COMPARISON OF EMITTER LOCALIZATION METHODS WITH A MOVING PLATFORM IN THREE DIMENSIONS

A THESIS SUBMITTED TO
THE GRADUATE SCHOOL OF NATURAL AND APPLIED SCIENCES
OF
MIDDLE EAST TECHNICAL UNIVERSITY

BY

BURCU TUFAN

IN PARTIAL FULLFILLMENT OF THE REQUIREMENTS
FOR
THE DEGREE OF MASTER OF SCIENCE
IN
ELECTRICAL AND ELECTRONICS ENGINEERING

SEPTEMBER 2012

Approval of the thesis:

COMPARISON OF EMITTER LOCALIZATION METHODS WITH A MOVING PLATFORM IN THREE DIMENSIONS

submitted by **BURCU TUFAN** in partial fulfillment of the requirements for the degree of **Master of Science in Electrical and Electronics Engineering Department, Middle East Technical University** by,

Prof. Dr. Canan Özgen
Dean, Graduate School of **Natural and Applied Sciences** _____

Prof. Dr. İsmet Erkmen
Head of Department, **Electrical and Electronics Engineering** _____

Prof. Dr. T. Engin Tuncer
Supervisor, **Electrical and Electronics Engineering Dept., METU** _____

Examining Committee Members:

Prof. Dr. A. Aydın Alatan
Electrical and Electronics Engineering Dept., METU _____

Prof. Dr. T. Engin Tuncer
Electrical and Electronics Engineering Dept., METU _____

Prof. Dr. Buyurman Baykal
Electrical and Electronics Engineering Dept., METU _____

Asst. Prof. Dr. Umut Orguner
Electrical and Electronics Engineering Dept., METU _____

Aydın Bayri, M.Sc.
ASELSAN Inc. _____

Date: **11.09.2012**

I hereby declare that all information in this document has been obtained and presented in accordance with academic rules and ethical conduct. I also declare that, as required by these rules and conduct, I have fully cited and referenced all material and results that are not original to this work.

Name, Last name : Burcu Tufan

Signature :

ABSTRACT

COMPARISON OF EMITTER LOCALIZATION METHODS WITH A MOVING PLATFORM IN THREE DIMENSIONS

Tufan, Burcu

M. Sc., Department of Electrical and Electronics Engineering
Supervisor: Prof. Dr. Temel Engin Tuncer

September 2012, 106 pages

In passive target localization, source position is estimated by only using the source signal. In this thesis, position of a stationary target is estimated by using the data collected by a moving platform. Since the focus of the thesis is the location estimation, the parameters used for localization such as angle-of-arrival (AOA), time-difference-of-arrival (TDOA), Doppler frequency shift are assumed to be known.

Different emitter localization methods are implemented in this thesis. Some of these methods are known in the literature and some are the modified or hybrid versions of these algorithms. Orthogonal Vector Estimator (OVE), Pseudolinear Estimator (PLE), Weighted Instrumental Variables Estimator (WIVE) and Maximum Likelihood Estimator (MLE) use only the AOA information. In MLE, Gauss Newton (GN) search algorithm is used to realize the search process effectively. AOA localization methods are also implemented together with the extended Kalman filter (EKF) realization.

Doppler Shifted Frequency (DSF) based Least Squares (LS) and MLE are implemented which use Doppler frequency shift only. AOA-DSF combined hybrid algorithm is shown to perform better.

LS and Maximum Likelihood (ML) TDOA localization methods are also implemented. AOA-DSF-TDOA combined hybrid algorithm is shown to perform better than the algorithms which use one type of parameter and AOA-DSF hybrid algorithm.

Estimator performances are analyzed in this thesis. Error ellipsoid is a useful tool to evaluate an estimator's performance. The parameters of the ellipsoids are drawn from Cramer-Rao Lower Bound (CRLB) matrices. The effect of target-sensor positioning is also investigated by using error ellipsoids.

Several experiments are done where a platform is assumed to be moving on a pre-determined path while the target is stationary. The effects of different parameters are considered for the location estimation accuracy.

Keywords: 3D Target Localization, AOA, CRLB, DSF, TDOA, Error Ellipsoid

ÖZ

HAREKETLİ TEK PLATFORM İLE ÜÇ BOYUTLU HEDEF KONUM BELİRLEME TEKNİKLERİNİN KARŞILAŞTIRILMASI

Tufan, Burcu

Yüksek Lisans, Elektrik Elektronik Mühendisligi Bölümü
Tez Yöneticisi: Prof. Dr. Temel Engin Tuncer

Eylül 2012, 106 sayfa

Pasif hedef konum bulma yönteminde, hedef konumu sadece kaynak sinyali kullanılarak bulunur. Bu tezde durağan hedefin konumu hareketli tek platform tarafından toplanan bilgiler kullanılarak kestirilmiştir. Tezin odak noktası hedef konum kestirimi olduğu için, konum bulurken kullanılan Geliş Açısı (GA), Varış Zaman Farkları (VZF), Doppler frekans kayması parametrelerinin değerleri biliniyor kabul edilmiştir.

Tez kapsamında farklı konum bulma yöntemleri incelenmiştir. Bu yöntemlerin bazıları literatürde bilinirken bazıları bu algoritmaların değiştirilmiş ya da birleştirilmiş halleridir. Dikgen Vektör Kestirici (DVK), Sahte-Doğrusal Kestirici (SDK), Ağırlıklı Etkili Değişken Kestirici (AEDK) ve En Büyük Olabilirlik Kestiricisi (EBOK) sadece GA bilgisini kullanarak konum bulmaktadır. EBOK, arama işlemini etkili bir şekilde yapabilmek için Gauss Newton (GN) arama algoritmasını kullanmaktadır. Genişletilmiş Kalman süzgeci kullanılarak GA ile konum bulma yöntemleri de incelenmiştir.

Sadece Doppler frekans kaymasını kullanarak konum bulan Doppler Kaymış Frekans (DKF) temelli En Küçük Kareler (EKK) ve EBOK yöntemleri gerçeklenmiştir. GA-DKF hibrit algoritmasının daha iyi sonuç verdiği gösterilmiştir.

Varış Zaman Farkları (VZF) temelli EKK ve EBOK yöntemleri de gerçeklenmiştir. GA-DKF-VZF hibrit algoritmasın tek parametre kullanan algoritmalardan ve GA-DKF hibrit algoritmasından daha iyi sonuç verdiği gösterilmiştir.

Tez kapsamında kestiricilerin performansları da incelenmistir. Hata elipsoidi bir kestiricinin performansını değerlendirmek için kullanılan yararlı bir araçtır. Elipsoidin parametreleri Cramer-Rao Alt Sınır (CRAS) matrisinden çıkarılmaktadır. Hedef-platform geometrisinin performansa etkisi de hata elipsoidleri kullanılarak incelenmiştir.

Hareketli platformun belirlenmiş bir güzergahta durağan bir hedef üzerinde hareket ettiği çeşitli deneyler yapılmıştır. Farklı parametrelerin konum kestirim doğruluğuna etkileri incelenmiştir.

Anahtar Kelimeler: 3B Hedef Konum Kestirimi, GA, CRAS, DKF, VZF, Hata Elipsoidi

To

The memory of my grandmother,

My mother and sister,

and

Alper

ACKNOWLEDGEMENTS

I would like to express my deepest gratitude to my supervisor Prof. Dr. Temel Engin Tuncer for his encouragements, guidance, advice and insight throughout the research.

I would like to thank ASELSAN Inc. for facilities provided for the competition of this thesis.

I would like to forward my appreciation to all my friends and colleagues who contributed to my thesis with their continuous encouragement.

I would also like to convey thanks to jury members for their valuable comments on this thesis.

Lastly but mostly, I would like to thank my mother Sıdıka ÖZÇELİK and sister Begüm ÇOLAKOĞLU for being such a great family. Also I have to send my special thanks to the love of my life, Alper TUFAN, who has always encouraged and motivated me on my thesis with his constant patience and understanding. Their support is very important for me throughout my life and they mean everything to me. This thesis is dedicated to them.

TABLE OF CONTENTS

LIST OF TABLES

TABLES

LIST OF FIGURES

FIGURES

LIST OF ABBREVIATIONS

AOA : Angle of Arrival
BM : Bearing Method
CM : Combined Method
CRLB : Cramer Rao Lower Bound
DF : Direction Finding
DSF : Doppler Shifted Frequency
DTED : Digital Terrain Elevation Data
EA : Electronic Attack
EKF : Extended Kalman Filter
EP : Electronic Protect
ES : Electronic Support
EW : Electronic Warfare
FIM : Fisher Information Matrix
GDOP : Geometric Dilution of Precision
GN : Gauss Newton
GPS : Global Positioning System
IV : Instrumental Variable
KF : Kalman Filter
LS : Least Squares
MLE : Maximum Likelihood Estimator
MSE : Mean Square Error
OVE : Orthogonal Vector Estimator
PLE : Pseudolinear Estimator
RDOA : Range Difference of Arrival
RMS : Root Mean Square
SNR : Signal-to-Noise Ratio
TDOA : Time Difference of Arrival

TOA : Time of Arrival

WIVE : Weighted Instrumental Variable Estimator

WLS : Weighted Least Squares

CHAPTER 1

INTRODUCTION

1.1 Background

Determining the location of an emitting target is one of the fundamental functions of Electronic Warfare (EW) systems [1]. It is generally accepted that EW has three distinct components: (1) *electronic support* (ES), (2) *electronic attack* (EA) and *electronic protect* (EP). Emitter localization is performed in ES systems. Beside military uses, localization is important in commercial uses such as localization of mobile phone calls to emergency services [2]. On the other hand, since the target does not cooperate, this is a complicated task. Estimation procedure consists of two steps. First the parameters which will be used in the estimation algorithm are estimated. Then by using these parameters the target position is estimated. These mentioned parameters can be TDOA, frequency and/or bearing measurements. Estimation of these parameters is out of scope of this thesis but brief information will be given in the following sections. In this thesis the focus is the location estimation given the parameter estimates.

In the literature, there are many papers about emitter localization. Bearing-only emitter localization algorithm is one of the most-common methods. In this method, emitter location is obtained by intersecting the bearing lines taken at different platform positions. This method is referred to as *triangulation*. Stansfield estimator [3] is one of the first bearing-only localization methods which is a Weighted Least-Squares (WLS) estimator. It can be viewed as a small error approximation of the

MLE [4]. On the other hand, Stansfield estimator is biased unlike MLE which is asymptotically unbiased. In [5], PLE is presented which requires no range information of the target different from the Stansfield's method. MLE is an effective method which is based on minimizing a cost function [5]. Taylor-Series method is used for solving simultaneous set of algebraic position equations (generally nonlinear), starting with a rough initial estimate [6]. The points where bearing measurements are collected play a crucial role in estimator accuracy. In [8] the impact of measurement points on localization performance is investigated. The method is based on minimizing the Mean-Square-Error (MSE) of the localization algorithm.

Doppler-shift is also used to locate an emitter when there is relative motion between locator platform and target. Due to relative motion, the emitted signal's frequency and the received frequency by the locator platform are different. In [9] a grid search method is proposed for DSF localization. LS and ML estimation methods are presented in [10]. Emitter localization using both bearing and frequency methods are also available [11]. In [12] target localization of radars which change their frequency in time (frequency-hopping radars) is presented. In this thesis, it is assumed that the target is emitting at a constant frequency. [13] uses digital terrain data while estimating target position with frequency measurements. Digital terrain data gives terrain altitude values as a function of (x, y). Effect of this data on estimator performance is analyzed and compared with the case where no terrain information is available.

TDOA based localization is known as quadratic position-fixing methods. In this method, the arrival times of the same pulse is measured between different sensors. Estimation of these arrival times is critical in position estimation accuracy. The measured TDOA values define a hyperboloid where the target lies. Position estimate is found by intersecting these hyperboloids. This is why TDOA localization is also called as hyperbolic positioning. Position estimate can be found by using closed-form estimators [14]. In [17], position is estimated by using

hyperbolic asymptotes. The property that the TDOA equations become linear in the far field is used and the equations are solved analytically as the intersection of hyperbolic asymptotes. Most TDOA localization algorithms process one set of TDOA measurements to estimate target position. In [18] a closed-form multi-platform localization algorithm is presented that exploits additional information available from multiple TDOA measurements. WLS and WIVE are analyzed. Different sensor placement strategies for TDOA based localization are investigated in literature [19].

Beside these methods emitter localization techniques based on antenna scan properties are available [20]. Unlike TDOA methods, high-precision TOA measurements are not required for these algorithms. However these methods are applicable for mechanically scanning radar with a narrow azimuth beamwidth.

Target-Platform geometry has a large effect on estimator accuracy. In [23] a path planning algorithm is presented which minimizes localization uncertainty. It is a nonlinear programming problem which uses an approximation of the Fisher Information Matrix (FIM) to generate optimum platform trajectories.

In literature it is stated that hyperbolic position-fixing methods based on TDOA and Dopplerized frequencies yield better accuracy than bearing-only methods. On the other hand for these methods, longer integration times are required than for the DF approaches [2].

1.2 Scope and Contributions of the Thesis

In this thesis, three main types of localization approaches are investigated. These are bearing based methods, frequency based methods and TDOA based methods. In addition, hybrid methods obtained from the combinations of these methods are considered. In the simulations, target is assumed to be stationary. The locator platform is flying over a path and collecting the parameters from the target.

The contribution of this thesis is the implementation and comparison of different localization methods under the same framework. Therefore, it is possible to have an

idea about the possible performance of different algorithms. While it is not possible to have a completely fair comparison between different methods, the comparisons give a good idea about the expected performance of different methods. Note that since different methods use different parameters such as AOA, frequency, TDOA, *etc*., a completely fair comparison is not possible. However, the accuracy achieved for the estimation of AOA, frequency and TDOA parameters is well known in practice and those values can be used to have an idea about the possible performances achieved by different methods.

Certain modifications to existing algorithms are done and these versions of the algorithms can be seen as partly novel algorithms. In addition hybrid algorithms are implemented which are reported in this thesis.

The thesis is organized in five chapters. In CHAPTER 2, localization techniques based on bearing measurements is analyzed. OVE, PLE, WIVE and MLE algorithms are presented and their performances are compared for different cases. The WIVE algorithm in literature is modified as WIVE2 and the performances of WIVE and WIVE2 are compared. Recursive position estimation using EKF is also implemented which uses bearing measurements at each time step. Information about error ellipsoid is given which is an important tool to analyze estimator performances. Calculating the parameters of an ellipsoid, taking slice or projection of the ellipsoid on a plane are explained. Error ellipsoid parameters are calculated for bearing-only method and the effect of target-platform geometry on estimator accuracy is analyzed by using error ellipsoids. In CHAPTER 3, localization techniques based on DSF measurements is analyzed. LS and ML solutions are presented. Combined method (CM) is presented which uses both bearing and frequency measurements. Both the target position and frequency are estimated using measurements. At the end of this chapter performances of the algorithms are compared for different cases. Also effect of different parameters on estimator performance, such as platform velocity, signal frequency is analyzed. In CHAPTER 4, TDOA based localization methods are presented. Localization

methods both for multi-platform and single platform are analyzed. At the end of this chapter a localization method which uses all parameters which are bearing, frequency and TDOA measurements is presented. The performance of this combined algorithm is compared with other presented algorithms and shown it outperforms all others. Finally CHAPTER 5 summarizes the thesis and proposes future work.

CHAPTER 2

BEARING-ONLY LOCALIZATION ALGORITHMS

2.1 General Information

In this chapter, bearing-only localization algorithms are presented. Bearing-only emitter localization is a passive localization technique that employs bearing (direction-of-arrival) measurements of the received signals originating from an emitter [24]. Algorithms are based on intersecting the Direction-Finding (DF) lines. In the absence of noise, the DF lines will intersect at a point where the target lies. But in real life this is not the case. Due to noise, lines will intersect each other at different points, so many intersection points will occur. At this point, estimation algorithms are used to obtain a single position estimate.

This chapter includes different localization algorithms which are performed in 3D. Since 3D scenarios are analyzed, both azimuth and elevation angles are used in the algorithms.

The chapter starts with a brief information about the DF methods. The algorithms used for estimating azimuth and elevation angles are explained. After the problem formulation part, which explains the scenarios considered, bearing-only localization algorithms are presented for 3D localization scenarios such as OVE, PLE, WIVE and ML.

2.2 Direction-Finding Methods

In this section, brief information about DF methods is given. However DF algorithms are not implemented and it is outside the scope of this thesis. It is assumed that DF is already estimated with an error distribution which is known. Then this information is used to evaluate the localization algorithms. In simulations, azimuth and elevation angles are generated by adding zero mean Gaussian noise to the actual values. The noises on azimuth and elevation angles are assumed to be independent.

$$\begin{aligned} \tilde{\theta}_k &= \theta_k + n_{\theta,k} \ , n_{\theta,k} \sim \mathcal{N}\left(0, \sigma_\theta^2\right) \\ \tilde{\phi}_k &= \phi_k + n_{\phi,k} \ , n_{\phi,k} \sim \mathcal{N}\left(0, \sigma_\phi^2\right) \end{aligned} \tag{2-1}$$

Direction of the target is found by using antenna arrays on the platform. The phase difference can be measured between the signals at different antenna elements. If the antennas have directionality, the amplitude difference can also be measured [2]. In AOA estimation algorithms, it is assumed that the target radar is located at the far field of the receiver array and radar is a point emitter.

In amplitude comparison methods the directional antennas are located on the platform. The one which is directed to the target will measure the highest amplitude value.

In phase comparison methods, AOA is estimated by using the differences of phases between different antennas. A phase difference between the antennas occurs depending on the distance between the sensors (d), carrier frequency of the received signal (f_c) and the angle between target and platform. Although the angle can be easily calculated from the phase difference between the signals, this method is prone to performance degradation. Thus, using sum and difference of the channels can generate more stable angle estimation results [26]. In amplitude and phase comparison methods proper antenna calibration is required.

AOA estimation with TDOA method finds the direction of arrival of a signal from the information of time difference of the signal at the sensors [25].

2.3 Problem Formulation

Azimuth and elevation angles of the target are assumed to be obtained by using the algorithms which are explained in Section 2.2 by DF-sites. In AOA based localization methods, input parameters are the DF angles and the DF platform coordinates. In the absence of noise, the DF lines will intersect at a single point as stated before. The errors in azimuth and elevation angles will create cone-shaped structures as shown in Figure 2-1. So the intersection of these cones will represent a volume instead of a single point. The shapes of the cones depend to the standard deviation of the azimuth and elevation measurement errors.

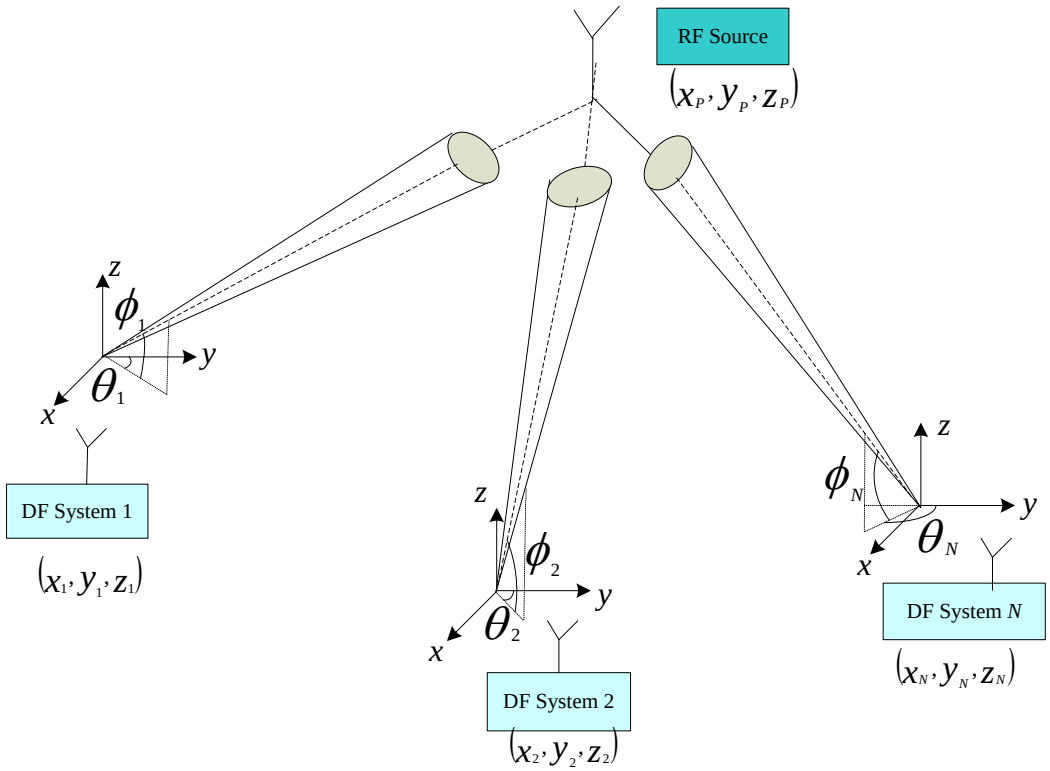

Figure 2-1 : 3D AOA Based Source Localization for Noisy Case

In bearing-only localization algorithms the inputs are the target DF angles, DF error variance and the platform coordinates. Target position can be estimated by many platforms which lie at different positions, or by a single moving platform which takes measurements at different points. In this thesis, a single moving platform is used which collects multiple DF measurements.

2.4 Bearing-Only Localization Algorithms

In this section, bearing-only localization algorithms have been presented. First OVE is given which is a closed form estimator. Then PLE and WIVE algorithms are analyzed which are also closed form estimators. In WIVE, the target estimate found in PLE is used. MLE follows these algorithms which constructs the estimate in an iterative way unlike closed form estimators. GN search algorithm which is an iterative method is used in ML estimator. In all these methods the data are collected from the moving platform and used in the estimator. On the other hand the ability to update a position estimate with a new measurement without using all previous measurements is important. By this ability it will be enough to store only the last position estimate and the new measurement information in the memory instead of all measurements. A recursive position estimator which starts with an initial estimate and updates this estimate with new measurements is analyzed in Section 2.4.5. Extended Kalman Filter (EKF) is used for this algorithm. At the end of the section, the simulation results of the mentioned algorithms and performance comparison of the methods are given. Effect of different parameters on estimator performance is analyzed.

In this thesis, the true location of the stationary target is represented by $\boldsymbol{p} = [x_P, y_P, z_P]^T$ where ^{T} denotes matrix transpose. The single moving platform takes N measurements along its path and the platform position where the k^{th} measurement taken is represented by $\boldsymbol{r_k} = [x_k, y_k, z_k]^T$.

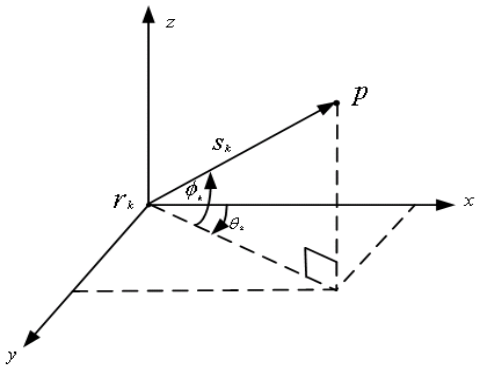

Figure 2-2 : Illustration of azimuth and elevation angles for noise-free case

The moving platform collects azimuth (θ_k) and elevation (ϕ_k) angle at each measurement point along its path. These angles are illustrated in Figure 2-2 and the relations between positions and angles are given in Equations (2-2) and (2-3).

$$\theta_k = \tan^{-1}\left(\frac{y_P - y_k}{x_P - x_k}\right) \tag{2-2}$$

$$\phi_k = \tan^{-1}\left(\frac{z_P - z_k}{\sqrt{(x_P - x_k)^2 + (y_P - y_k)^2}}\right) \tag{2-3}$$

As seen in Figure 2-2, $\boldsymbol{s_k}$ is a vector between the platform and the emitter. This vector can be written for noise-free case as

$$\boldsymbol{s_k} = \|\boldsymbol{s_k}\| \begin{bmatrix} \cos\phi_k \cos\theta_k \\ \cos\phi_k \sin\theta_k \\ \sin\phi_k \end{bmatrix} \tag{2-4}$$

The relationship between the platform position and the target is given by Equation (2-5)

$$\boldsymbol{p} = \boldsymbol{r_k} + \boldsymbol{s_k} \tag{2-5}$$

Since the position of the target is unknown, the information about $\boldsymbol{s_k}$ vector is unavailable. This $\boldsymbol{s_k}$ term can be eliminated from Equation (2-5) by multiplying Equation (2-5) with a unit vector $(\boldsymbol{a_k})$ which is orthogonal to $\boldsymbol{s_k}$ $\left(\boldsymbol{i.e.}\ \boldsymbol{a_k^T s_k} = 0\right)$. The orthogonal vector is obtained by increasing the elevation angle by $\pi / 2$ radians in $\boldsymbol{s_k}$.

$$\boldsymbol{a_k} = \begin{bmatrix} \cos\left(\phi_k + {}^{\pi}/_{2}\right)\cos\theta_k \\ \cos\left(\phi_k + {}^{\pi}/_{2}\right)\sin\theta_k \\ \sin\left(\phi_k + {}^{\pi}/_{2}\right) \end{bmatrix} = \begin{bmatrix} -\sin\phi_k \cos\theta_k \\ -\sin\phi_k \sin\theta_k \\ \cos\phi_k \end{bmatrix} \tag{2-6}$$

Since $\boldsymbol{s_k}$ and $\boldsymbol{a_k}$ are orthogonal $\boldsymbol{a_k^T s_k} = 0$.

After multiplying both sides of Equation (2-5) with the orthogonal vector of $\boldsymbol{s_k}$ and using the property $\boldsymbol{a_k^T s_k} = 0$ the following is obtained:

$$\boldsymbol{a_k^T p} = \boldsymbol{a_k^T r_k} \tag{2-7}$$

Above equality is used in the following estimator. It is obvious that exact azimuth and elevation angles are not known. These angles are estimated by DF algorithms. So $\boldsymbol{a_k}$ vector is obtained with generated angles $(\tilde{\theta}_k, \tilde{\phi}_k)$ which are true angles corrupted with zero-mean Gaussian noise.

$$\begin{aligned} \tilde{\theta}_k &= \theta_k + n_{\theta,k}\ , n_{\theta,k} \sim \mathcal{N}\left(0, \sigma_\theta^2\right) \\ \tilde{\phi}_k &= \phi_k + n_{\phi,k}\ , n_{\phi,k} \sim \mathcal{N}\left(0, \sigma_\phi^2\right) \end{aligned} \tag{2-8}$$

2.4.1 Orthogonal Vector Estimator (Least Squares Estimator)

In this estimator, the property derived in Equation (2-7) is used. The generated azimuth and elevations are used for defining $\tilde{\boldsymbol{a}}_{\boldsymbol{k}}$ which is the noise corrupted version of $\boldsymbol{a_k}$.

$$\tilde{\boldsymbol{a}}_{\boldsymbol{k}} = \begin{bmatrix} -\sin\tilde{\phi}_k \cos\tilde{\theta}_k \\ -\sin\tilde{\phi}_k \sin\tilde{\theta}_k \\ \cos\tilde{\phi}_k \end{bmatrix} \tag{2-9}$$

In noisy case, Equation (2-7) becomes $\tilde{\boldsymbol{a}}_k^T \boldsymbol{p} = \tilde{\boldsymbol{a}}_k^T \boldsymbol{r}_k + \boldsymbol{n}_k$. It is obvious that the noise term is non-linear function of the azimuth and elevation angles' measurement noise. If the equation is written for all measurements taken at *N* different points and expressed in matrix form, following relation is obtained

$$\underbrace{\begin{bmatrix} \tilde{\boldsymbol{a}}_1^T \\ \vdots \\ \tilde{\boldsymbol{a}}_N^T \end{bmatrix}}_{\boldsymbol{A}} \boldsymbol{p} = \underbrace{\begin{bmatrix} \tilde{\boldsymbol{a}}_1^T \boldsymbol{r}_1 \\ \vdots \\ \tilde{\boldsymbol{a}}_N^T \boldsymbol{r}_N \end{bmatrix}}_{\boldsymbol{b}} + \underbrace{\begin{bmatrix} \boldsymbol{n}_1 \\ \vdots \\ \boldsymbol{n}_N \end{bmatrix}}_{\boldsymbol{n}} \tag{2-10}$$

In Equation (2-10), sizes of $\boldsymbol{A}$ matrix, $\boldsymbol{p}$ and $\boldsymbol{b}$ vectors are *Nx3*, *3x1* and *Nx1* respectively. $\tilde{\boldsymbol{a}}_{\boldsymbol{k}}$ terms are obtained with generated bearing angles and platform has its own position data $\boldsymbol{r}_{\boldsymbol{k}}$. LS solution of $\boldsymbol{Ap} = \boldsymbol{b}$ is given by

$$\hat{\boldsymbol{p}} = (\boldsymbol{A}^T \boldsymbol{A})^{-1} \boldsymbol{A}^T \boldsymbol{b} \tag{2-11}$$

which is the closed-form 3D orthogonal vector estimator [24]. Since $\boldsymbol{A}$ and $\boldsymbol{n}$ are correlated, this estimator exhibits bias and the bias gets larger as bearing noise and range-to-baseline ratio increases.

OVE Algorithm:

1. Estimate the AOA of the target signal at each measurement point with a direction-finding algorithm.
2. Obtain the matrix $\boldsymbol{A}$ and vector $\boldsymbol{b}$ as mentioned in Equations (2-9) and (2-10) by using the generated AOA measurements and platform positions.
3. Estimate the target position $\hat{\boldsymbol{p}}$ by using the closed form solution given in Equation (2-11).

2.4.2 Pseudolinear Estimator (PLE)

PLE is another closed form estimator used in target localization. In this method, problem is first analyzed as a 2D problem and only azimuth angles are used to estimate the target's x and y coordinates. Then by using the estimates and the elevation angles, z-coordinate of the platform is estimated. Equation (2-2) can be written as follows for noisy case

$$\tan\tilde{\theta}_k = \frac{\sin\tilde{\theta}_k}{\cos\tilde{\theta}_k} = \frac{y_P - y_k}{x_P - x_k} \tag{2-12}$$

$$\sin\tilde{\theta}_k x_P - \sin\tilde{\theta}_k x_k = \cos\tilde{\theta}_k y_p - \cos\tilde{\theta}_k y_k \tag{2-13}$$

$$\sin\tilde{\theta}_k x_P - \cos\tilde{\theta}_k y_P = \sin\tilde{\theta}_k x_k - \cos\tilde{\theta}_k y_k \tag{2-14}$$

The equations written for all N measurements can be expressed in matrix form:

$$\underbrace{\begin{bmatrix} \sin\tilde{\theta}_1 & -\cos\tilde{\theta}_1 \\ \vdots & \vdots \\ \sin\tilde{\theta}_N & -\cos\tilde{\theta}_N \end{bmatrix}}_{\mathbf{A}_1} \underbrace{\begin{bmatrix} x_P \\ y_P \end{bmatrix}}_{p_{xy}} \approx \underbrace{\begin{bmatrix} \sin\tilde{\theta}_1 x_1 - \cos\tilde{\theta}_1 y_1 \\ \vdots \\ \sin\tilde{\theta}_N x_N - \cos\tilde{\theta}_N y_N \end{bmatrix}}_{b_1} \tag{2-15}$$

Note that the $\boldsymbol{A_1}$ matrix and $\boldsymbol{b_1}$ vector in Equation (2-15) are different from $\boldsymbol{A}$ matrix and $\boldsymbol{b}$ vector used in OVE.

By using Equation (2-15), pseudolinear estimate of target's x and y coordinates can be found as:

$$\hat{\boldsymbol{p}}_{xy} = (\boldsymbol{A_1^T A_1})^{-1} \boldsymbol{A_1^T b_1} \tag{2-16}$$

At this point x and y coordinates of the target is estimated ($\hat{x}_P$ and $\hat{y}_P$). By using these estimates and Equation (2-3), z coordinate of the target can be found. Noisy

elevation measurements ($\tilde{\phi}_k$) are used instead of the actual elevation angles. The z_P term in the equation is calculated for all N measurements and the average of these values is calculated. This value is the estimate of the z coordinate, $\hat{z}_P$. Since the relation between elevation angle and target position is non-linear, the corresponding equations cannot be written in matrix form as in Equation (2-15). So following formula is used

$$\hat{z}_P = \frac{1}{N}\sum_{k=1}^{N}\left(z_k + \sqrt{(\hat{x}_P - x_k)^2 + (\hat{y}_P - y_k)^2}\tan\tilde{\phi}_k\right) \tag{2-17}$$

PLE Algorithm:

1. Estimate the AOA of the target signal at each measurement point with a direction-finding algorithm.
2. Obtain the matrix $\boldsymbol{A_1}$ and vector $\boldsymbol{b_1}$ as defined in Equation (2-15) by using the generated azimuth measurements and platform positions.
3. Estimate x and y coordinates of the target $\widehat{\boldsymbol{p}}_{xy}$ by using the closed form solution given in Equation (2-16).
4. Estimate the z coordinate of the target by using $\widehat{\boldsymbol{p}}_{xy}$, generated elevation measurements and platform positions with Equation (2-17).

2.4.3 Weighted Instrumental Variables Estimator (WIVE) [24]

In the PLE above, since the measurement matrix $\boldsymbol{A}_1$ is correlated with bearing noise, the 3D PLE is not consistent. That is, $\widehat{\boldsymbol{p}}_{xy}$ does not converge to the true location vector $\boldsymbol{p}_{xy}$ as $N \to \infty$ and it is biased [24]. Instrumental variables are used to solve this problem.

In localization problem, a linear model $\boldsymbol{A_1 p}_{xy} = \boldsymbol{b}_1 + \boldsymbol{n}$ is used where some of the $\boldsymbol{A_1}$ variables are correlated with $\boldsymbol{n}$. This occurs when $\boldsymbol{A_1}$ contains measurement

errors. For general case $\boldsymbol{A_1}$ is *nxk*, $\boldsymbol{p_{xy}}$ is *kx1*, $\boldsymbol{b_1}$ and $\boldsymbol{n}$ are *nx1*. Suppose there is a *nxk* array of variables $\boldsymbol{G_1}$, called *instruments*, which have the property that the variables in $\boldsymbol{G_1}$ are uncorrelated with $\boldsymbol{n}$. Premultiplying the linear model equation with $\boldsymbol{G_1^T}$ yields

$$\boldsymbol{G_1^T A_1 p_{xy}} = \boldsymbol{G_1^T b_1} + \boldsymbol{G_1^T n} \tag{2-18}$$

The idea of an IV estimator of $\boldsymbol{p_{xy}}$ is to approximate $\boldsymbol{G_1^T n}$ by zero, and solve Equation (2-19).

$$(\boldsymbol{G_1^T A_1})\hat{\boldsymbol{p}}_{IV} = \boldsymbol{G_1^T b_1} \tag{2-19}$$

The IV estimate of the target is:

$$\hat{\boldsymbol{p}}_{IV} = (\boldsymbol{G_1^T A_1})^{-1}\boldsymbol{G_1^T b_1} \tag{2-20}$$

The only change is in $\boldsymbol{G_1}$ which is called as instrumental variable (IV) matrix. By using an instrumental variable matrix which is uncorrelated with the bearing noise, the consistency of the estimate is established and the estimator becomes asymptotically unbiased. In some algorithms in literature, uncorrelation between IV matrix and the bearing noise is established by using an iterative process for calculating an IV matrix [24]. Noise free version of the A_1 matrix is an optimal IV matrix, but since the actual angle values are not known, this is not practical. However by using the PLE found in Section 2.4.2, azimuth angles can be re-calculated and a suboptimal IV matrix can be obtained. In other words, instead of the noisy azimuth angles $(\tilde{\theta}_k)$, azimuth angle estimates $(\hat{\theta}_k)$ calculated by using the position estimate will be used.

$$\hat{\theta}_k = \tan^{-1}\left(\frac{\hat{y}_P - y_k}{\hat{x}_P - x_k}\right) \tag{2-21}$$

IV matrix is constructed by using estimated azimuth angles:

$$\boldsymbol{G_1} = \begin{bmatrix} \boldsymbol{g_1^T} \\ \vdots \\ \boldsymbol{g_N^T} \end{bmatrix} = \begin{bmatrix} sin\hat{\theta}_1 & -cos\hat{\theta}_1 \\ \vdots & \vdots \\ sin\hat{\theta}_N & -cos\hat{\theta}_N \end{bmatrix} \tag{2-22}$$

By using the PLE estimate found in 2.4.2, the distances between emitter and the platform positions can be estimated. The measurements taken at closer points are more trustworthy. This information is used in the estimation by introducing a weighting matrix which is:

$$\boldsymbol{W} = diag(\hat{d}_1^2, \dots, \hat{d}_N^2) \tag{2-23}$$

$$\hat{d}_k = \sqrt{(\hat{x}_P - x_k)^2 + (\hat{y}_P - y_k)^2} \tag{2-24}$$

By using the IV matrix and the weighting matrix, the Weighted Instrumental Variable (WIV) estimate of the target is obtained with the following equation. As in PLE, first x and y coordinates of the target are estimated. Then by using these estimates, z coordinate of the target is found.

$$\hat{\boldsymbol{p}}_{WIV} = (\boldsymbol{G_1^T W^{-1} A_1})^{-1} \boldsymbol{G_1^T W^{-1} b_1} \tag{2-25}$$

$$\hat{z}_{P,WIV} = \frac{1}{N} \sum_{k=1}^{N} \left(z_k + \sqrt{(\hat{x}_{P,WIV} - x_k)^2 + (\hat{y}_{P,WIV} - y_k)^2} tan\tilde{\phi}_k \right) \tag{2-26}$$

WIVE Algorithm:

1. Estimate the AOA of the target signal at each measurement point with a direction-finding algorithm.
2. Calculate the azimuth angles $(\hat{\theta}_k)$ by using the $\hat{\boldsymbol{p}}_{xy}$ estimate obtained with PLE as in Equation (2-21).
3. Obtain the IV matrix $\boldsymbol{G_1}$ by using the calculated azimuth angles in Step 2 as in Equation (2-22).

4. Calculate the distance between target and platform positions by using the $\hat{\boldsymbol{p}}_{xy}$ estimate obtained with PLE and obtain the weighting matrix $\boldsymbol{W}$ as in Equation (2-23).
5. Estimate x and y coordinates of the target $\hat{\boldsymbol{p}}_{WIV}$ by using the closed form solution given in Equation (2-25).
6. Estimate the z coordinate of the target $\hat{z}_{P,WIV}$ by using the generated elevation angles and the $\hat{\boldsymbol{p}}_{WIV}$ obtained in Step 5.

In WIVE algorithm, the IV matrix $\boldsymbol{G_1}$ is calculated by using the PLE estimate. In this thesis the same procedure is repeated such that the IV matrix is updated by using the position estimate obtained by WIVE. This algorithm is named as WIVE2.

WIVE2 Algorithm:

1. Calculate the azimuth angles $(\hat{\theta}_k)$ by using the $\hat{\boldsymbol{p}}_{WIV}$ estimate obtained with WIVE.
2. Update the IV matrix $\boldsymbol{G_1}$ by using the calculated azimuth angles in Step 1.
3. Estimate x and y coordinates of the target $\hat{\boldsymbol{p}}_{WIV}$ by using the updated IV matrix.
4. Estimate the z coordinate of the target $\hat{z}_{P,WIV}$ by using the generated elevation angles and the $\hat{\boldsymbol{p}}_{WIV}$ obtained in Step 3.

2.4.4 Maximum Likelihood Estimator

The maximum likelihood estimator (MLE) is obtained from the maximization of the joint probability density function of the bearing measurements $\left(\tilde{\theta}_k, \tilde{\phi}_k\right)$, $k=1,\ldots,N$ [24].

Assuming the bearing noise is zero mean Gaussian, the MLE of the target position can be written as

$$\widehat{\boldsymbol{p}}_{ML=} \underset{\boldsymbol{p}}{\operatorname{argmin}}\, J_{ML}(\boldsymbol{p}) \tag{2-27}$$

where the ML cost function is given by

$$J_{ML}(\boldsymbol{p}) = \boldsymbol{e}^T(\boldsymbol{p})\boldsymbol{K}^{-1}\boldsymbol{e}(\boldsymbol{p}) \tag{2-28}$$

$\boldsymbol{K}$ is the $2Nx2N$ covariance matrix of the bearing noise and $\boldsymbol{e}(\boldsymbol{p})$ is the $2Nx1$ error vector which are defined as

$$\boldsymbol{K} = diag\{\sigma_{\theta_1}^2, \sigma_{\theta_2}^2, \dots, \sigma_{\theta_N}^2, \sigma_{\phi_1}^2, \sigma_{\phi_2}^2, \dots, \sigma_{\phi_N}^2\} \tag{2-29}$$

$$\boldsymbol{e}(\boldsymbol{p}) = [\tilde{\theta}_1 - \theta_1(\boldsymbol{p}), \dots, \tilde{\theta}_N - \theta_N(\boldsymbol{p}), \tilde{\phi}_1 - \phi_1(\boldsymbol{p}), \dots, \tilde{\phi}_N - \phi_N(\boldsymbol{p})] \tag{2-30}$$

It is seen that the ML estimator does not have a closed form solution. A search algorithm should be used to find the target position that maintains the minimum cost. GN algorithm is used for this purpose which is a batch iterative minimization technique. The method is as follows

$$\widehat{\boldsymbol{p}}_{i+1} = \widehat{\boldsymbol{p}}_i - (\boldsymbol{J}_i^T\boldsymbol{K}^{-1}\boldsymbol{J}_i)^{-1}\boldsymbol{J}_i^T\boldsymbol{K}^{-1}\boldsymbol{e}(\widehat{\boldsymbol{p}}_i)\ for\ i = 0,1, \dots, N_{iteration} \tag{2-31}$$

where $\boldsymbol{J}_i$ is the *2Nx3* Jacobian matrix evaluated at the current position estimate:

$$\mathbf{J}_i = \left[\begin{array}{ccc} \dfrac{-(y_P - y_1)}{(x_P - x_1)^2\left(\dfrac{(y_P - y_1)^2}{(x_P - x_1)^2}+1\right)} & \dfrac{1}{(x_P - x_1)\left(\dfrac{(y_P - y_1)^2}{(x_P - x_1)^2}+1\right)} & 0 \\ \vdots & \vdots & \vdots \\ \dfrac{-(y_P - y_N)}{(x_P - x_N)^2\left(\dfrac{(y_P - y_N)^2}{(x_P - x_N)^2}+1\right)} & \dfrac{1}{(x_P - x_N)\left(\dfrac{(y_P - y_N)^2}{(x_P - x_N)^2}+1\right)} & 0 \\ \dfrac{-(x_P - x_1)(z_P - z_1)}{\|p - r_1\|^2\sqrt{(x_P - x_1)^2 + (y_P - y_1)^2}} & \dfrac{-(y_P - y_1)(z_P - z_1)}{\|p - r_1\|^2\sqrt{(x_P - x_1)^2 + (y_P - y_1)^2}} & \dfrac{\sqrt{(x_P - x_1)^2 + (y_P - y_1)^2}}{\|p - r_1\|^2} \\ \vdots & \vdots & \vdots \\ \dfrac{-(x_P - x_N)(z_P - z_N)}{\|p - r_N\|^2\sqrt{(x_P - x_N)^2 + (y_P - y_N)^2}} & \dfrac{-(y_P - y_N)(z_P - z_N)}{\|p - r_N\|^2\sqrt{(x_P - x_N)^2 + (y_P - y_N)^2}} & \dfrac{\sqrt{(x_P - x_N)^2 + (y_P - y_N)^2}}{\|p - r_N\|^2} \end{array} \right]_{p=\hat{p}_i} \quad (2\text{-}32)$$

In the algorithm an initial estimate is required. The estimate obtained with pre-mentioned algorithms (PLE, WIVE) can be used. Jacobian matrix is evaluated at this estimate $\widehat{\boldsymbol{p}}_i = \boldsymbol{p} = [x_P, y_P, z_P]^T$. Then the estimate is updated according to the Equation (2-31). This procedure is repeated for a defined iteration number ($N_{iteration}$) or until the norm of the position update is smaller than a sufficiently small number. In MLE, the important point is choosing the initial estimate. If the initial estimate is not close enough to the actual target position, due to non-convex structure of cost function the estimator can diverge.

MLE Algorithm:

1. Estimate the AOA of the target signal at each measurement point with a direction-finding algorithm.
2. Obtain the measurement covariance matrix $\boldsymbol{K}$ as defined in Equation (2-29).
3. Start with an initial position estimate $\widehat{\boldsymbol{p}}_0$ and calculate the error vector for this estimate which is defined in Equation (2-30).
4. Calculate the Jacobian matrix $\boldsymbol{J}_0$ for the initial estimate as in Equation (2-32).

5. Perform GN search algorithm which updates position estimate by updating error vector and Jacobian matrix at each step as in Equation (2-31).
6. End the search algorithm when the defined update criterions are met.

2.4.5 Recursive Estimation with Extended Kalman Filter

In previous sections, information about different bearing-only localization algorithms is given. In these methods, bearings are used all at once to find the target location. In certain cases, recursive location estimation may be preferred where the location estimation is updated as the new data is collected. In situations where memory is limited in the platform, there may not be enough space to store all measurements. Also the calculation capacity of the platform can be restrictive. At this point a recursive estimator can be used which stores the position estimate and the new measurement only. First, a few measurements are taken and a position estimate is obtained which may be far from the actual position. By using this position and the new measurement, a new position estimate is obtained. The user does not need to store old measurements. Kalman filter (KF) is used for this problem.

KF can be used in linear-Gaussian systems. The 'linear' term means the relation between the observations and the state which is desired to estimate is linear. In emitter localization system the state is the target location. Since the target is stationary, the state is constant. The measurements are azimuth and elevation angles. As seen in Equations (2-2) and (2-3) the relation between measurements and state is non-linear which means KF cannot be used in this problem directly.

While KF is the optimal solution when the system model is linear, the real life systems are usually non-linear. For non-linear cases, the idea is to linearize the system equations such that the assumptions hold, and then run the standard KF algorithm. This is called the Extended Kalman Filter (EKF) [28]. The important

point is that the linearization is done recursively on the current state estimate. The system equations are as follows:

$$\boldsymbol{x}_{k+1} = f_k(\boldsymbol{x}_k) + \boldsymbol{w}_k \tag{2-33}$$

$$\boldsymbol{y}_k = h_k(\boldsymbol{x}_k) + \boldsymbol{v}_k \tag{2-34}$$

where $f_k(.)$ represents system model and $h_k(.)$ represents measurement model. $\boldsymbol{w}_k$ and $\boldsymbol{v}_k$ are the process noise and measurement noise, respectively.

In the emitter localization problem $\boldsymbol{x}_k$ represents the target position for the k^{th} time instant and $\boldsymbol{y}_k$ represents the measurements which are azimuth and elevation angles. Since the target is stationary the following equation holds:

$$\boldsymbol{x}_{k+1} = \boldsymbol{x}_k \tag{2-35}$$

Since the state model is linear, the linearization process is only done for the measurement model. The measurement relation is linearized around the predicted state $\hat{\boldsymbol{x}}_{k+1|k}$.

$$\boldsymbol{y}_{k+1} = h_{k+1}\left(\hat{\boldsymbol{x}}_{k+1|k}\right) + \boldsymbol{H}_{k+1}\left(\boldsymbol{x}_{k+1} - \hat{\boldsymbol{x}}_{k+1|k}\right) + \boldsymbol{v}_{k+1} \tag{2-36}$$

$$\boldsymbol{H}_{k+1} = \left(\nabla_{\boldsymbol{x}_{k+1}} h_{k+1}^T(\boldsymbol{x}_{k+1})\right)^T \Big|_{\boldsymbol{x}_{k+1}=\hat{\boldsymbol{x}}_{k+1|k}} \tag{2-37}$$

Time update and measurement update equations are as follows:

Time Update Step:

$$\hat{\boldsymbol{x}}_{k+1|k} = \hat{\boldsymbol{x}}_{k|k} \tag{2-38}$$

$$\boldsymbol{P}_{k+1|k} = \boldsymbol{P}_{k|k} \tag{2-39}$$

Since the emitter is stationary there is no time update. $\boldsymbol{P}_{k|k}$ is the covariance matrix of the state estimate.

Measurement Update Step:

$$\hat{\boldsymbol{x}}_{k+1|k+1} = \hat{\boldsymbol{x}}_{k+1|k} + \boldsymbol{K}_{k+1}\left(\boldsymbol{y}_{k+1} - \boldsymbol{h}_{k+1}\left(\hat{\boldsymbol{x}}_{k+1|k}\right)\right) \tag{2-40}$$

$$\boldsymbol{K}_{k+1} = \boldsymbol{P}_{k+1|k}\boldsymbol{H}_{k+1}^{T}\left(\boldsymbol{H}_{k+1}\boldsymbol{P}_{k+1|k}\boldsymbol{H}_{k+1}^{T} + \boldsymbol{R}_{k+1}\right)^{-1} \tag{2-41}$$

$$\boldsymbol{P}_{k+1|k+1} = (\boldsymbol{I} - \boldsymbol{K}_{k+1}\boldsymbol{H}_{k+1})\boldsymbol{P}_{k+1|k} \tag{2-42}$$

where $\boldsymbol{R}_k$ is the covariance matrix of the measurement noise and $\boldsymbol{K}_{k+1}$ is the Kalman gain. In the analyzed problem, since measurement noise is not changing with time, the sub index *k* may be removed. Covariance matrix of the initial position estimate $\left(\boldsymbol{P}_{0|0}\right)$ is required in the algorithm. The covariance matrix of the algorithm which is used to find the initial target estimate is used as $\boldsymbol{P}_{0|0}$. Then the matrix is updated with measurement update step as seen above. The cycle of EKF is seen in Figure 2-3.

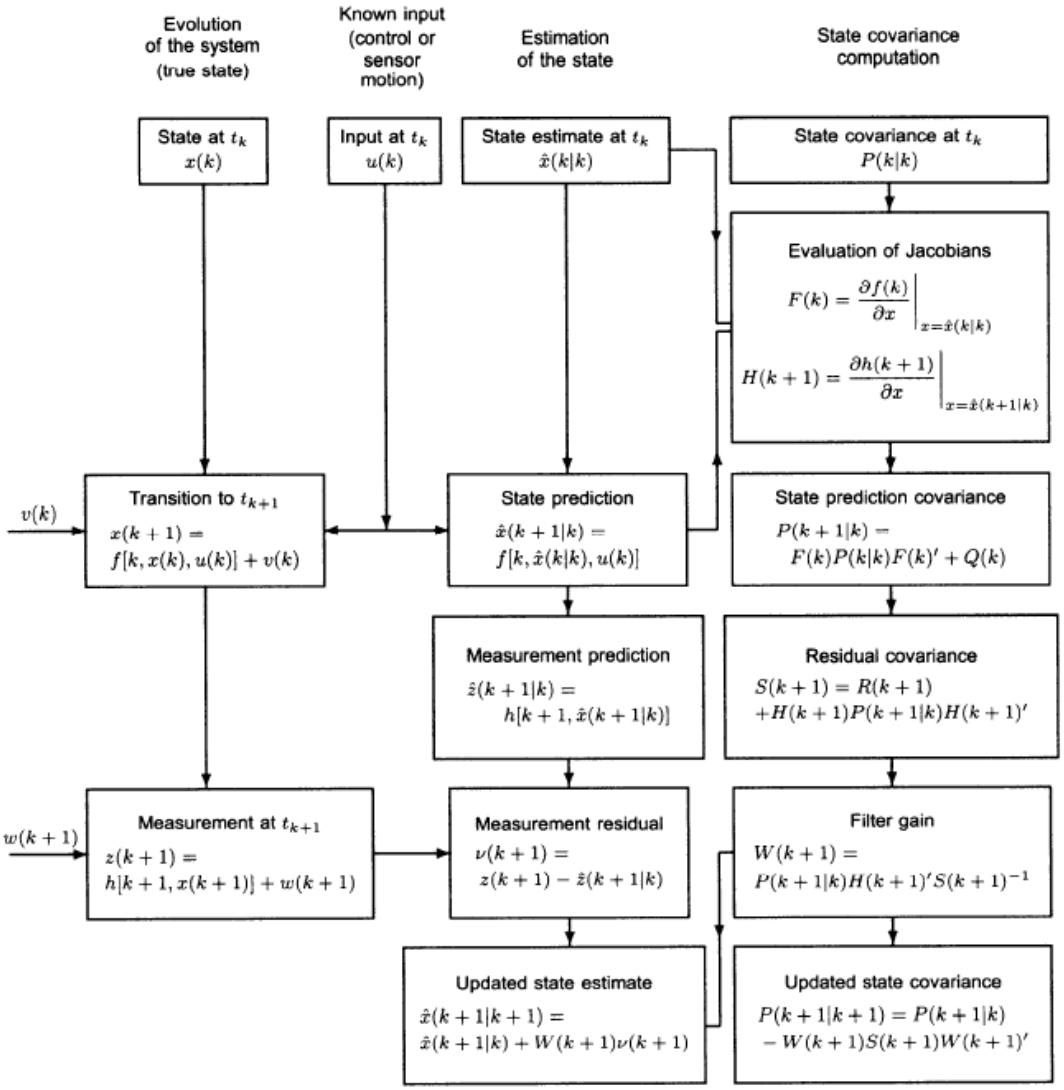

Figure 2-3 : Cycle of EKF [29]

In emitter localization problem the state is target position and the measurement vector consists of azimuth and elevation angles.

$$\boldsymbol{x}_k = \begin{bmatrix} x_P \\ y_P \\ z_P \end{bmatrix} \quad \boldsymbol{y}_k = \begin{bmatrix} \theta_k \\ \phi_k \end{bmatrix} \tag{2-43}$$

$$\boldsymbol{x}_{k+1} = \boldsymbol{x}_k \tag{2-44}$$

$$\boldsymbol{y}_k = h_k(\boldsymbol{x}_k) + \boldsymbol{v}_k \tag{2-45}$$

The linearization of the measurement model is done by calculating the gradient of the measurements vector with respect to the state variables which are coordinates of the target. The calculation of $\boldsymbol{H}_k$ matrix is same as the calculation of Jacobian matrix in MLE which is given in Section 2.4.4.

To sum up, in recursive position estimation with EKF, first *K* measurements are taken and an initial position estimate is obtained. Then with new measurements the position estimate is updated without the necessity of storing old measurements. Only the current estimate and the new measurements are used.

2.5 Error Ellipsoids

In emitter localization problems, algorithm performances depend on the geometry between emitter and the platform positions. For bearing-only localization algorithms, the measured angle measurements should differ from each other for a good estimate. If the difference between angles is too small, then the DF lines will be parallel to each other, and the lines can intersect at far from the true target position.

While implementing a localization algorithm, analyzing the emitter-target geometry is useful. For 3D problem, which is the case analyzed in this thesis, an error ellipsoid is used for this purpose. The error ellipsoid around the true target position represents the area that the target estimate will lie with a defined probability. For example a %90 error ellipsoid around the true target position will include the target estimate which is estimated by an unbiased estimator with a 0.9 probability. By using error ellipsoids, one can comment on which target position, the estimator performs better. A smaller error ellipsoid means estimator accuracy is better.

An error ellipsoid can be drawn around the estimated target position instead of actual target position. This ellipsoid represents the area where the true target lies with P probability. Ellipsoid around the true target position and the target estimate are similar concepts. Both represents an area that the target or estimate will lie. The only difference is the covariance matrix which is used to compute the ellipsoid parameters. If ellipsoid is drawn around position estimate, the covariance matrix of the estimate is used. In this thesis the error ellipsoid around true target position is analyzed. So the CRLB matrix which is calculated at the actual target position is used.

In 2D error ellipses, in 3D error ellipsoids are used. For higher dimensions hyperellipsoids are used but they are hard to visualize. In that case slice or projection of the hyperellipsoid can be used for desired parameters. Details of these concepts will be given in this chapter.

2.5.1 Calculating the Ellipsoid Parameters

The aim is to obtain the smallest error ellipsoid around the true target position which an unbiased estimator can achieve. For this purpose CRLB matrix is used to compute the ellipsoid parameters. Let the parameters which are desired to be estimated are represented by vector $\boldsymbol{x}$. Then the measured parameters (e.g. angle, phase, time of arrival) are a function of the vector $\boldsymbol{x}$. These parameters are modeled by adding Gaussian noise on the actual value. For time t_i, the data vector is

$$\tilde{f}(t_i, \boldsymbol{x}) = f(t_i, \boldsymbol{x}) + n(t_i) \tag{2-46}$$

In this case where N measurements are taken, the data vector used to estimate the desired parameters is defined as,

$$\tilde{f}(x) = \left[\tilde{f}(t_1, x)\ \tilde{f}(t_2, x)\ \ldots\ \tilde{f}(t_N, x)\right]^T \tag{2-47}$$

The data vector is distributed according to $\tilde{f}(x) = \mathcal{N}(f(x), \boldsymbol{C})$ where $\boldsymbol{C}$ is the covariance matrix of the zero-mean Gaussian noise. To calculate CRLB matrix, first Fisher Information Matrix (FIM) is calculated with the following equation:

$$FIM = \boldsymbol{J} = \boldsymbol{H}^T \boldsymbol{C}^{-1} \boldsymbol{H} \tag{2-48}$$

where $\boldsymbol{H}$ matrix is defined as

$$\boldsymbol{H} = \frac{\partial}{\partial x} f(t, \boldsymbol{x})\Big|_{x=true\ value} = \left[\boldsymbol{h}_1 | \boldsymbol{h}_2 | \ldots | \boldsymbol{h}_{n_p}\right] \tag{2-49}$$

$$\boldsymbol{h}_j = \begin{bmatrix} \frac{\partial}{\partial x_j} f(t_1, \boldsymbol{x}) \\ \frac{\partial}{\partial x_j} f(t_2, \boldsymbol{x}) \\ \vdots \\ \frac{\partial}{\partial x_j} f(t_N, \boldsymbol{x}) \end{bmatrix} \tag{2-50}$$

In the equations n_p represents the number of the estimated parameters.

Thus, for a given "emitter-platform geometry", it is possible to compute $\boldsymbol{H}$ matrix and then use it to compute the CRLB covariance matrix, from which an eigen-analysis can be done [30]. CRLB is the inverse of the FIM

$$\boldsymbol{C}_{\boldsymbol{CRLB}}(\boldsymbol{x}) = \boldsymbol{J}^{-1} = [\boldsymbol{H}^T \boldsymbol{C}^{-1} \boldsymbol{H}]^{-1} \tag{2-51}$$

After CRLB matrix is derived, the ellipsoid parameters can be calculated. Principle axes and principle axes lengths are required to define an ellipsoid completely. The principle axes are determined from eigenvectors and lengths of the axes are determined from eigenvalues. In Figure 2-4, parameters of an ellipse are shown for simplicity instead of an ellipsoid. The relation between eigenvalues, eigenvectors and ellipse parameters is given on figure. The eigenvalues of the CRLB matrix are represented by λ_1 and λ_2 , eigenvectors are represented by v_1 and v_2 respectively.

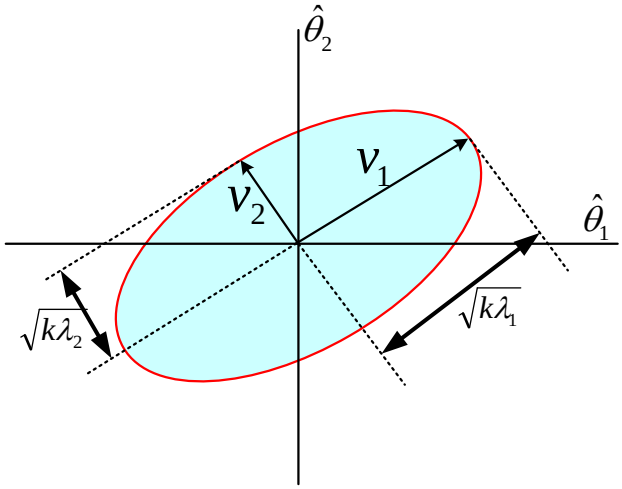

Figure 2-4: Error ellipse parameters

The off-diagonal elements of the CRLB matrix determine the tilt angles of the ellipsoid. Location accuracy characteristics depend on the CRLB structure. In Figure 2-5 scatter plots for the estimated target location is seen for 2D. Although each case has the same variances, the first one's CRLB matrix has off-diagonal terms different form the second one, so ellipses are not aligned with the axes. Since $\hat{x}_e$ and $\hat{y}_e$ are correlated, the ellipses are tilted. Location accuracy characteristics are very different.

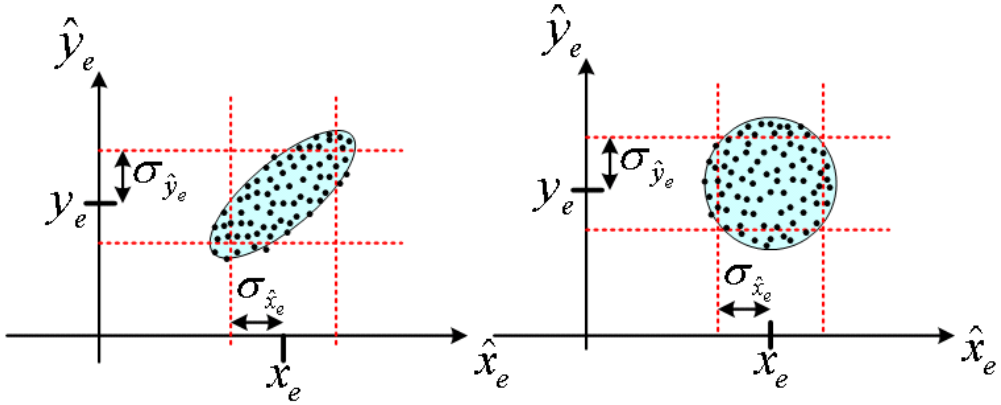

Figure 2-5: The effect of off-diagonal elements of CRLB matrix

For creating error ellipsoid, eigenvectors and eigenvalues of the 3x3 CRLB matrix are used. Ellipsoid axes are aligned with the three eigenvectors. Axes lengths are square root of the eigenvectors multiplied with a *k* term. This *k* term takes different values according to the probability *P* indicated by the ellipsoid. As explained before *P* value is the probability that the estimate will lie in the ellipsoid. The larger the *P* value is, bigger the ellipsoid is. Most common values of *P* are 0.9 and 0.95. According to *P* value, *k* value and consequently axes lengths of the ellipsoid are changed. For calculating the *k* value, the following property is used:

Given n-dimensional Gaussian random vector $\boldsymbol{x}$*, with mean* $\boldsymbol{m_x}$ *and covariance matrix* $\boldsymbol{\Sigma_x}$ *, the scalar random variable k defined by the quadratic form*

$$[\boldsymbol{x} - \boldsymbol{m_x}]^T \boldsymbol{\Sigma}_{\mathrm{X}}^{-1} [\boldsymbol{x} - \boldsymbol{m_x}] = k \tag{2-52}$$

has a chi-square distribution with n degrees of freedom [31].

In the emitter localization problem $\boldsymbol{m_x}$ is the true target position, $\boldsymbol{\Sigma_x}$ is the CRLB matrix. This equation defines an n-dimension hyperellipsoid.

The probability that the scalar random variable *k* is less than or equal to a given constant, (χ_P^2)

$$Pr\{k \leq \chi_P^2\} = Pr\{[\boldsymbol{x} - \boldsymbol{m_x}]^T \boldsymbol{\Sigma}_{\mathrm{X}}^{-1} [\boldsymbol{x} - \boldsymbol{m_x}] \leq \chi_P^2\} = P \tag{2-53}$$

is given in the following table where *n* is the number of degrees of freedom [31].

Table 1: Chi-square values

n	$\chi^2_{0.995}$	$\chi^2_{0.99}$	$\chi^2_{0.975}$	$\chi^2_{0.95}$	$\chi^2_{0.90}$	$\chi^2_{0.75}$	$\chi^2_{0.50}$	$\chi^2_{0.25}$	$\chi^2_{0.10}$	$\chi^2_{0.05}$
1	7.88	6.63	5.02	3.84	2.71	1.32	0.455	0.102	0.0158	0.0039
2	10.6	9.21	7.38	5.99	4.61	2.77	1.39	0.575	0.211	0.103
3	12.8	11.3	9.35	7.81	6.25	4.11	2.37	1.21	0.584	0.352
4	14.9	13.3	11.1	9.49	7.78	5.39	3.36	1.92	1.06	0.711

According to the Table 1, for 3D problem, k value is 6.25 for %90 error ellipsoid. So principle axes are square root of 6.25 times eigenvalues.

2.5.2 Slice of Error Ellipsoid

After creating the error ellipsoid, a slice of the ellipsoid can be taken on the desired surface. For hyperellipsoids which are hard to visualize, desired estimated parameters can be chosen and the error ellipse (for 2 parameters) or error ellipsoid (for 3 parameters) can be obtained. Also the projection of the ellipsoid can be taken. At this point, it is important not to confuse slice and projection. In Figure 2-6, the distinction is seen for an ellipse:

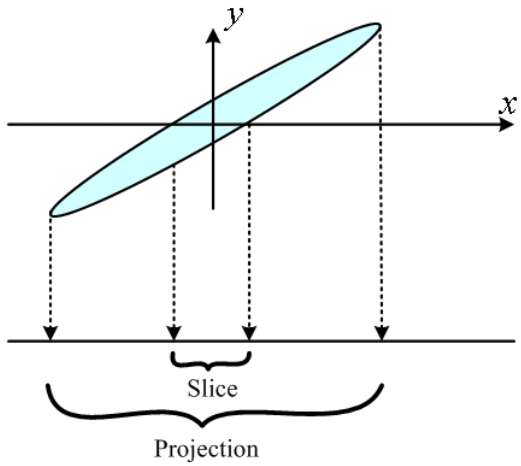

Figure 2-6 : Comparison of slice and projection

Same projection matrix is used for taking slice and projection on the surface. It is a matrix where each row has a single one in it at the location of one of the parameters that remains in desired subspace. For example, in a case where x, y and z coordinates of a target is estimated, for taking a slice over x-y surface, the projection matrix is defined as follows:

$$\boldsymbol{P} = \begin{bmatrix} 1 & 0 & 0 \\ 0 & 1 & 0 \end{bmatrix} \tag{2-54}$$

By using this matrix, the new CRLB matrix is obtained:

$$\boldsymbol{C}_{CRLB,slice} = (\boldsymbol{P}\boldsymbol{C}_{CRLB}^{-1}\boldsymbol{P}^T)^{-1} \tag{2-55}$$

By using the 2x2 $\boldsymbol{C}_{CRLB,slice}$ matrix, the ellipse parameters are calculated as explained in 2.5.1. While calculating ellipse parameters, the same "*k*" value which is used while calculating ellipsoid parameters is used.

2.5.3 Projection of Error Ellipsoid

The projection of error ellipsoid can be taken on desired surface. This provides convenience while analyzing the results. The projected CRLB matrix is obtained as follows:

$$\boldsymbol{C}_{CRLB,proj} = \boldsymbol{P}\boldsymbol{C}_{CRLB}\boldsymbol{P}^T \tag{2-56}$$

2.6 Error Ellipsoid for Bearing-Only Localization

In bearing-only localizations the measurements are azimuth and elevation angles. So the $\boldsymbol{H}$ matrix defined in Section 2.5.1 is calculated by using these measurements. The azimuth and elevation angles are defined in Equations (2-2) and (2-3).

For the case where N measurements are taken, the data vector is a $2Nx1$ vector which consists of N azimuth and N elevation angles.

$$f(\boldsymbol{p}) = [f_1^T(\boldsymbol{p})\ \ f_2^T(\boldsymbol{p})]^T \tag{2-57}$$

$$f_1(\boldsymbol{p}) = [\theta_1 \quad \theta_2 \quad \dots \quad \theta_N]^T \tag{2-58}$$

$$f_2(\boldsymbol{p}) = [\phi_1 \quad \phi_2 \quad \dots \quad \phi_N]^T \tag{2-59}$$

The $\boldsymbol{H}$ matrix is calculated as

$$H = \begin{bmatrix} \nabla_p f_1(p) \\ \nabla_p f_2(p) \end{bmatrix} = \begin{bmatrix} \frac{\partial f_1(p)}{\partial x_P} & \frac{\partial f_1(p)}{\partial y_P} & \frac{\partial f_1(p)}{\partial z_P} \\ \frac{\partial f_2(p)}{\partial x_P} & \frac{\partial f_2(p)}{\partial y_P} & \frac{\partial f_3(p)}{\partial z_P} \end{bmatrix} \tag{2-60}$$

where ∇ is the gradient operator.

The first N rows of $\boldsymbol{H}$ are partial derivatives of azimuth angles with respect to x, y and z coordinates of the target which are calculated as:

$$\frac{\partial f_1(p)}{\partial x_P} = \begin{bmatrix} \frac{-(y_P - y_1)}{(x_P - x_1)^2\left(\frac{(y_P - y_1)^2}{(x_P - x_1)^2} + 1\right)} \\ \frac{-(y_P - y_2)}{(x_P - x_2)^2\left(\frac{(y_P - y_2)^2}{(x_P - x_2)^2} + 1\right)} \\ \vdots \\ \frac{-(y_P - y_N)}{(x_P - x_N)^2\left(\frac{(y_P - y_N)^2}{(x_P - x_N)^2} + 1\right)} \end{bmatrix} \tag{2-61}$$

$$\frac{\partial f_1(p)}{\partial y_P} = \begin{bmatrix} \frac{1}{(x_P - x_1)\left(\frac{(y_P - y_1)^2}{(x_P - x_1)^2} + 1\right)} \\ \frac{1}{(x_P - x_2)\left(\frac{(y_P - y_2)^2}{(x_P - x_2)^2} + 1\right)} \\ \vdots \\ \frac{1}{(x_P - x_N)\left(\frac{(y_P - y_N)^2}{(x_P - x_N)^2} + 1\right)} \end{bmatrix} \tag{2-62}$$

$$\frac{\partial f_1(p)}{\partial z_P} = 0_{Nx1} \tag{2-63}$$

In a similar way, the derivatives of the elevation angles are taken and the second N rows of $\boldsymbol{H}$ matrix are obtained,

$$\frac{\partial f_2(p)}{\partial x_P} = \begin{bmatrix} \dfrac{-(x_P - x_1)(z_P - z_1)}{\|p - r_1\|^2 \sqrt{(x_P - x_1)^2 + (y_P - y_1)^2}} \\ \dfrac{-(x_P - x_2)(z_P - z_2)}{\|p - r_2\|^2 \sqrt{(x_P - x_2)^2 + (y_P - y_2)^2}} \\ \vdots \\ \dfrac{-(x_P - x_N)(z_P - z_N)}{\|p - r_N\|^2 \sqrt{(x_P - x_N)^2 + (y_P - y_N)^2}} \end{bmatrix} \tag{2-64}$$

$$\frac{\partial f_2(p)}{\partial y_P} = \begin{bmatrix} \dfrac{-(y_P - y_1)(z_P - z_1)}{\|p - r_1\|^2 \sqrt{(x_P - x_1)^2 + (y_P - y_1)^2}} \\ \dfrac{-(y_P - y_2)(z_P - z_2)}{\|p - r_2\|^2 \sqrt{(x_P - x_2)^2 + (y_P - y_2)^2}} \\ \vdots \\ \dfrac{-(y_P - y_N)(z_P - z_N)}{\|p - r_N\|^2 \sqrt{(x_P - x_N)^2 + (y_P - y_N)^2}} \end{bmatrix} \tag{2-65}$$

$$\frac{\partial f_2(p)}{\partial z_P} = \begin{bmatrix} \dfrac{\sqrt{(x_P - x_1)^2 + (y_P - y_1)^2}}{\|p - r_1\|^2} \\ \dfrac{\sqrt{(x_P - x_2)^2 + (y_P - y_2)^2}}{\|p - r_2\|^2} \\ \vdots \\ \dfrac{\sqrt{(x_P - x_N)^2 + (y_P - y_N)^2}}{\|p - r_N\|^2} \end{bmatrix} \tag{2-66}$$

The covariance matrix of the measurements is defined as

$$\boldsymbol{C} = diag\{\sigma_{\theta_1}^2, \sigma_{\theta_2}^2, \dots, \sigma_{\theta_N}^2, \sigma_{\phi_1}^2, \sigma_{\phi_2}^2, \dots, \sigma_{\phi_N}^2\} \tag{2-67}$$

By using the calculated $\boldsymbol{H}$ matrix and the above covariance matrix, FIM and CRLB matrices are computed as in Equations (2-48) and (2-51). By using CRLB matrix, ellipsoid parameters are calculated as explained in Section 2.5.1. The slice and projection of the ellipsoid can be taken as explained in Sections 2.5.2 and 2.5.3.

In Figure 2-7, there is an illustration of the *P=0.9* error ellipsoid. The target lies at $(0,0,0)$ and the platform flies through a straight path. The standard deviations of azimuth and elevation angles are $\sigma = 0.5^{\circ}$. The center of the ellipsoid is the true target position. 100 Monte Carlo simulations are run for the ML estimator and the estimates are seen on the figure.

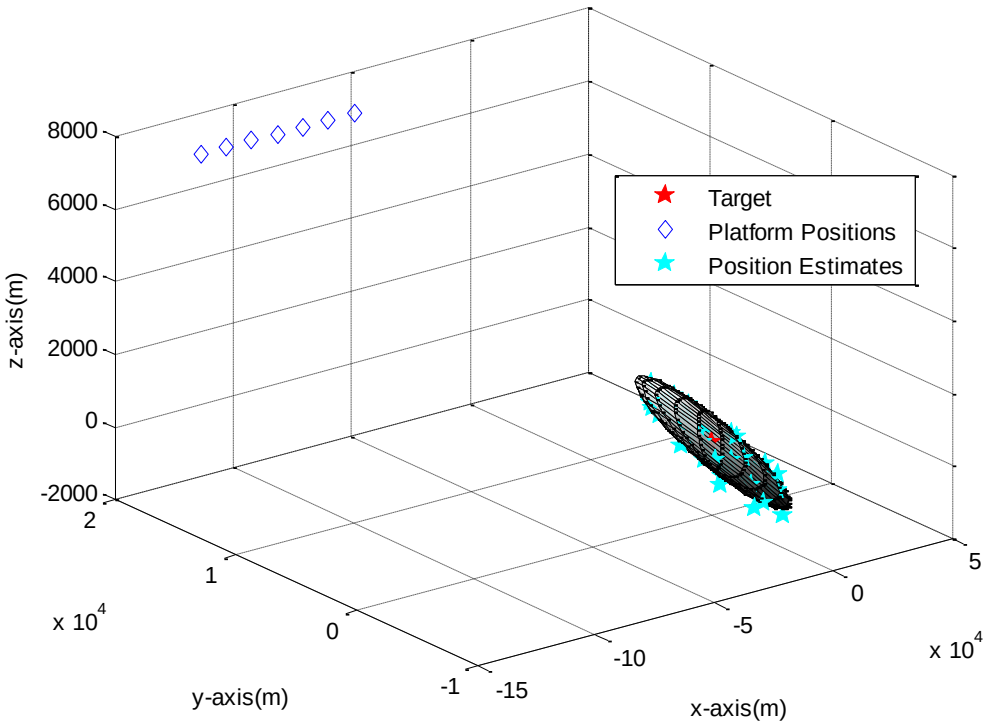

Figure 2-7 : Error ellipsoid around true target position

The zoomed version of the error ellipsoid is in Figure 2-8. As seen from the figure, most of the estimates are in the 0.9 error ellipsoid (nearly %90 of the estimates)

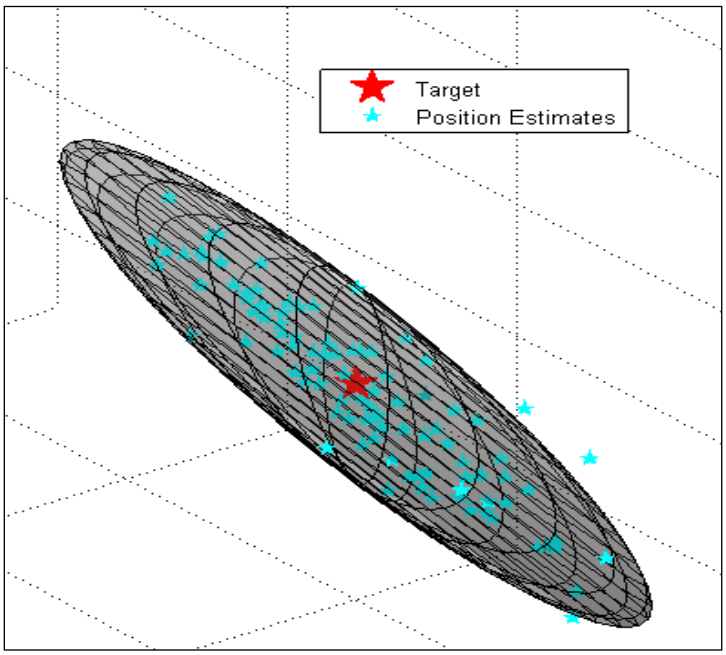

Figure 2-8 : Error ellipsoid and the position estimates

In the scenario examined above, no information is available about the target position. If there was information that the target's z coordinate is zero $(z_P = 0)$ and only x and y coordinates of the target are estimated, this would be a different case. The error ellipsoid for the case of not estimating a parameter is found by taking a slice through the full-parameter error ellipsoid with the plane defined by setting the eliminated error variable to zero [13]. In Figure 2-9 the case of knowing z coordinate of the target is analyzed. The slice of the ellipsoid and the estimates are seen on the figure. The estimates are found by moving forward the 3D estimates along the direction of ellipsoid and intersect with $z = 0$ plane.

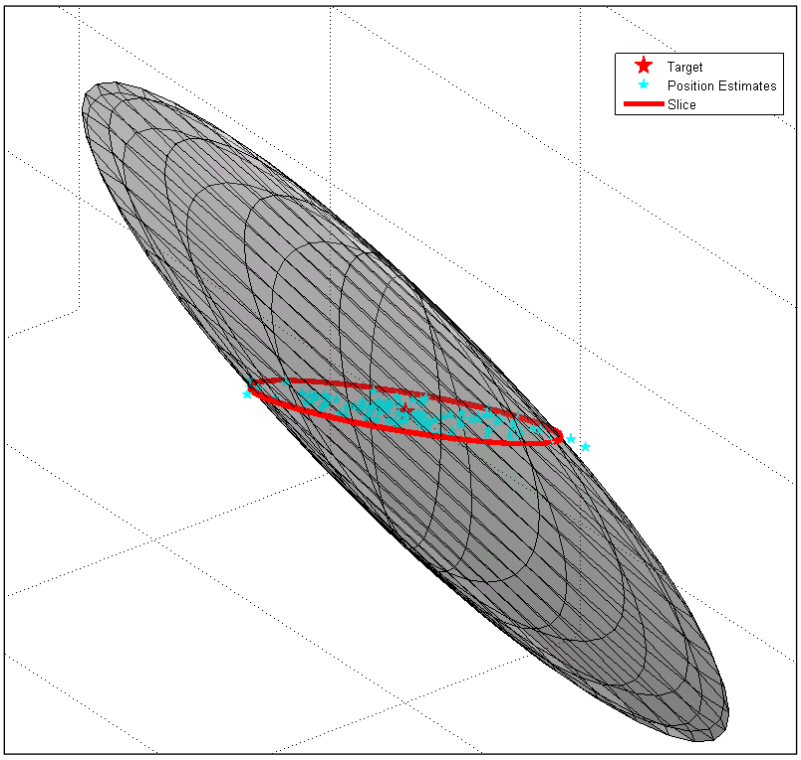

Figure 2-9 : Slice of the error ellipsoid (known $z_P = 0$)

By using the error ellipsoids, the effect of target-platform geometry on accuracy can be observed. In Figure 2-10 the error ellipsoids for different target positions are plotted. The smaller is the ellipsoid, the better is the accuracy.

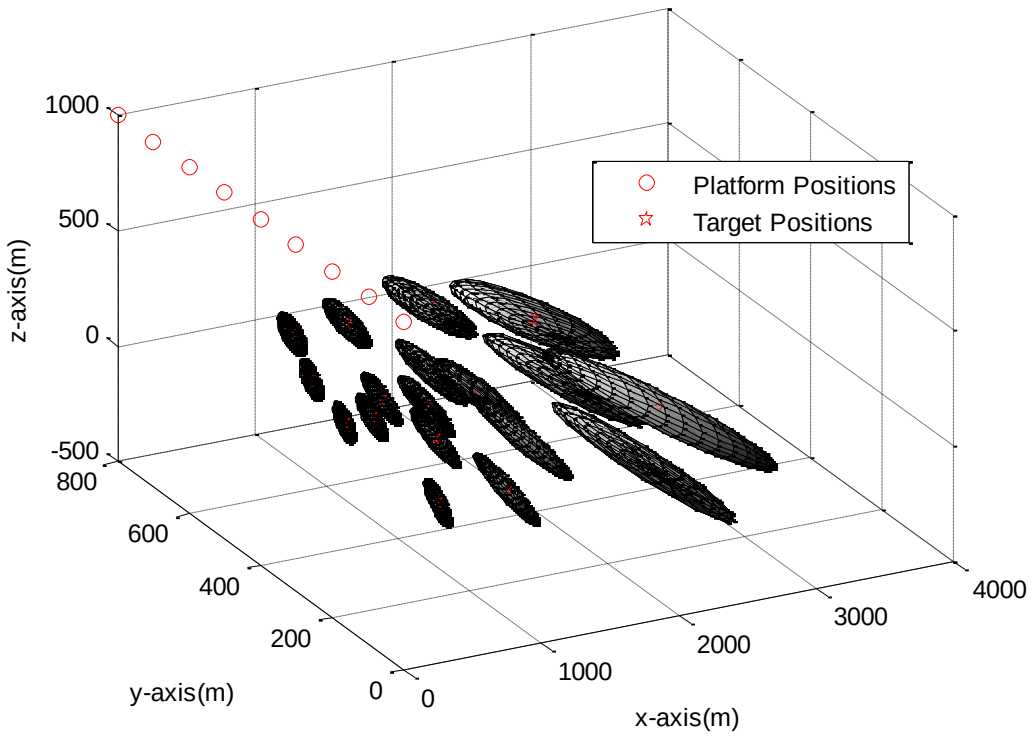

Figure 2-10 : Error ellipsoids for different target locations

By taking the projection of the above error ellipsoids on x-y plane, the effect of geometry can be observed better. In Figure 2-11 projection of the ellipsoids can be seen.

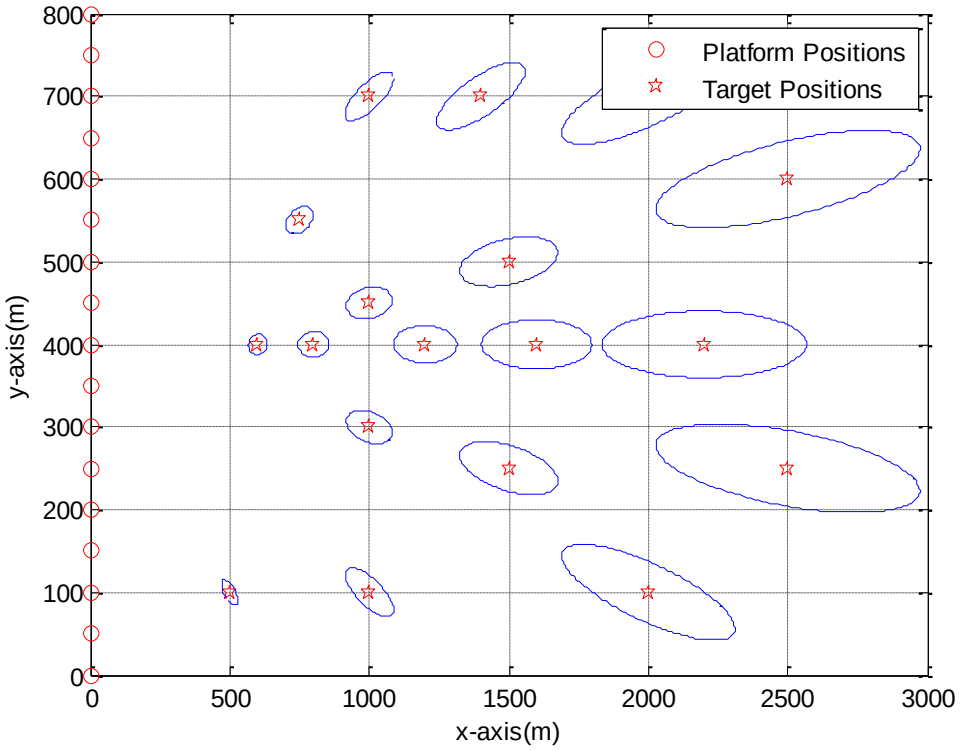

Figure 2-11 : Projection of the error ellipsoids for different target positions

In Figure 2-10 and Figure 2-11 the effect of geometry on accuracy can be observed easily. As target distance increases, the accuracy degrades. Another observation is that as the difference between measured angles increases, the accuracy gets better. It is seen that as target gets closer to $y = 400$, ellipses get smaller. For targets which lie on same $x = k$ plane, the maximum azimuth angle change between measurements occurs at $y = 400$ for above scenario.

2.7 Simulation Results

In this section, performances of the bearing-only localization algorithms are compared for different scenarios. In the simulations, the target position is $(x_P, y_P, z_P) = (4000,3000,0)$. The platform is traveling with a constant speed

$V = 100m/s$ and collects bearing measurements at every 10 seconds. Platform starts its path at $(x_1, y_1, z_1) = (0,0,2000)$ with a velocity vector in the direction of $\theta = 90$ and $\phi = 0$. After collecting 4 measurements, velocity vector changes in the direction of $\theta = 45$ and $\phi = -5$. 4 measurements are taken along this path and the velocity vector changes to the direction $\theta = 310$ and $\phi = 0$ and collects 4 more measurements. The scenario is as shown in Figure 2-12.

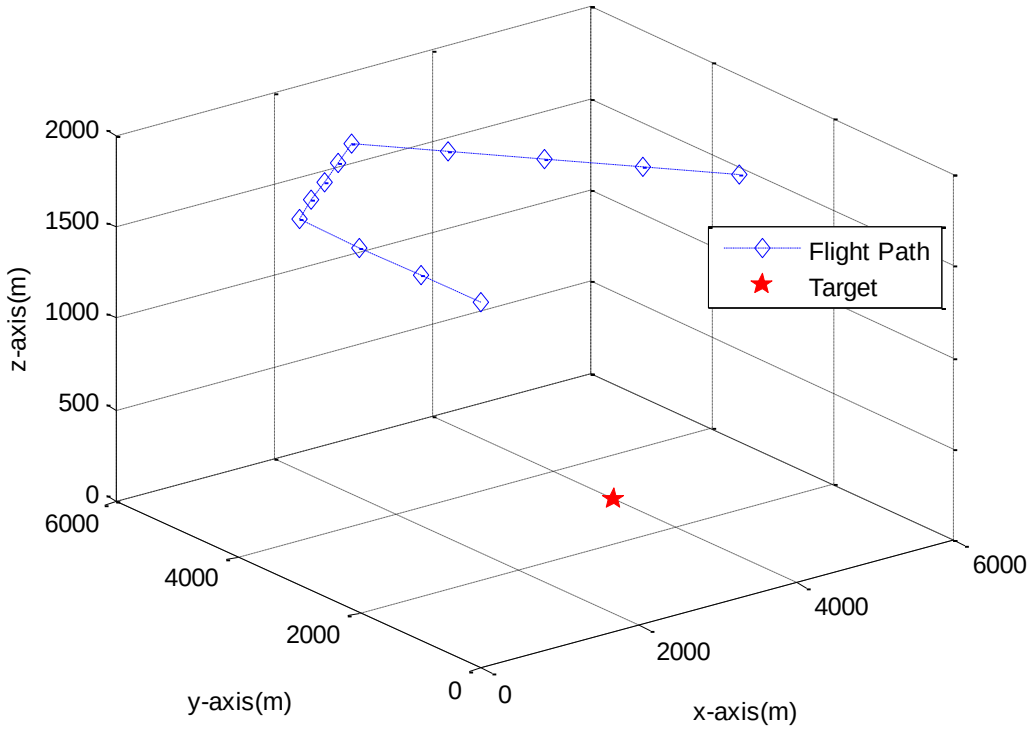

Figure 2-12 : Scenario used in the simulations

In the simulations, the performances are compared with CRLB which is the minimum achievable error. The derivations of CRLB matrix were given in Section 2.6. The 3x3 CRLB matrix contains the axial minimum achievable variances on its diagonals and the trace of the CRLB matrix gives the minimum achievable localization variance [27].

$$diag(CRLB) = \left\{\sigma_{x_P}^2, \sigma_{y_P}^2, \sigma_{z_P}^2\right\} \tag{2-68}$$

$$\sigma_P^2 = trace(CRLB) \tag{2-69}$$

Simulation results are obtained by running 1000 Monte Carlo runs and the RMS errors are calculated. Results are compared for four different algorithms which are OVE, PLE, WIVE and MLE for different standard deviation values. In MLE, the estimates obtained in WIVE are used as initial estimates. Performance analyses are also done for WIVE2 algorithm.

In the first scenario, both azimuth and elevation angle errors have the same standard deviation values which are changing between 0.5° and 5°. The results are seen in Figure 2-13. It is observed that OVE has the worst; MLE has the best performance among all algorithms. MLE performance is very close to the CRLB. Another important point is that WIVE has a significant improvement over PLE and OVE. Since it is a closed form estimator, its computational complexity is much lower than MLE. So in systems where low complexity of implementation is an important consideration, WIVE would be a reasonable choice. WIVE and WIVE2 have approximately the same performances. There is a slight improvement in WIVE2 method's accuracy. So it can be concluded that updating the instrumental variable matrix is not useful.

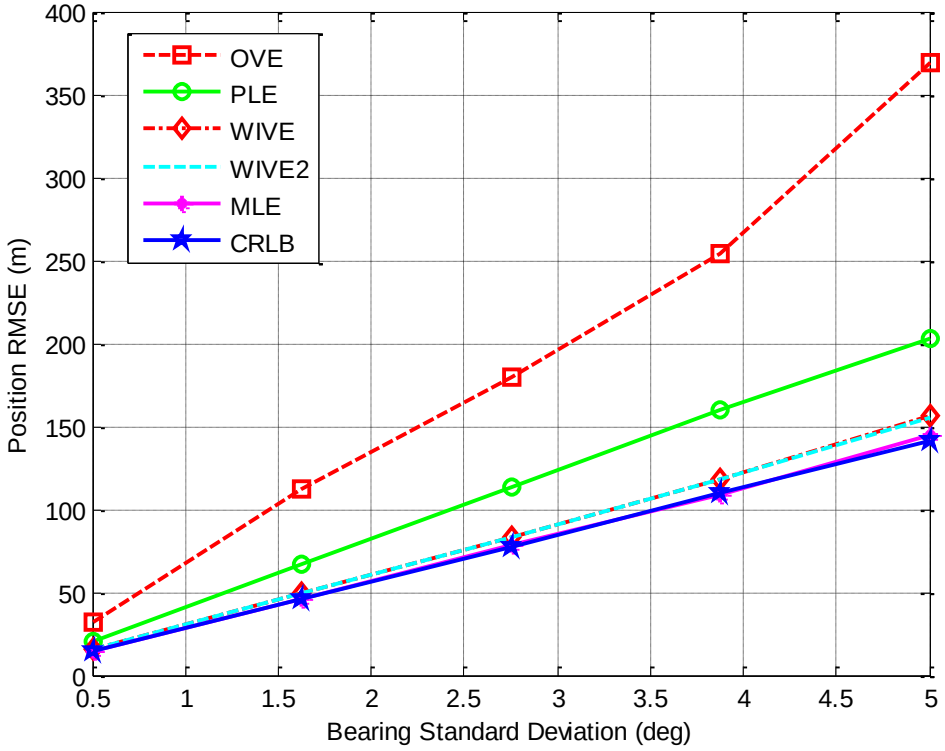

Figure 2-13 : Performance comparison of bearing-only localization algorithms for $\sigma_\theta = \sigma_\phi$ case

To see the effect of azimuth and elevation errors individually, two scenarios are analyzed. In the first one, elevation deviation is fixed to 3° and only azimuth deviation is changed between 0.5° and 5°. In the second scenario azimuth deviation is fixed to 3° and elevation deviation is changed between 0.5° and 5° . The results are in Figure 2-14 and Figure 2-15 respectively.

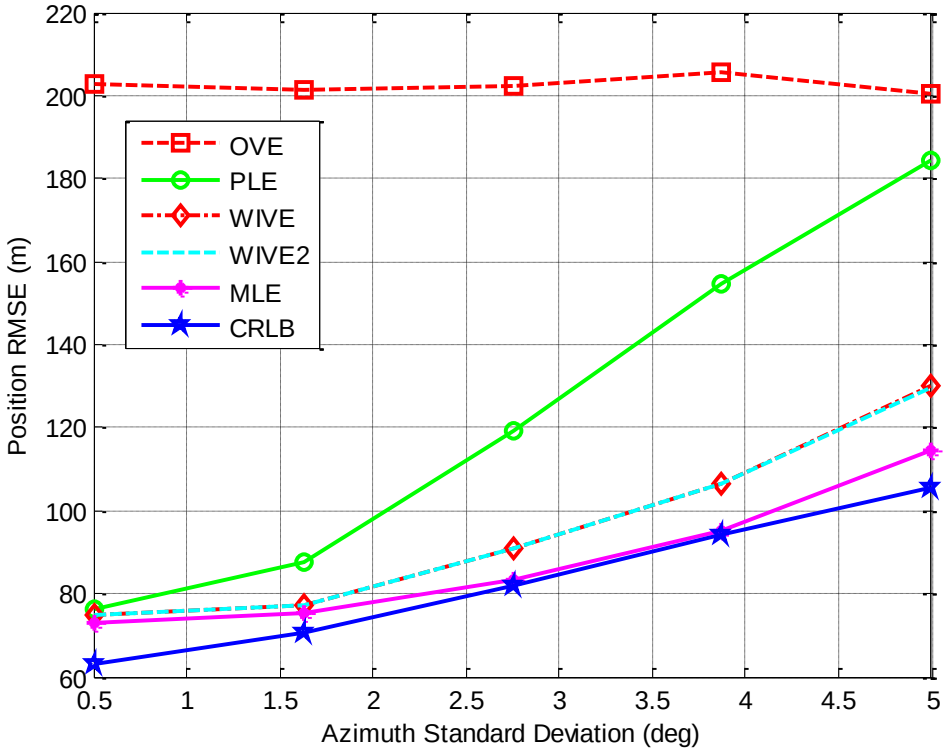

Figure 2-14: Performance comparison of bearing-only localization algorithms for fixed $\sigma_\phi = 3^\circ$ case

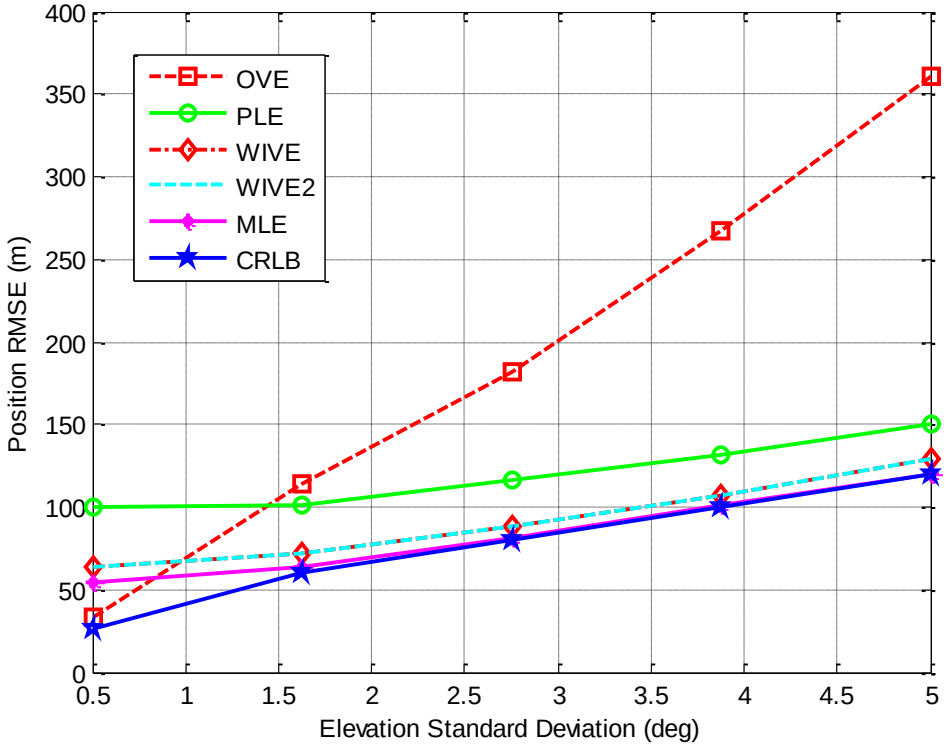

Figure 2-15 : Performance comparison of bearing-only localization algorithms for fixed $\sigma_\theta = 3^\circ$ case

In the above figures there is an interesting point that the performance of OVE changes only slightly with azimuth error. The main error source that affects the performance is the elevation error. When the noise vector $\boldsymbol{n}$ in OVE is written in explicit form and the values for different azimuth and elevation noises are calculated, it is observed that noise vector's elements change slightly with azimuth noise, but highly dependent to elevation noise.

Different from the above localization algorithms, recursive estimation by using EKF is analyzed. In this method, position is estimated with a few measurements and as new measurement arrives, position estimate is updated. In simulations the same flight path is used. First *K=3* measurements are used to find the initial position

estimate. Then, as new measurement arrives the position is updated. In below figures the x-axis represents the new measurement number. $N=3+9=12$ measurements are used as in the above scenarios. Simulation results are obtained by running 100 Monte Carlo runs. The RMS of the position error is calculated for each update time. As seen in Figure 2-16 and Figure 2-17, as new measurement arrives the position error gets smaller.

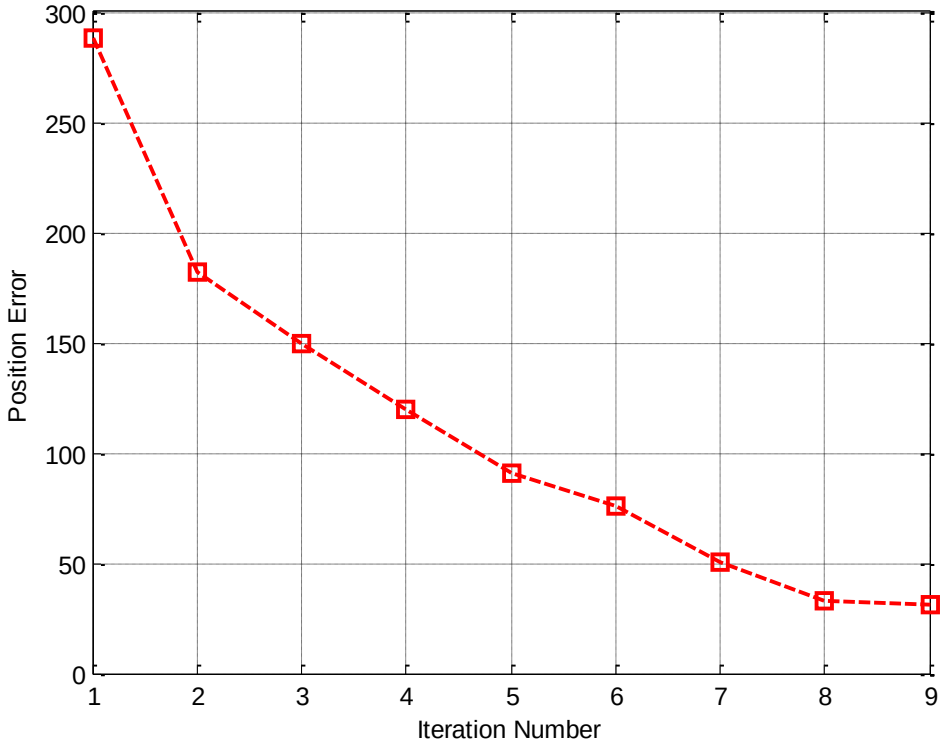

Figure 2-16 : RMS error of recursive estimator as new measurement arrived for $\sigma_\theta = \sigma_\phi = 1^o$ case

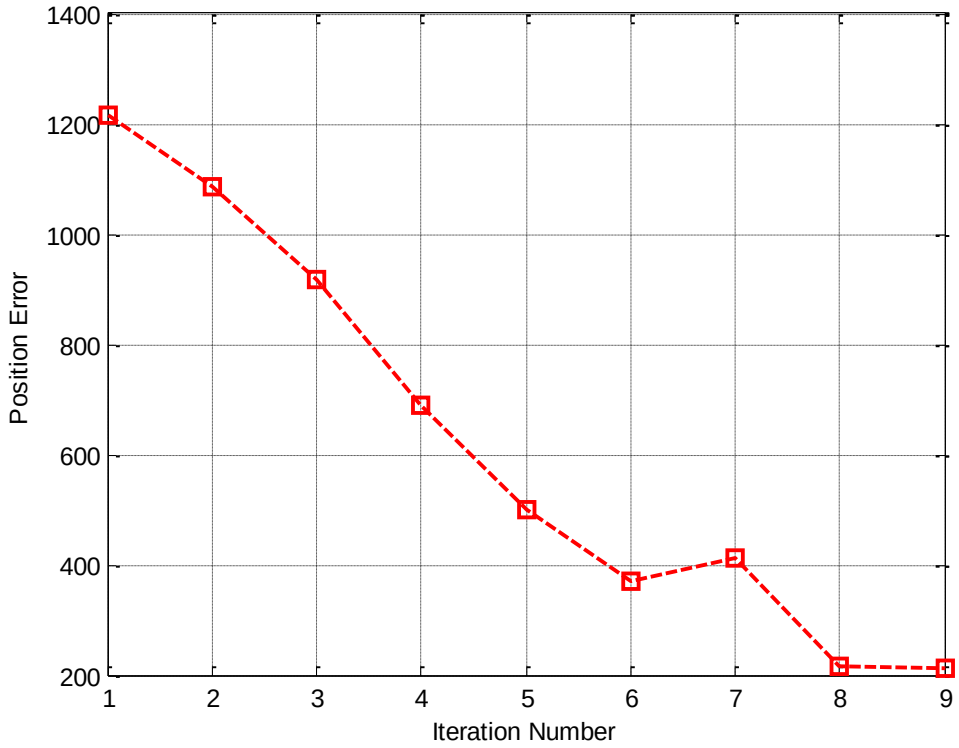

Figure 2-17 : RMS error of recursive estimator as new measurement arrived for $\sigma_\theta = \sigma_\phi = 3^o$ case

When the performance of the recursive estimator is compared with other algorithms, it is seen that collecting all measurements and using all of them in the algorithm at the same time has better performance than the recursive estimator. On the other hand, these algorithms need more memory and time to calculate the estimate. Recursive estimator stores only the current estimate and the measurement at that moment.

CHAPTER 3

LOCALIZATION ALGORITHMS USING DOPPLER FREQUENCY SHIFT

3.1 General Information

In this thesis, a moving platform such as a plane or UAV is considered to estimate the position of a stationary RF transmitter. When there is relative motion between the emitter (target) and the receiver (platform), the measured frequencies by the receiver will differ from the original emitted frequency. These frequencies which are different from the actual frequency are called Doppler-shifted frequencies (DSF). In localization algorithms based on DSF, the measured frequencies from target, platform positions and velocities are used as input to the algorithm and target position and the frequency of the emitted signal are estimated.

The measured DSFs depend on the emitter location and frequency. However relationship between them is non-linear. In the special case where the moving receiver measures frequencies along a straight path at constant speed, the relationship becomes linear [10]. By using this special case, location of the target and the transmitted frequency is estimated by a LS estimator. By using the LS estimate as initial estimate, ML estimates are obtained. Results are compared with the CRLB.

In the second part of the chapter, emitter localization by using both frequency and bearing measurements is analyzed. It is shown that the location methods based on bearing and frequency measurements differ significantly [11]. So combining these two methods lead to a significant performance improvement. In the rest of this section, the method where only frequencies are used will called as Doppler-Shifted Frequency (DSF) method, both bearings and frequencies are used will called as combined method (CM).

3.2 Frequency Estimation

Emitter localization by Doppler-shifted frequencies consists of two main steps. First, the platform estimates the Doppler-shifted frequencies and then by using these frequencies with an estimator, target position is estimated. Frequency estimation concept is out of scope of this thesis. However brief information about this concept will be given. In simulations, frequency estimates are obtained by adding zero mean Gaussian noise on the actual frequency values.

Several techniques can be used to estimate the frequency of a signal such as ML estimation, FFT-based techniques [32], *etc*. In FFT approach, center frequency of the bin which contains the most energy is used as frequency estimate. Step size of frequency spacing determines the accuracy of the estimation. As the size of the FFT increases, the performance gets better but this also increases computational complexity and needs larger memory. Zoom-FFT is another technique which deals with only the bins that contain most energy [33]. In [34], interpolation is done using bins adjacent to the maximum bin and avoids increasing the FFT size.

3.3 Problem Formulation

In DSF method, the problem is estimating the position of the stationary target which is represented by $\boldsymbol{p} = [x_P, y_P, z_P]^T$. The single moving platform takes N measurements along its path which consists of different straight line segments. The

platform position where the k^{th} measurement is taken is represented by $\boldsymbol{r_k} = [x_k, y_k, z_k]^T$ and the velocity of the platform at that point is represented by $\boldsymbol{V_k} = [\dot{x}_k, \dot{y}_k, \dot{z}_k]^T$. The target is transmitting a radar signal at an unknown carrier frequency f_0. Due to the relative motion between target and the moving platform, received carrier frequency is different from the transmitted carrier frequency. For different time instants, since the relative motion changes, the received carrier frequencies also change.

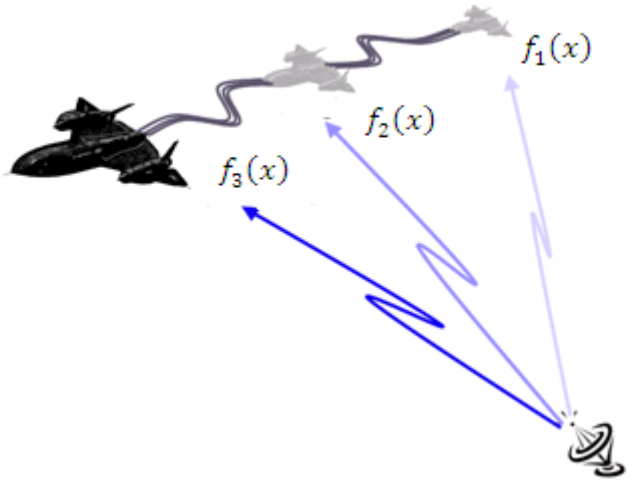

Figure 3-1: Measured frequencies at different points [30]

The received frequency depends on transmitter's carrier frequency f_0 and target's position $\boldsymbol{p} = [x_P, y_P, z_P]^T$. If these parameters are shown with a parameter vector, then the received frequencies are function of time and this parameter vector.

Parameter vector is given as $\boldsymbol{x} = [x_P\ y_P\ z_P\ f_0]^T$

The received frequency can be written as

$$f_k(\boldsymbol{x}) = f_0 + \frac{f_0}{c}\left[\frac{\dot{x}_k(x_k - x_P) + \dot{y}_k(y_k - y_P) + \dot{z}_k(z_k - z_P)}{\sqrt{(x_k - x_P)^2 + (y_k - y_P)^2 + (z_k - z_P)^2}}\right]$$
$$= f_0\left(1 + \frac{V cos\alpha_k}{c}\right) for\ k = 1, \dots, N \quad (3\text{-}1)$$

where V is the speed of the platform and c is the propagation speed. The angle between the platform's velocity vector and the vector from platform to emitter is represented by α_k. Since target position is not known, there is no information about this angle too.

The measured Doppler frequencies are created by adding zero mean, independent and identically distributed Gaussian noise (n_k) on the actual Doppler-shifted frequencies:

$$\tilde{f_k} = f_k + n_k\ , n_k \sim \mathcal{N}(0, \sigma^2) \quad (3\text{-}2)$$

The platform position and velocity at k^{th} time instant are shown by the following vectors

$$\vec{\boldsymbol{r}}_{\boldsymbol{k}} = x_k\vec{\boldsymbol{x}} + y_k\vec{\boldsymbol{y}} + z_k\vec{\boldsymbol{z}} \quad (3\text{-}3)$$

$$\vec{\boldsymbol{V}}_{\boldsymbol{k}} = \dot{x}_k\vec{\boldsymbol{x}} + \dot{y}_k\vec{\boldsymbol{y}} + \dot{z}_k\vec{\boldsymbol{z}} \quad (3\text{-}4)$$

The target position is represented by the following vector

$$\vec{\boldsymbol{p}} = x_p\vec{\boldsymbol{x}} + y_p\vec{\boldsymbol{y}} + z_p\vec{\boldsymbol{z}} \quad (3\text{-}5)$$

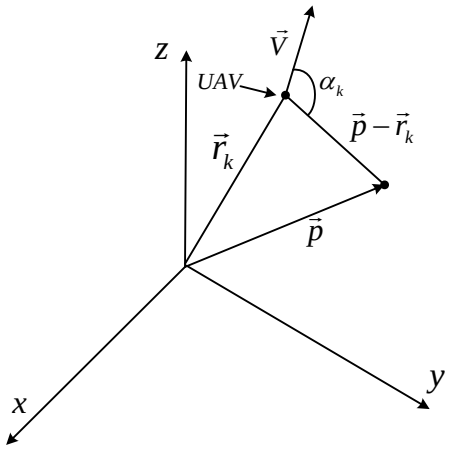

Figure 3-2 : Target and platform vectors

In emitter localization scenario, the moving platform is following a path which consists of different straight segments. In other words, the direction of the velocity vector changes. The direction of the velocity at k^{th} time instant may be represented by azimuth and elevation angles. Azimuth angle (θ_k) represents the angle between velocity vector and the x-axis, elevation angle (ϕ_k) represents the angle with respect to the x-y plane. The components of the velocity can be written as follows:

$$V_x = V cos\phi_k cos\theta_k$$
$$V_y = V cos\phi_k sin\theta_k \quad (3\text{-}6)$$
$$V_z = V sin\phi_k$$

where Vrepresents the speed of the moving platform.

3.4 Least Squares Estimator

In least squares method, a closed form estimate of the target position is obtained. Since the frequency of the emitted signal is not available, first 1-D discrete search is

done for frequency estimation, and then with LS estimator a coarse estimate of the emitter coordinates is obtained [10].

According to Figure 3-2 the inner product of velocity vector and the vector from target to emitter is:

$$\vec{\boldsymbol{V}}(\vec{\boldsymbol{p}} - \overrightarrow{\boldsymbol{r}_k}) = VR_k cos\alpha_k \tag{3-7}$$

$$R_k = |\vec{\boldsymbol{p}} - \overrightarrow{\boldsymbol{r}_k}| = \sqrt{(x_P - x_k)^2 + (y_P - y_k)^2 + (z_P - z_k)^2} \tag{3-8}$$

By substituting Equation (3-6) and Equation (3-8) into Equation (3-7) the following equation is obtained

$$R_k cos\alpha_k - m_k = b_k x_P + c_k y_P + d_k z_P \tag{3-9}$$

where b_k, c_k, d_k and m_k are defined as

$$b_k = cos\phi_k cos\theta_k \tag{3-10}$$

$$c_k = cos\phi_k sin\theta_k \tag{3-11}$$

$$d_k = sin\phi_k \tag{3-12}$$

$$m_k = -(x_k b_k + y_k c_k + z_k d_k) \tag{3-13}$$

In Figure 3-3, the platform is moving on a straight path, such that azimuth and elevation angles of the velocity vector are constant.

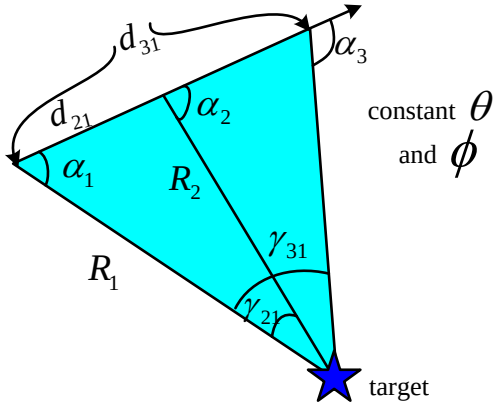

Figure 3-3: Non-manoeuvring path of the moving platform

According to Figure 3-3, the following equality can be written by applying the sine law, i.e,

$$\frac{d_{21}}{sin\gamma_{21}} = \frac{R_1}{sin\alpha_2} \tag{3-14}$$

$$\frac{d_{k1}}{sin\gamma_{k1}} = \frac{R_k}{sin\alpha_1} \; for\; k = 2,3,\dots N \tag{3-15}$$

d_{k1} represents the distance between platform position at *k=1* and *k=2,3,…N*. Also as seen from Figure 3-3 the angle γ_{k1} may be written as

$$\gamma_{k1} = \alpha_k - \alpha_1 \; for\; k \geq 2 \tag{3-16}$$

Combining the above equations results in

$$R_1 = \frac{d_{21} sin\alpha_2}{sin(\alpha_2 - \alpha_1)} \tag{3-17}$$

$$R_k = \frac{d_{k1} sin\alpha_1}{sin(\alpha_k - \alpha_1)} \; for \; k = 2, \dots, N \tag{3-18}$$

By writing Equation (3-9) for all measurements $k = 1,2, \dots N$ the following matrix equation is obtained

$$\boldsymbol{Ap} = \boldsymbol{b} \tag{3-19}$$

$$\boldsymbol{p} = \begin{bmatrix} x_P \\ y_P \\ z_P \end{bmatrix}, \boldsymbol{A} = \begin{bmatrix} b_1 & c_1 & d_1 \\ \vdots & \vdots & \vdots \\ b_N & c_N & d_N \end{bmatrix}, \boldsymbol{b} = \begin{bmatrix} R_1 cos\alpha_1 - m_1 \\ \vdots \\ R_N cos\alpha_N - m_N \end{bmatrix} \tag{3-20}$$

Then the LS solution for the target position is

$$\hat{\boldsymbol{p}} = (\boldsymbol{A}^T \boldsymbol{A})^{-1} \boldsymbol{A}^T \boldsymbol{b} \tag{3-21}$$

In this algorithm the important point is the measurement equation is linear in $\boldsymbol{p} = [x_P, y_P, z_P]^T$ for a fixed f_0 along a non-manoeuvring path of constant coarse and speed [10]. So the above equations are written for different non-manoeuvring path segments individually and then equations are combined as a matrix.

To find $\hat{\boldsymbol{p}}$ in Equation (3-21), the elements of $\boldsymbol{A}$ matrix and $\boldsymbol{b}$ vector should be known. However since α_k terms in $\boldsymbol{b}$ are not known, a 1D search algorithm is implemented over frequency and α_k values are calculated for each frequency in the search space.

Since the frequency of the emitted signal is unknown, a search over frequency is developed. The average of the measured frequencies is calculated $(\widetilde{f_a})$ and a range is defined for the search space, from $\widetilde{f_a} - \Delta$ to $\widetilde{f_a} + \Delta$. Δ is the maximum frequency shift and calculated as $\Delta \approx \widetilde{f_a} \frac{v}{c}$. Search starts from $\hat{f}_0 = \widetilde{f_a} - \Delta$ and by using Equation (3-1) $\alpha_k$values are calculated for *k=1,2,…,N*. Generated frequency values $(\tilde{f}_k)$ are used for f_k and $\hat{f}_0$ is used for f_0 in Equation (3-1). Then by using these calculated α_k values, R_k values are estimated with Equations (3-17) and

(3-18). Now all the elements of $\boldsymbol{b}$ matrix is available and by using Equation (3-21), LS estimate of target is obtained. For this position estimate, α_k and R_k values are re-calculated and predicted Doppler-shifted frequency $(\hat{f}_k)$ is found by using these values. Finally a cost function is evaluated which measures the difference between the predicted frequency and the generated frequency. The cost function ρ is given as

$$\rho = \sum_{k=1}^{N} (\hat{f}_k - \tilde{f}_k)^2 \tag{3-22}$$

This procedure is done for all frequencies in the search space. The frequency granularity can be chosen as 1Hz. Then the frequency value and the corresponding $\hat{\boldsymbol{p}} = [x_P, y_P, z_P]^T$ value that give the minimum cost are chosen as LS estimate.

As will be shown in simulations parts, the LS estimates do not meet CRLB, however they are close enough to the actual values to be chosen as initial estimates in ML estimate.

LS Algorithm:

1. Estimate the Doppler shifted frequencies with a frequency estimation algorithm at each measurement point.
2. Obtain the $\boldsymbol{A}$ matrix by using the direction of platform's velocity vector and platform positions as defined in Equations (3-10), (3-11), (3-12) and (3-20).
3. Define a search space for frequency, from $\tilde{f}_a - \Delta$ to $\tilde{f}_a + \Delta$ where $(\tilde{f}_a)$ is the average of the estimated frequencies in Step 1 and $\Delta \approx \tilde{f}_a \frac{V}{c}$.
4. For each frequency value in search space, calculate the α_k values as in Equation (3-1) by substituting f_0 with this frequency value and $f_k(\boldsymbol{x})$ with the measured frequency for *k=1,2,…N.*
5. By using these α_k values, estimate R_k values with Equations (3-17) and (3-18).

6. Obtain the $\boldsymbol{b}$ vector by using R_k, m_k and α_k as in Equation (3-20).
7. Estimate the target position $\hat{\boldsymbol{p}}$ by using the closed form estimator in Equation (3-21).
8. Re-calculate the α_k and R_k values for this position estimate $\hat{\boldsymbol{p}}$ and by using these values with Equation (3-1) find the predicted Doppler-shifted frequencies$(\hat{f}_k)$.
9. Calculate the cost function defined in Equation (3-22).
10. Repeat Step 4-9 for each frequency in the search space and choose the frequency value which gives the minimum cost and the corresponding position estimate $\hat{\boldsymbol{p}}$ as LS estimate.

3.5 Maximum Likelihood Estimator

The optimum MLE is obtained from the maximization of the joint probability density function of the Doppler-shifted frequency measurements $(\tilde{f}_k)$, *k=1,...,N* .

Assuming the frequency measurement noise is Gaussian distributed, the ML estimate of the target position and the signal frequency can be written as

$$\hat{\boldsymbol{x}}_{ML} = arg \min_{P} J_{ML}(\boldsymbol{x}) \tag{3-23}$$

where the ML cost function is given by

$$J_{ML}(\boldsymbol{x}) = \boldsymbol{e}^T(\boldsymbol{x})\boldsymbol{K}^{-1}\boldsymbol{e}(\boldsymbol{x}) \tag{3-24}$$

As indicated in Section 3.3 the target position and the signal frequency are combined in parameter vector

$$\boldsymbol{x} = [x_P \; y_P \; z_P \; f_0]^T \tag{3-25}$$

In the cost function, $\boldsymbol{K}$ is the *NxN* covariance matrix of the frequency noise and $\boldsymbol{e}(\boldsymbol{x})$ is the *Nx1* error vector which are defined as

$$\boldsymbol{K} = diag\{\sigma_{f_1}^2, \sigma_{f_2}^2, \dots, \sigma_{f_N}^2\} \tag{3-26}$$

$$\boldsymbol{e}(\boldsymbol{x}) = [\tilde{f_1} - f_1(\boldsymbol{x}) \quad \dots \quad \tilde{f_N} - f_N(\boldsymbol{x})] \tag{3-27}$$

It is seen that the ML estimator does not have a closed form solution. A search algorithm should be used to find the target position that maintains the minimum cost. GN algorithm is used for this purpose which is a batch iterative minimization technique. The update for the parameter vector is done as follows

$$\hat{\boldsymbol{x}}_{i+1} = \hat{\boldsymbol{x}}_i - (\boldsymbol{J}_i^T \boldsymbol{K}^{-1} \boldsymbol{J}_i)^{-1} \boldsymbol{J}_i^T \boldsymbol{K}^{-1} \boldsymbol{e}(\hat{\boldsymbol{x}}_i) \; for \; i = 0,1, \dots, N_{iteration} \tag{3-28}$$

where $\boldsymbol{J}_i$ is the *Nx4* Jacobian matrix evaluated at the current frequency and position estimate:

$$\boldsymbol{J}_i = \begin{bmatrix} \frac{\partial f_1(\boldsymbol{x})}{\partial x_P} & \frac{\partial f_1(\boldsymbol{x})}{\partial y_P} & \frac{\partial f_1(\boldsymbol{x})}{\partial z_P} & \frac{\partial f_1(\boldsymbol{x})}{\partial f_0} \\ \vdots & \vdots & \vdots & \vdots \\ \frac{\partial f_N(\boldsymbol{x})}{\partial x_P} & \frac{\partial f_N(\boldsymbol{x})}{\partial y_P} & \frac{\partial f_N(\boldsymbol{x})}{\partial z_P} & \frac{\partial f_N(\boldsymbol{x})}{\partial f_0} \end{bmatrix}_{\boldsymbol{x}=\hat{\boldsymbol{x}}_i} \tag{3-29}$$

The terms of the Jacobian matrix are calculated as follows:

$$K = \frac{f_0 V}{c} \tag{3-30}$$

$$n_k = \sqrt{(x_P - x_k)^2 + (y_P - y_k)^2 + (z_P - z_k)^2} \tag{3-31}$$

$$m_k = b_k x_P - b_k x_k + c_k y_P - c_k y_k + d_k z_P - d_k z_k \tag{3-32}$$

$$\frac{\partial f_k(\boldsymbol{x})}{\partial x_P} = K\left(\frac{b_k}{c n_k} - \frac{(x_P - x_k) m_k}{c n_k^3}\right) \tag{3-33}$$

$$\frac{\partial f_k(\boldsymbol{x})}{\partial y_P} = K\left(\frac{c_k}{c n_k} - \frac{(y_P - y_k) m_k}{c n_k^3}\right) \tag{3-34}$$

$$\frac{\partial f_k(\boldsymbol{x})}{\partial z_P} = K\left(\frac{d_k}{cn_k} - \frac{(z_P - z_k)m_k}{cn_k^3}\right) \tag{3-35}$$

$$\frac{\partial f_k(\boldsymbol{x})}{\partial f_0} = \left(1 + \frac{Vm_k}{cn_k}\right) \tag{3-36}$$

While calculating the above elements the current estimate values are used for $\boldsymbol{x} = [x_P\ y_P\ z_P\ f_0]^T$. In the algorithm an initial estimate is required. The LS estimate obtained in Section 3.4 is used as initial estimate. Jacobian matrix is evaluated at this estimate. Then the estimate is updated according to the Equation (3-28). This procedure is repeated for a defined iteration number or until the norm of the position update is smaller than a sufficiently small number.

MLE Algorithm:

1. Estimate the Doppler shifted frequencies with a frequency estimation algorithm at each measurement point
2. Obtain the measurement covariance matrix $\boldsymbol{K}$ as defined in Equation (3-26).
3. Start with an initial estimate (LS estimate) and calculate the error vector for this estimate which is defined in Equation (3-27).
4. Calculate the Jacobian matrix $\boldsymbol{J}_0$ for the initial estimate as in Equation (3-29).
5. Perform GN search algorithm which updates position estimate by updating error vector and Jacobian matrix at each step as in Equation (3-28).
6. End the search algorithm when the defined update criterions are met. The final $\hat{\boldsymbol{x}}_i$ value is the ML estimate of the parameters.

The covariance matrix of the ML estimator is calculated by using the Jacobian matrix obtained in the last iteration and the measurement error covariance matrix.

$$\boldsymbol{Q}_{ML} = (\boldsymbol{J}^T\boldsymbol{K}^{-1}\boldsymbol{J})^{-1} \tag{3-37}$$

By using the covariance matrix of the estimator, the error ellipsoid around the estimated target position can be plotted as explained in Section 2.5.1. The error ellipsoid with probability P represents the area that the true target is in with probability P.

By using the Jacobian matrix evaluated at the true signal frequency, actual target position and the measurement covariance matrix, CRLB matrix is evaluated as in Equation (3-37). By using CRLB matrix, the error ellipsoid around true target position can be plotted.

3.6 Combined Method for Position Estimation

In the previous sections, localization algorithms based on bearings and frequency measurements are presented individually. Combined set of bearing and frequency measurements can also be exploited for emitter position estimation [11]. In the remaining of this section, this method is called as Combined Method (CM). In CM, position estimation is obtained in ML sense. ML estimators for bearing-only and DSF methods are presented in Sections 2.4.4 and 3.5. In CM, the error vector and Jacobian matrix are evaluated such that they include information about both bearings and frequencies. In DSF method, the Jacobian matrix is $Nx4$ where the last column is calculated for dependence of measurements on center frequency of the emitted signal. On the other hand, in bearing-only method Jacobian matrix is $2Nx3$, since there is no dependence of bearing measurements to center frequency. In CM, Jacobian matrices of bearing-method and DSF method are combined by adding a $2Nx1$ zeros column at the end of Jacobian matrix of bearing method. The $\boldsymbol{x}$ vector used in Equation (3-39) is defined in Equation (3-25). In MLE the covariance matrix of the measurement noise is used in the update step. In Section 2.4.4 covariance matrix of bearing noise, in Section 3.5 covariance matrix of frequency noise is used which are defined in Equations (2-29) and (3-26) respectively. In CM covariance matrix of both bearing noise and frequency noise is used which is defined as follows

$$\boldsymbol{K}_{comb} = diag\{\sigma_{\theta_1}^2, \sigma_{\theta_2}^2, \dots, \sigma_{\theta_N}^2, \sigma_{\phi_1}^2, \sigma_{\phi_2}^2, \dots, \sigma_{\phi_N}^2, \sigma_{f_1}^2, \sigma_{f_2}^2, \dots, \sigma_{f_N}^2\} \tag{3-38}$$

The error vector is also combined as in above case. The error vectors are defined in Equations (2-30) and (3-27) for bearing-only method and DSF method respectively. In CM, the error vector which combines these error vectors is used.

$$\begin{aligned}\boldsymbol{e}_{comb}(\boldsymbol{x}) = [&\tilde{\theta}_1 - \theta_1(\boldsymbol{x}), \dots, \tilde{\theta}_N - \theta_N(\boldsymbol{x}), \tilde{\phi}_1 - \phi_1(\boldsymbol{x}), \dots, \tilde{\phi}_N - \phi_N(\boldsymbol{x}), \tilde{f}_1 \\ &- f_1(\boldsymbol{x}), \dots, \tilde{f}_N - f_N(\boldsymbol{x})]\end{aligned} \tag{3-39}$$

The Jacobian matrix used in CM is obtained by combining the Jacobian matrices used in bearing-only method and DSF method.

$$\boldsymbol{J}_{comb} = \begin{bmatrix} \boldsymbol{J}_{Bearing} \\ \boldsymbol{J}_{DSF} \end{bmatrix} \tag{3-40}$$

In above equation $\boldsymbol{J}_{Bearing}$ represents the Jacobian matrix of bearing-only method which a $2Nx1$ zeros column is added to the end of the matrix to indicate independence of angle measurements and frequency. By using these combined vectors and matrices, the ML estimate is obtained as described in Sections 2.4.4 and 3.5. The update for the parameter vector is done as follows

$$\begin{aligned}\hat{\boldsymbol{x}}_{i+1} = \hat{\boldsymbol{x}}_i - \left(\boldsymbol{J}_{comb,i}^T K_{comb}^{-1} \boldsymbol{J}_{comb,i}\right)^{-1} \boldsymbol{J}_{comb,i}^T K_{comb}^{-1} \boldsymbol{e}(\hat{\boldsymbol{x}}_i) \\ for\ i = 0,1, \dots, N_{iteration}\end{aligned} \tag{3-41}$$

An initial position estimate found by bearing-only or DSF-only method can be used in the MLE.

MLE Algorithm:

1. Estimate the AOA and received frequency of the target signal at each measurement point with a direction-finding and frequency estimation algorithm.

2. Obtain the measurement covariance matrix $\boldsymbol{K}$ as defined in Equation (3-38).
3. Start with an estimate and calculate the error vector for this estimate which is defined in Equation (3-39).
4. Calculate the Jacobian matrix $\boldsymbol{J}_{comb}$ for the initial estimate as in Equation (3-40). The calculated Jacobian matrices in Equations (2-32) and (3-29) are combined.
5. Perform GN search algorithm which updates estimate by updating error vector and Jacobian matrix at each step as in Equation (3-41).
6. End the search algorithm when the defined update criterions are met. The final $\hat{\boldsymbol{x}}_i$ value is the ML estimate of the parameters.

3.7 Simulation Results

In simulations the same scenario used in bearing-only algorithm is used. The target is at $(x_P, y_P, z_P) = (4000,3000,0)$. The platform is traveling with a constant speed $V = 100m/s$ and collects frequency measurements at every 10 seconds. Platform starts its path at $(x_1, y_1, z_1) = (0,0,2000)$ with a velocity vector in the direction of $\theta = 90$ and $\phi = 0$. After collecting 4 measurements, velocity vector changes in the direction of $\theta = 45$ and $\phi = -5$. 4 measurements are taken along this path and the velocity vector changes to the direction $\theta = 310$ and $\phi = 0$ and collects 4 more measurements. The scenario is as shown in Figure 3-4. As the algorithm required, the path consists of non-maneuvering path segments where a linear relation between frequency measurements and target position can be written.

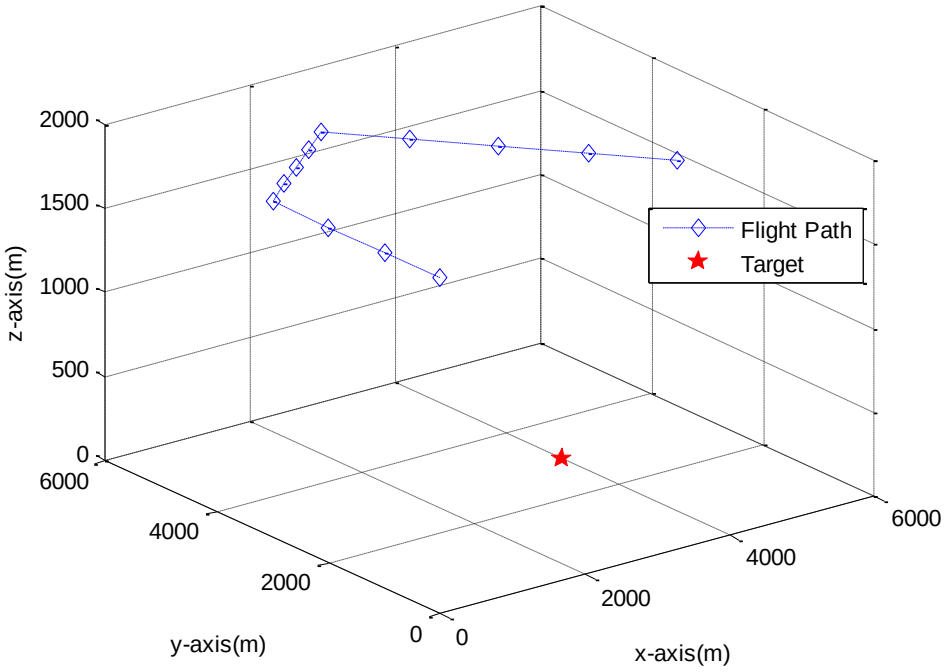

Figure 3-4 : Scenario used in the simulations

First, the performance of the DSF algorithm is considered. The frequency measurement error standard deviation is changed between 1Hz and 15Hz. Results are obtained by running 1000 Monte Carlo runs and RMS errors in target position and frequency estimation are calculated. The results are as in Figure 3-5 and Figure 3-6.

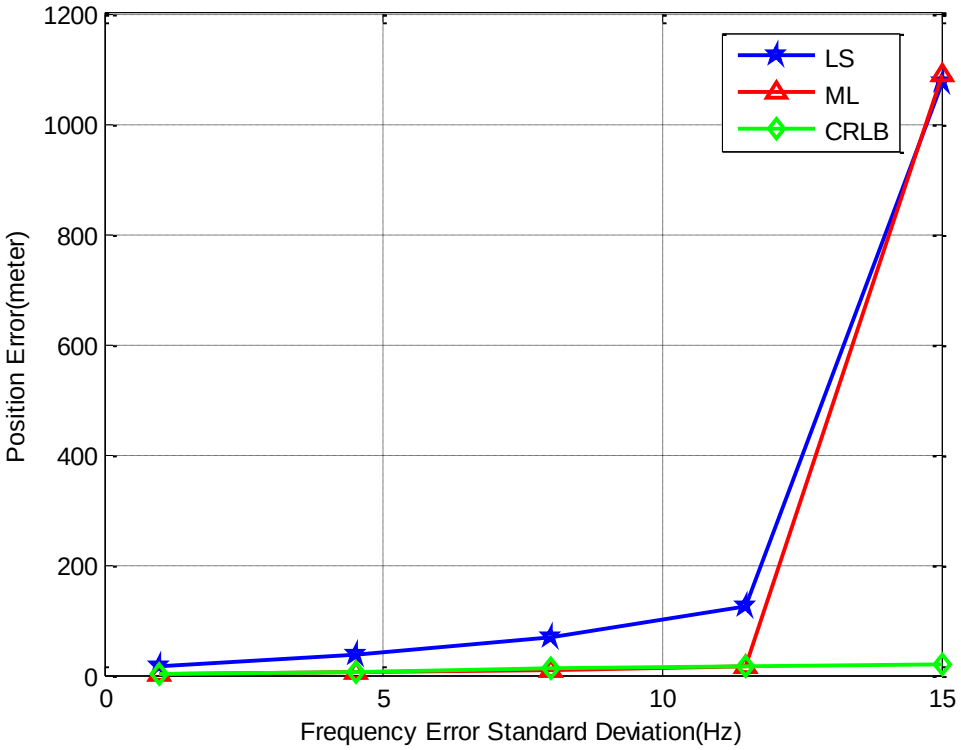

Figure 3-5 : RMS error for target position

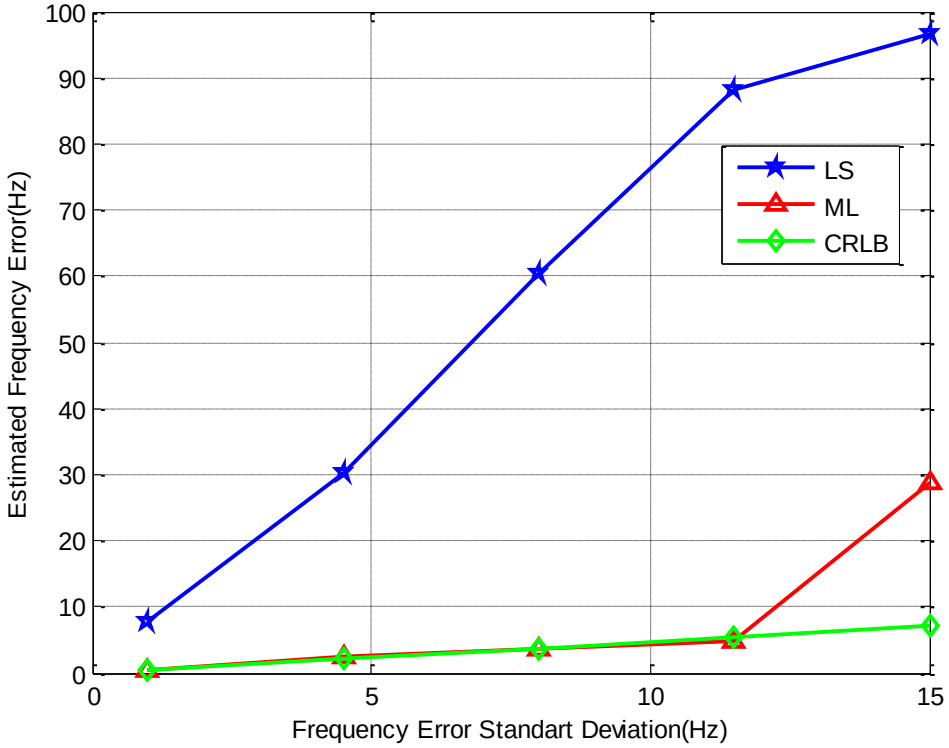

Figure 3-6 : RMS error for frequency

As seen from figures, the LS estimates do not meet CRLB. As the frequency error gets larger, the difference between LS estimates and CRLB increases. However it provides a good initial estimate for ML estimator which meets the CRLB. Up to approximately $\sigma_f = 12Hz$, ML estimator is nearly the same with the CRLB. On the other hand, as frequency error gets larger, since LS estimator does not provide close enough initial estimates the error increases and diverges from the actual position.

In the second part of this section, the performance of the combined method (CM) is compared with the DSF only method. Same flight path is used in the simulations.

To compare the performances of DSF only method, Bearing-Only method and combined method, error ellipsoids, which are calculated from CRLB, are used. Calculating the ellipsoid parameters and taking a slice from the ellipsoid and

projecting the ellipsoid on desired plane were explained in Section 2.5. So the details are not repeated in this section. An ellipsoid around true target position represents the volume where the estimates obtained from an unbiased estimator will lie with a probability *P*. So it can be concluded that a smaller error ellipsoid represents a better estimator performance since the estimates will lie in a smaller area. The alignment and size of the ellipsoids cannot be seen clearly when plotted on the same plot since they overlap. So the projections of the ellipsoids on x-y plane are plotted. The ellipses are plotted for the case where azimuth and elevation errors standard deviation is 3 degrees and frequency error standard deviation is 70Hz. The probabilities of the ellipsoids are 0.9.

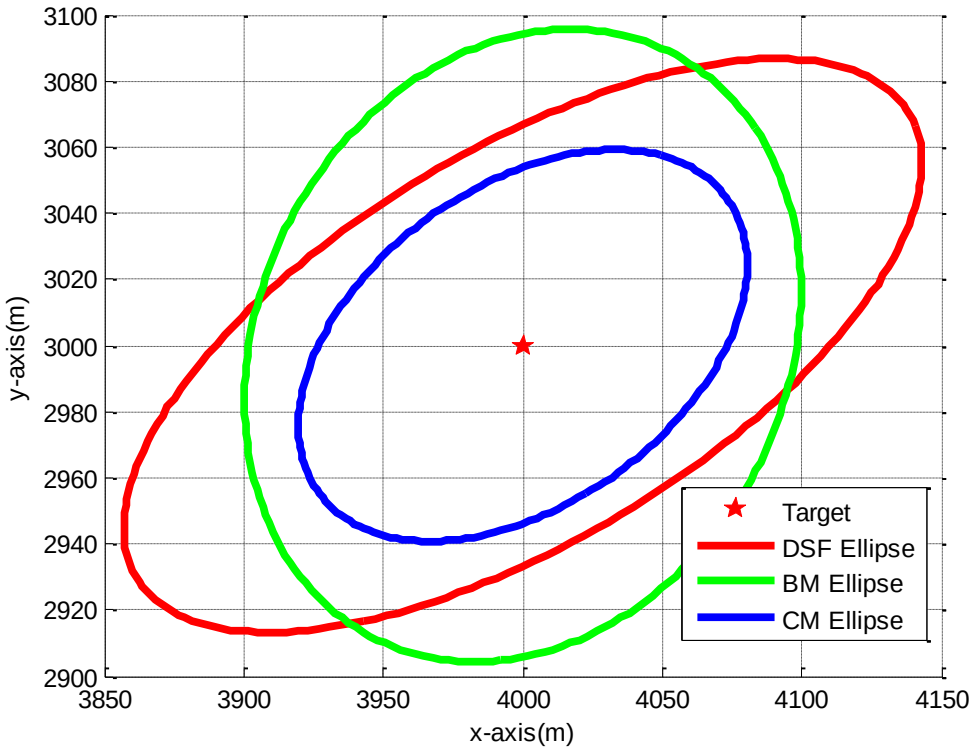

Figure 3-7: Projection of error ellipsoids for different methods

The algorithms are run 100 times. It is assumed that the information that the target is on $z = 0$ plane is available. So the algorithms which use this information are used. The estimates are expected to be in the area which is defined by the slice of the ellipsoid taken at $z = 0$.

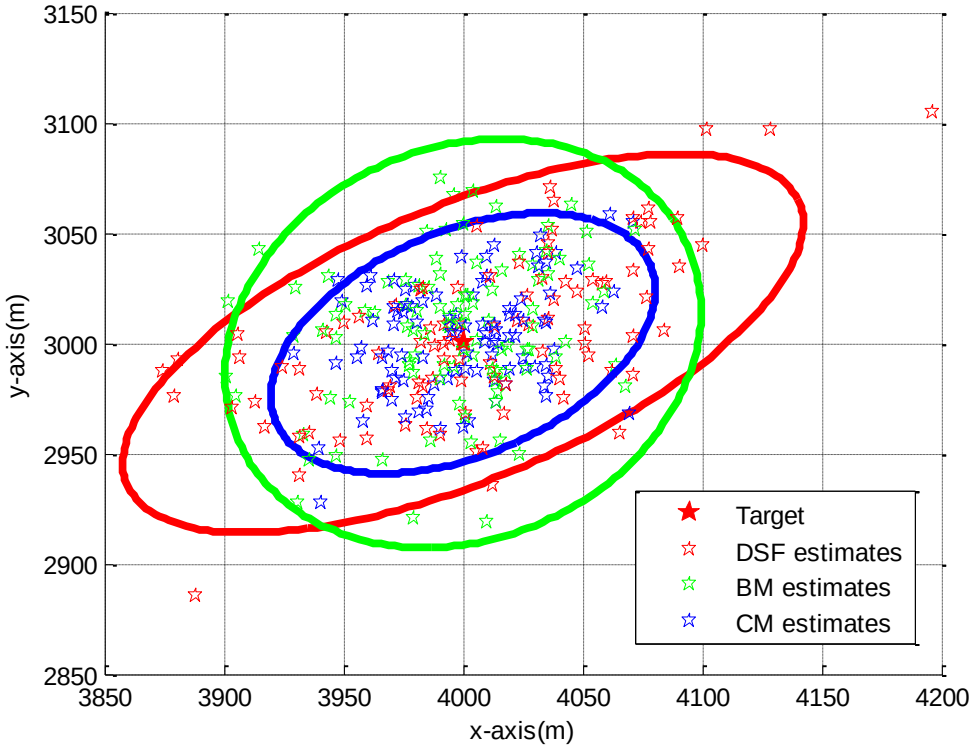

Figure 3-8: The estimates obtained with different algorithms

As seen from Figure 3-7 the alignment of the ellipsoids for DSF method and bearing-only method are different. Combining these ellipsoids yields a smaller ellipsoid which means the performance of the combined method is better than DSF method and bearing-only method individually. With the following simulations, this claim is supported.

First, the case where standard deviations of azimuth and elevation angles are fixed to 3 degrees is examined. The standard deviation of the frequency measurements are changed between 10Hz and 90Hz.

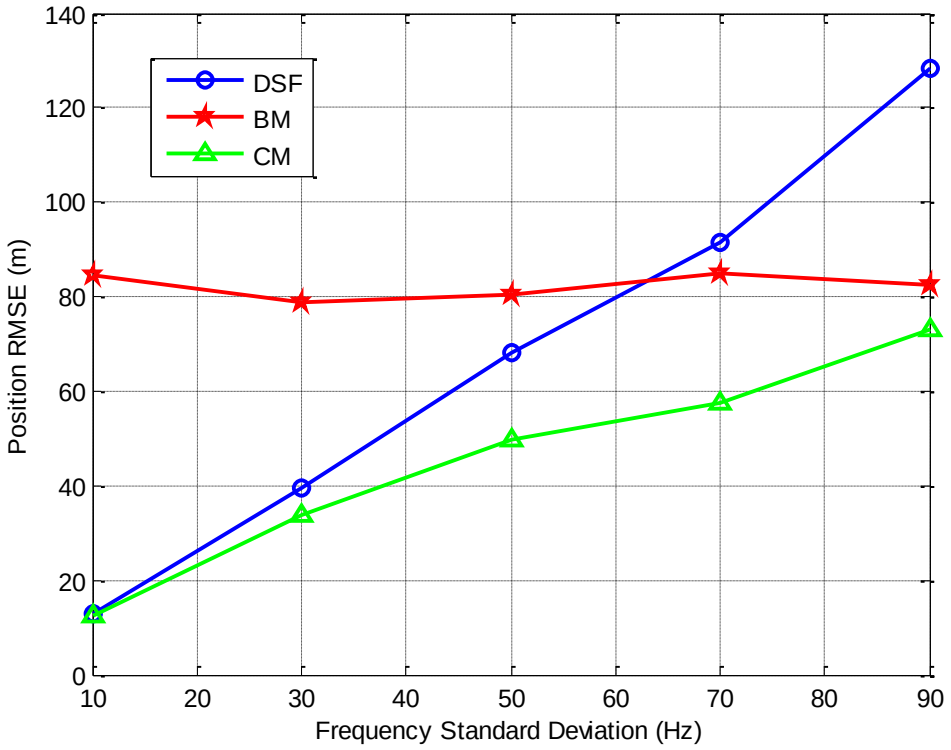

Figure 3-9: Performance comparison of algorithms for different frequency standard deviations

As seen from Figure 3-9, since angle measurements' standard deviation is fixed, the position error for bearing-only method is nearly the same for different frequency errors. For DSF method ML estimator is used which meets CRLB. To compare the performance of the algorithms for larger errors, the initial position estimate used in ML estimator is chosen as a close position near to the actual position. Otherwise as frequency error gets larger, the LS estimate gets further than the actual position and the ML estimator starts to diverge. The position error gets larger for DSF method as

frequency standard deviation values gets larger as expected. The important point is that CM always has a better performance than DSF method and bearing-only method as seen from the error ellipsoids in Figure 3-7.

In Figure 3-10, the performance of the CM is compared with the CRLB. As seen from the figure, the error is nearly equal to the best achievable error.

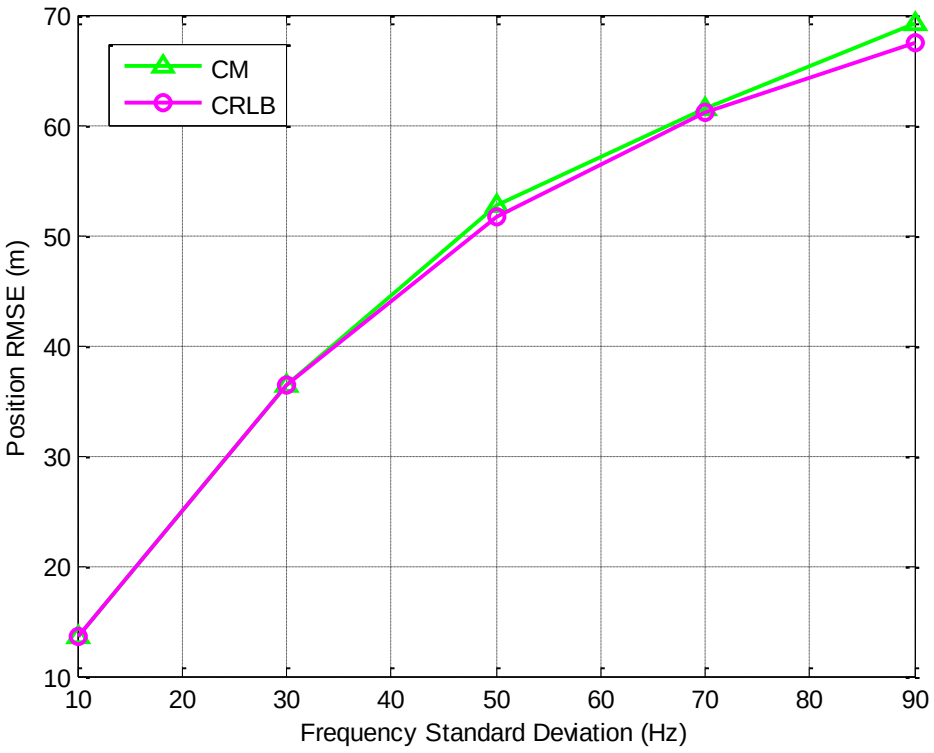

Figure 3-10: Comparison of position accuracy with CRLB of the combined algorithm

Beside the position estimation, the frequency of the emitted signal from target is also estimated with DSF method and CM. With the same simulation parameters, the accuracy of frequency estimation is considered for DSF and CM. Since there is no frequency estimation in BM, it is not included in the comparison.

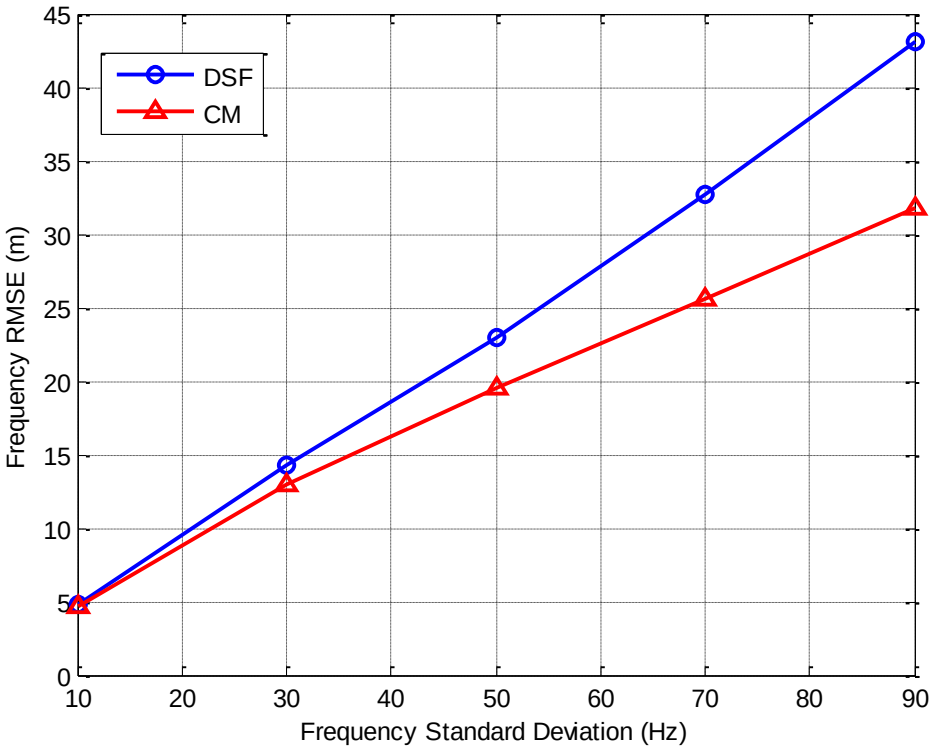

Figure 3-11: Frequency estimation accuracies for DSF and CM

At first sight it might be thought that the frequency estimation performance does not change between DSF and CM. Since in bearing-only method there is no information about signal frequency and including angle measurements will not provide extra information about frequency. However as seen in Figure 3-11, the frequency estimation accuracy is also higher in CM. This situation is relevant with the position estimation accuracy. In CM, since position estimation performance is better, the minimization of the cost function in ML estimation performed better and this is why the frequency estimates are more accurate.

In Figure 3-12, frequency estimation accuracy is compared with the CRLB. It is observed that it is nearly equal to the best achievable error.

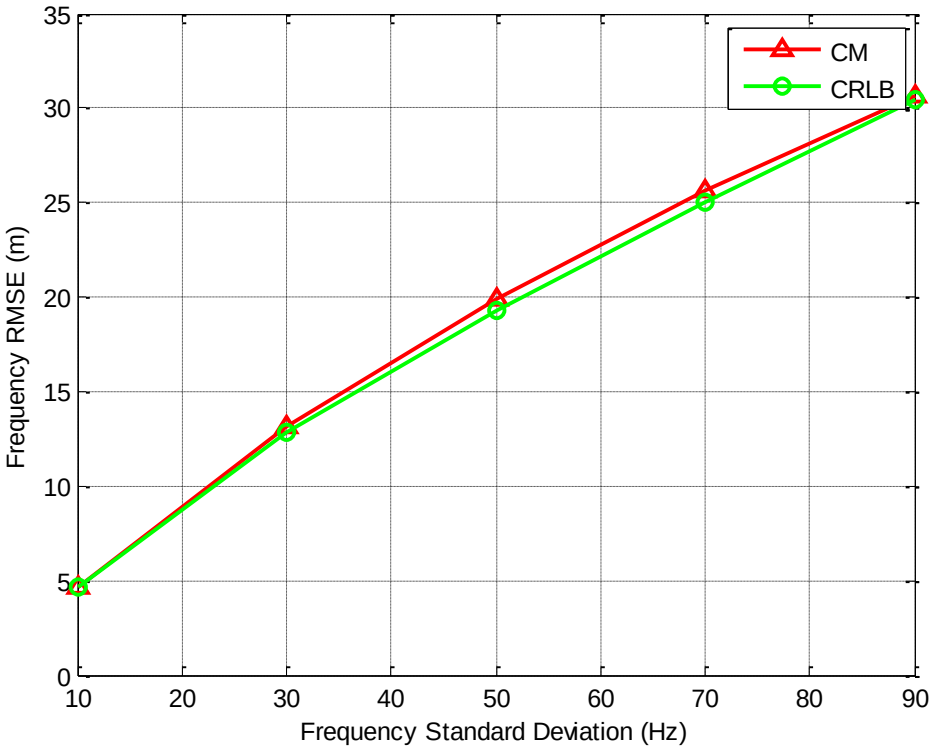

Figure 3-12: Comparison of frequency accuracy with CRLB for different frequency standard deviations

To see the algorithm performances for different angle measurement standard deviations, bearing standard deviations are changed between 1 and 5 degrees and frequency standard deviation is fixed to 50Hz.

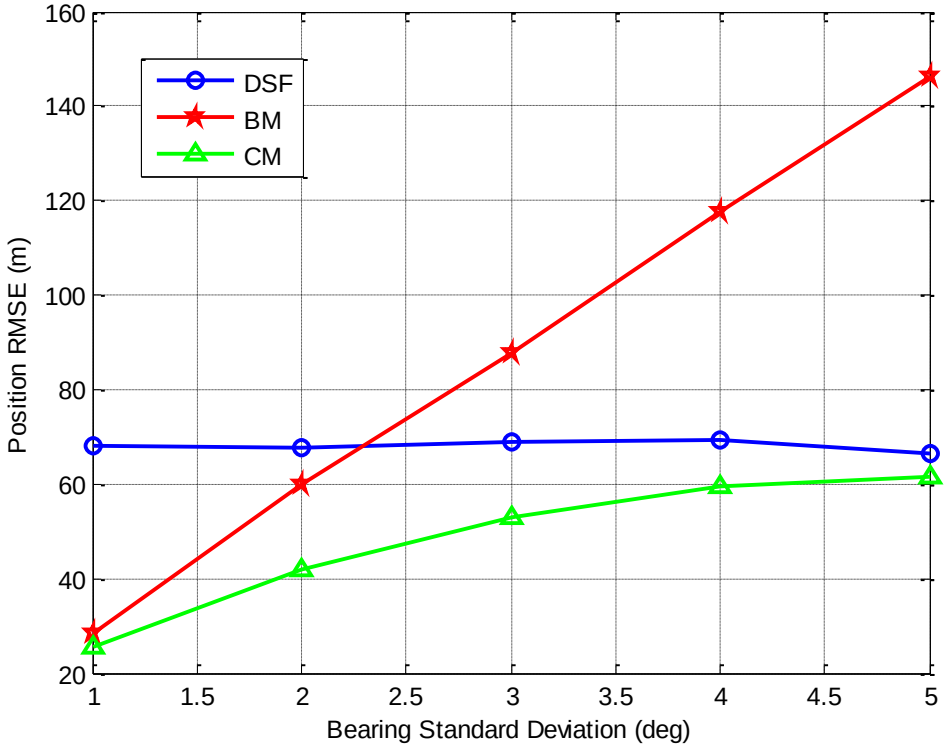

Figure 3-13: Performance comparison of algorithms for different bearing standard deviations

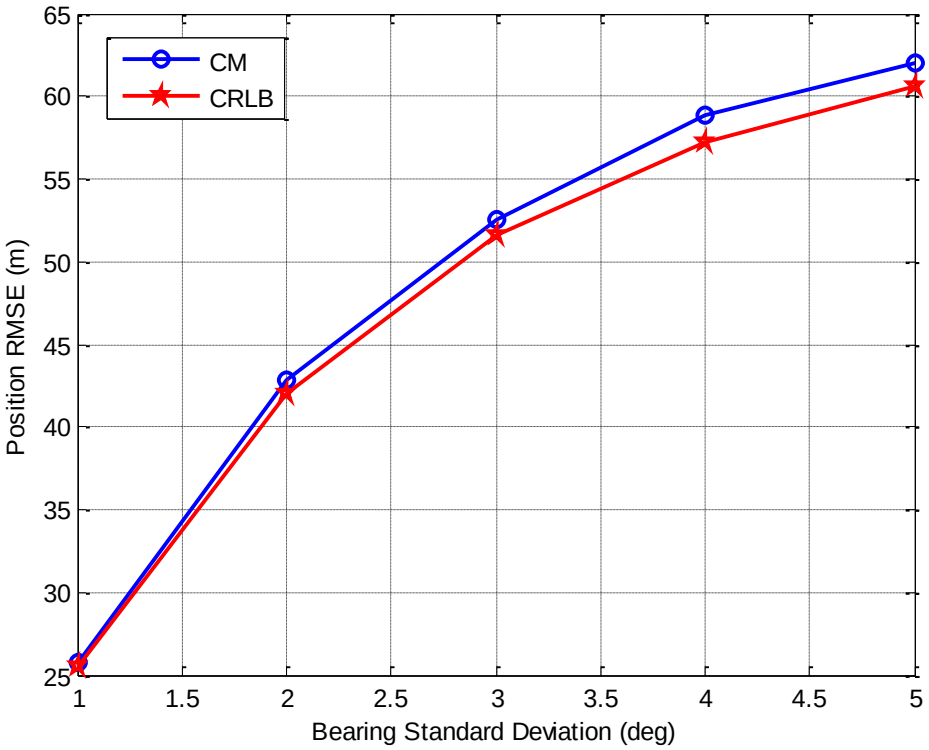

Figure 3-14 : Comparison of position accuracy with CRLB for different bearing standard deviations

As seen from Figure 3-13 since frequency measurements' standard deviation is fixed the position error for DSF method is nearly the same for different bearing errors. For BM method, ML estimator is used which meets CRLB. To compare the performance of the algorithms for larger errors, the initial position estimate used in the ML estimator is chosen as a close position near to the actual position. The position error gets larger for BM as bearing standard deviation values gets larger as expected.

Remember that the measured frequency from the platform was defined as in Equation (3-1). It is seen from the equation that the measured frequencies depend

on the target's signal frequency (f_0) and platform velocity (V). To see the effect of these parameters on estimation performance, followings simulations are performed.

To see the effect of platform velocity on position estimation accuracy, the platform velocity is changed between $100m/s$ and $500m/s$ and all other parameters kept constant. As seen from Figure 3-15, as platform velocity gets larger, the position RMSE gets smaller both for DSF method and CM. Since higher platform velocities cause higher Doppler shifts, the effect of noise gets smaller.

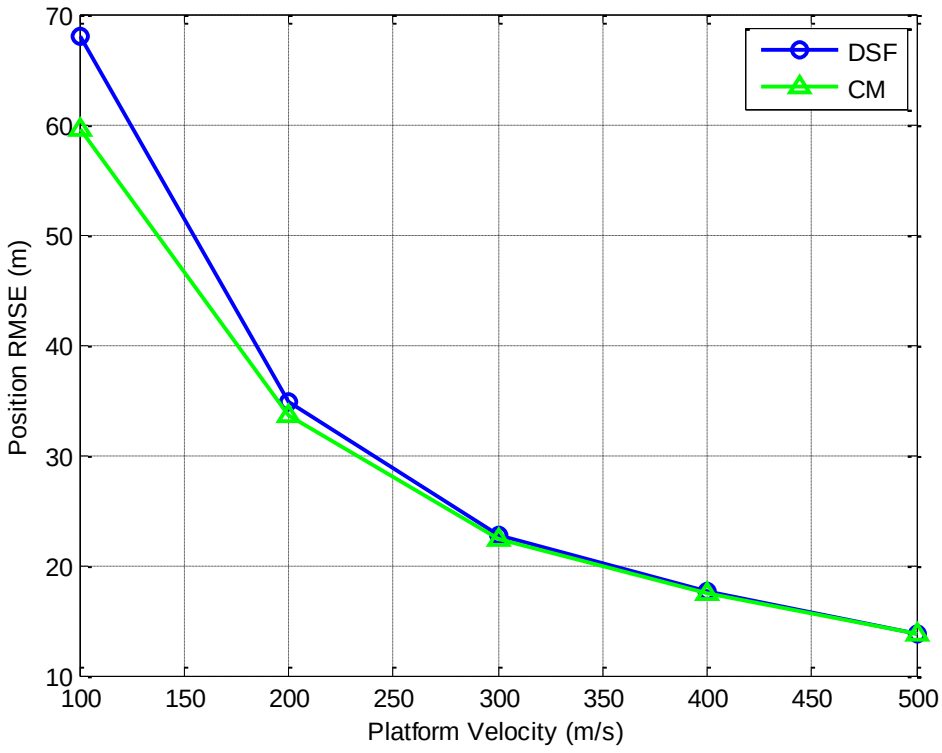

Figure 3-15 : Effect of platform velocity on position estimation accuracy

To see the effect of signal frequency on position estimation accuracy, the emitted signal frequency (f_0) is changed between 5GHz and 10GHz and all other parameters kept constant. As seen from Figure 3-16, as signal frequency gets larger,

the position RMSE gets smaller both for DSF method and CM. Similar with the above case, as frequency gets larger, according to Equation (3-1) Doppler shift becomes larger too. So the effect of noise is smaller for higher Doppler shifts.

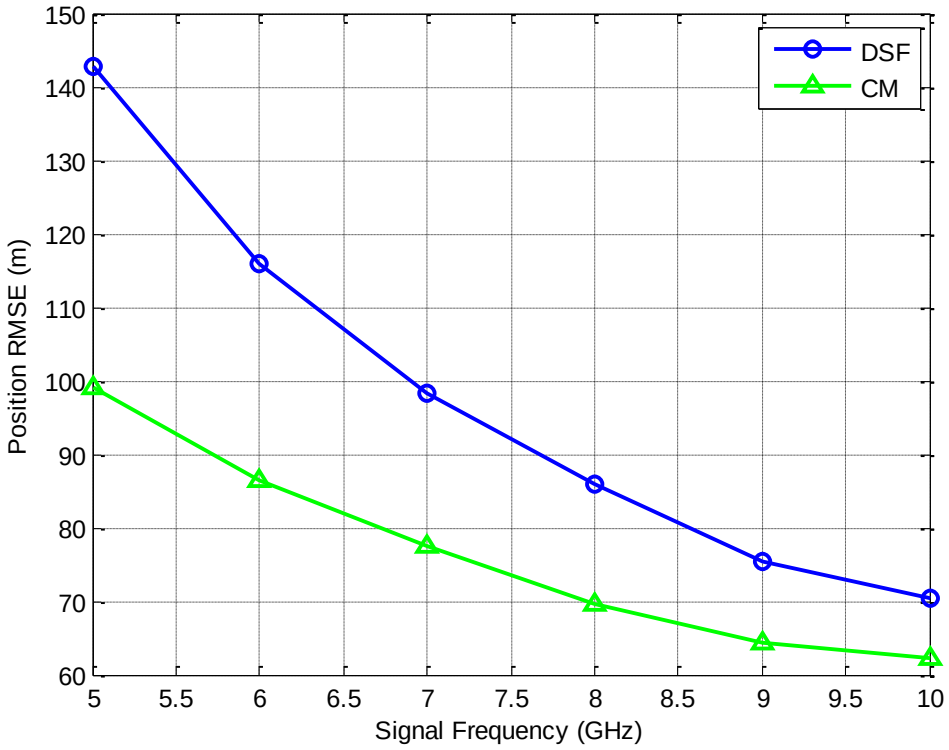

Figure 3-16 : Effect of signal frequency on position estimation accuracy

CHAPTER 4

TDOA BASED LOCALIZATION ALGORITHMS

4.1 General Information

Passive emitter localization by time difference of arrival (TDOA) has applications in a wide range of areas such as localization of lightning strikes, geolocation of mobile phones, radar, sonar and electronic warfare [35]. In this method, the emitter is transmitting a signal and receivers at different locations receive this signal. The TDOA values between the pairs of the receivers are used to estimate the target position. In passive localization, there is no information about the pulse transmission times. So the arrival time of the signal does not provide information about the target. The time differences are measured at multiple receivers with known locations, and subsequently used for computing a location estimate [18].

For 2D problem, the TDOA value between two receivers defines a hyperbola. For noise-free case, target is at the intersection of hyperbolas defined by different sensor pairs. In 3D, the TDOA value defines hyperboloids. Target position is found by solving *N-1* non-linear equations. Solution can be found in closed-form or by using a maximum likelihood estimator. In this thesis, target is first estimated with the closed-form estimator. Then by using this closed-form estimate in ML estimator, a better estimate is obtained which attains CRLB. As explained in previous sections, ML estimator does not have a closed form solution, so an iterative GN method is used to obtain the estimate. Because of the non-convex topology of ML cost

function, the iterative ML estimators require an initial estimate close to the solution in order to avoid divergence [15].

The localization accuracy in TDOA method depends on three factors which are the accuracy of TDOA estimates, the choice of the location estimator and the sensor position relative to the source [19]. The effect of sensor placement on localization accuracy can be examined in terms of CRLB matrix. This can be done by calculating the CRLB matrix and plotting the error ellipsoid. The optimum sensor placement is the one which minimizes the trace of the CRLB, in other words, which maximizes the trace of FIM.

There are two important advantages of estimating the target position with TDOA. Localization is realized without any knowledge about received waveform of the signal [36]. The arrival times of the pulse are sufficient for localization. The other advantage is that antenna array calibration is not needed different from bearing-only localization algorithms. On the other hand, this method is very sensitive to time synchronization between platforms.

4.2 TDOA Estimation

In this section, a short summary of TDOA estimation methods is given. However these methods are not implemented. It is outside the scope of this thesis. In simulations, TDOA values are generated by adding zero mean Gaussian noise to the actual values.

One of the methods for estimating TDOA between two sensors is “Leading-Edge TDOA”. In this method, arrival times of the signals are measured at the sensors and their difference is taken. The arrival time of the signal can be determined by measuring the time at which the signal crosses an adaptive threshold level [25]. This problem is analyzed in literature [37]. Another TDOA estimation method is “Cross-Correlation Method”. In this method the cross-correlation of the received waveforms is calculated and the delay value is estimated as the value which maximizes this function. Let model the received signals at the sensors as [38]:

$$r_1(t) = s(t) + n_1(t) \tag{4-1}$$

$$r_2(t) = s(t - D) + n_2(t)\ for\ 0 \le t \le T \tag{4-2}$$

where $s(t)$ represents the emitted signal from target, $n_1(t)$ and $n_2(t)$ represent the noise in the receivers. Observation time is denoted by T. In Equation (4-2), D is the unknown delay which is desired to be estimated. In the method, it is assumed that the correlation durations of the signals is very small compared to the observation time. The estimate of time delay $(\tau = \widehat{D})$ is found as

$$\tau = arg \max_{\tau} \int_0^T r_1(t) r_2(t - \tau) dt \tag{4-3}$$

There is also "Generalized Cross Correlation Method" which finds the maximum value of the cross correlation of prefiltered signals [38].

TDOA estimation accuracy is one of the most important factors that determine the TDOA based localization estimator performance. The accuracy of TDOA estimation depends on receiver noise, center frequency of the signal, received SNR and observation time. All these parameters also affect the localization performance. Increase in SNR, bandwidth, frequency of the signal and/or integration time result in better position estimates. In [39], CRLB of variance for the time delay estimate is examined in a detailed way for low and high SNR cases. It is stated that the standard deviation of the time delay estimate varies inversely to the square root of the SNR for high SNR case (SNR>>1), whereas for low SNR case, it varies inversely to the SNR. The effects of other parameters are same for both low and high SNR's. The derived CRLB values for TDOA estimations are as follows [39]:

$$\sigma_{TDOA} \ge \sqrt{\frac{3}{8\pi^2 T}} \frac{1}{SNR} \frac{1}{\sqrt{f_2^3 - f_1^3}} \quad \text{for SNR<<1} \tag{4-4}$$

$$\sigma_{TDOA} \geq \sqrt{\frac{3}{8\pi^2 T}} \frac{1}{\sqrt{SNR}} \frac{1}{\sqrt{f_2^3 - f_1^3}} \quad \text{for SNR>>1} \tag{4-5}$$

In [39], it is assumed that the TDOA estimation is evaluated under the assumption that both noise and signal have constant power spectral density over the bandwidth specified by f_1 and f_2 $(f_2 > f_1)$. As seen from the above equations, TDOA estimation accuracy degrades as signal bandwith decreases. So it can be concluded that TDOA based localization methods are not suitable for narrowband communication waveforms [27].

4.3 Problem Formulation

In TDOA localization, the problem is estimating the position of the stationary target which is represented by $\boldsymbol{p} = [x_P, y_P, z_P]^T$ given the TDOA values for different sensor pairs. The arrival time of the signal which is emitted by target is measured at N different points. By using the difference between these arrival times, location of the target is estimated. The platform position where the k^{th} measurement is taken is represented by $\boldsymbol{r_k} = [x_k, y_k, z_k]^T$ for $k = 1,2,\ldots,N$. The geometry between the target and the measurement points is seen in Figure 4-1. r_1 is chosen as the reference point and the time difference of arrivals are calculated according to this reference point.

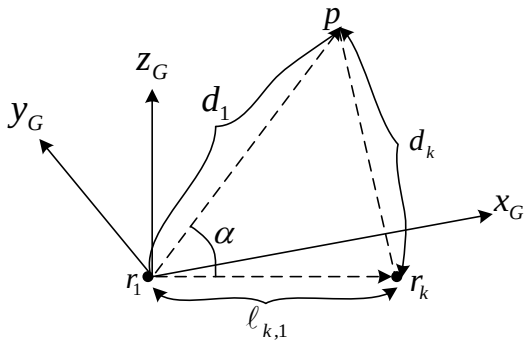

Figure 4-1: The geometry of the emitter localization problem

The distance between the target and the k^{th} measurement point is represented by d_k. ℓ_{k1} is the distance between the k^{th} measurement point and the reference point. Using r_1 as the reference receiver and computing the range difference of arrival (RDOA) measurements with respect to r_1, i.e., $g_{1k}, k = 2, \dots, N$, the target location can be obtained by solving the $N - 1$ non-linear equations [18]:

$$\begin{matrix} \|\boldsymbol{p} - \boldsymbol{r_2}\| - \|\boldsymbol{p} - \boldsymbol{r_1}\| = g_{12} \\ \vdots \\ \|\boldsymbol{p} - \boldsymbol{r_N}\| - \|\boldsymbol{p} - \boldsymbol{r_1}\| = g_{1N} \end{matrix} \tag{4-6}$$

The RDOA measurements are generated by adding a zero-mean Gaussian noise to the actual RDOA values:

$$\tilde{g}_{1k} = g_{1k} + n_{1k} \; for \; k = 2, \dots, N \tag{4-7}$$

In Equation (4-7), n_{1k} is the RDOA noise which is assumed to be stationary zero-mean Gaussian with covariance matrix [18]

$$\boldsymbol{\Sigma} = E\left\{ \begin{bmatrix} n_{12} \\ \vdots \\ n_{1N} \end{bmatrix} [n_{12} \quad \dots \quad n_{1N}] \right\} = \sigma_n^2 \begin{bmatrix} 1 & 1/2 & \dots & 1/2 \\ 1/2 & \ddots & \ddots & \vdots \\ \vdots & \ddots & \ddots & 1/2 \\ 1/2 & \dots & 1/2 & 1 \end{bmatrix} \tag{4-8}$$

where σ_n^2 is the RDOA noise variance. In [14], the details about the approximation of the covariance matrix as in Equation (4-8) are given. Since RDOA measurements are calculated by using a reference sensor, the measurements are correlated and the covariance matrix is not diagonal.

4.4 Multi Platform Emitter Localization

TDOA localization method is usually used in multi-platform emitter localization problems. Platforms at different positions receive the same signal at different arrival times and use the difference of these arrival times to estimate the position. LS and ML estimators are used for localization. The focus of thesis is emitter localization

with a single moving platform. However first details of multi-platform emitter localization method is given. Then this algorithm is modified for single-platform case and the differences are indicated for these two cases.

4.4.1 Least Squares Estimator

In LS estimator, a closed-form solution of the target is obtained. For the triangle in Figure 4-1, Law of Cosines property is used, i.e.,

$$d_k^2 = d_1^2 + \ell_{k1}^2 - 2d_1\ell_{k1}cos\alpha \tag{4-9}$$

The relation between d_1 and d_k is written by using RDOA values which is equal to speed of signal times TDOA values.

$$d_k = d_1 + g_{1k} = d_1 + c\tau_{1k} \tag{4-10}$$

where τ_{1k} is the TDOA value between the reference first platform and the k^{th} platform.

Combining the above two equations:

$$(d_1 + c\tau_{1k})^2 = d_1^2 + \ell_{k1}^2 - 2d_1\ell_{k1}cos\alpha \tag{4-11}$$

Using the vector product property,

$$\boldsymbol{x}^T\boldsymbol{y} = |\boldsymbol{x}||\boldsymbol{y}|cos\alpha \tag{4-12}$$

Equation (4-11) can be written as,

$$(d_1 + c\tau_{1k})^2 = d_1^2 + \ell_{k1}^2 - 2(\boldsymbol{r_k} - \boldsymbol{r_1})(\boldsymbol{p} - \boldsymbol{r_1}) \tag{4-13}$$

Arranging this equation results:

$$\ell_{k1}^2 - 2d_1c\tau_{1k} - c^2\tau_{1k}^2 - 2(\boldsymbol{r_k} - \boldsymbol{r_1})^T(\boldsymbol{p} - \boldsymbol{r_1}) = 0 \tag{4-14}$$

$$\ell_{k1}^2 - 2d_1 c\tau_{1k} - c^2\tau_{1k}^2 - 2(\boldsymbol{r_k} - \boldsymbol{r_1})^T\boldsymbol{p} + 2(\boldsymbol{r_k} - \boldsymbol{r_1})^T\boldsymbol{r_1} = 0 \quad (4\text{-}15)$$

$$\ell_{k1}^2 - 2d_1 g_{1k} - g_{1k}^2 - 2(\boldsymbol{r_k} - \boldsymbol{r_1})^T\boldsymbol{p} + 2(\boldsymbol{r_k} - \boldsymbol{r_1})^T\boldsymbol{r_1} = 0 \quad (4\text{-}16)$$

Equation (4-16) is written for all platforms for $k = 2, \dots, N$ and $N-1$ equations are obtained. These $N-1$ equations can be written in matrix form as follows:

$$\boldsymbol{Ax} = \boldsymbol{b} \quad (4\text{-}17)$$

where $\boldsymbol{A}$, $\boldsymbol{x}$ and $\boldsymbol{b}$ are defined as follows

$$\boldsymbol{A} = \begin{bmatrix} (r_2 - r_1)^T & g_{12} \\ (r_3 - r_1)^T & g_{13} \\ \vdots & \vdots \\ (r_N - r_1)^T & g_{1N} \end{bmatrix} \boldsymbol{x} = \begin{bmatrix} \boldsymbol{p} \\ d_1 \end{bmatrix} \boldsymbol{b} = \begin{bmatrix} 0.5(\ell_{21}^2 - g_{12}^2) + (r_2 - r_1)^T r_1 \\ 0.5(\ell_{31}^2 - g_{13}^2) + (r_3 - r_1)^T r_1 \\ \vdots \\ 0.5(\ell_{N1}^2 - g_{1N}^2) + (r_N - r_1)^T r_1 \end{bmatrix} \quad (4\text{-}18)$$

$$\hat{\boldsymbol{x}} = (\boldsymbol{A}^T\boldsymbol{A})^{-1}\boldsymbol{A}^T\boldsymbol{b} \quad (4\text{-}19)$$

In the simulations, instead of actual RDOA values the measured noisy RDOAs $(\tilde{g}_{1k})$ are used.

LS Algorithm:

1. Estimate the TDOA values between the reference platform and other platforms with a TDOA estimation algorithm.
2. Obtain the $\boldsymbol{A}$ matrix and $\boldsymbol{b}$ vector as defined in Equation (4-18) by using platform positions, TDOA values and the distance between platforms.
3. Estimate the target position and the distance between target and reference platform (d_1) with a closed form estimator as in Equation (4-19).

4.4.2 Maximum Likelihood Estimator

Under the Gaussian noise assumption, ML estimate of the solution can be found by maximizing the joint probability density function of the RDOA measurements resulting in [35],

$$\widehat{\boldsymbol{p}}_{ML=}\underset{\boldsymbol{p}}{\operatorname{argmin}}\, J_{ML}(\boldsymbol{p}) \tag{4-20}$$

where $J_{ML}(p)$ is the ML cost function

$$J_{ML}(\boldsymbol{p}) = \boldsymbol{h}^T(\boldsymbol{p})\boldsymbol{\Sigma}^{-1}\boldsymbol{h}(\boldsymbol{p}) \tag{4-21}$$

and $\boldsymbol{h}(\boldsymbol{p})$is the RDOA error vector which is defined by:

$$\boldsymbol{h}(\boldsymbol{p}) = \begin{bmatrix} \|\boldsymbol{p}-\boldsymbol{r_2}\| - \|\boldsymbol{p}-\boldsymbol{r_1}\| - \tilde{g}_{12} \\ \vdots \\ \|\boldsymbol{p}-\boldsymbol{r_N}\| - \|\boldsymbol{p}-\boldsymbol{r_1}\| - \tilde{g}_{1N} \end{bmatrix}_{(N-1)x1} \tag{4-22}$$

The aim is to find the point which makes the cost function minimum. Gauss-Newton algorithm is used to find the solution. In this method, Jacobian matrix of $\boldsymbol{h}(\boldsymbol{p})$ is evaluated at $\boldsymbol{p} = \widehat{\boldsymbol{p}}_{ML}(k)$. Algorithm starts with an initial estimate $\left(\widehat{\boldsymbol{p}}_{ML}(0)\right)$ and this estimate is updated according to the following expression,

$$\widehat{\boldsymbol{p}}_{ML}(k+1) = \widehat{\boldsymbol{p}}_{ML}(k) - \left(\boldsymbol{J}^T(k)\boldsymbol{\Sigma}^{-1}J(k)\right)^{-1}\boldsymbol{J}^T(k)\boldsymbol{\Sigma}^{-1}\boldsymbol{h}\left(\widehat{\boldsymbol{p}}_{ML}(k)\right) \quad for\ i = 0,1,\dots,N_{iteration} \tag{4-23}$$

The update is done for a defined iteration number or until the norm of the difference of the position update is smaller than a defined small value. The Jacobian matrix is calculated as follows:

$$\boldsymbol{J}(k) = \begin{bmatrix} \dfrac{(\widehat{\boldsymbol{p}}_{ML}(k)-r_2)^T}{\|\widehat{\boldsymbol{p}}_{ML}(k)-r_2\|} - \dfrac{(\widehat{\boldsymbol{p}}_{ML}(k)-r_1)^T}{\|\widehat{\boldsymbol{p}}_{ML}(k)-r_1\|} \\ \vdots \\ \dfrac{(\widehat{\boldsymbol{p}}_{ML}(k)-r_N)^T}{\|\widehat{\boldsymbol{p}}_{ML}(k)-r_N\|} - \dfrac{(\widehat{\boldsymbol{p}}_{ML}(k)-r_1)^T}{\|\widehat{\boldsymbol{p}}_{ML}(k)-r_1\|} \end{bmatrix} \tag{4-24}$$

ML estimate diverges when initial estimate $\left(\widehat{\boldsymbol{p}}_{ML}(0)\right)$ is not close enough to the actual position. Despite the convergence difficulties, the ML estimator is an efficient method and asymptotically unbiased [35].

MLE Algorithm:

1. Estimate the TDOA values between the reference platform and other platforms with a TDOA estimation algorithm.
2. Obtain the measurement covariance matrix $\boldsymbol{\Sigma}$ as defined in Equation (4-8).
3. Start with an initial estimate (LS estimate) and calculate the error vector for this estimate which is defined in Equation (4-22).
4. Calculate the Jacobian matrix $\boldsymbol{J}(0)$ for the initial estimate as in Equation (4-24).
5. Perform GN search algorithm which updates position estimate by updating error vector and Jacobian matrix at each step as in Equation (4-23).
6. End the search algorithm when the defined update criterions are met. The final $\widehat{\boldsymbol{p}}_{ML}(k)$ value is the ML estimate of the target position.

4.5 Single Platform Emitter Localization

In single-platform emitter localization with TDOA method, there is a single platform flying on its path. There are two sensors sufficiently separated from each other on the platform. Platform is measuring the TDOA value for these two sensors. Since the distance between sensors is relatively small, the measured TDOA values are not as large as in multi-platform case. In multi-platform case, the distance between the platform pairs where the TDOA values are calculated are in kilometers. On the other hand the distance between the sensors on the same platform is in meters. This is why single platform emitter localization is more sensitive to TDOA error. One advantage of single-platform emitter localization is that since the sensors are on the same platform there is nearly no synchronization error between the

sensors. For multi-platform case, synchronization error is much larger since TDOA is measured between different platforms at different positions. Highly synchronized clocks are needed to align the data collected by distributed receivers [20]. Another important point that has to be taken in consideration is that the receivers are required to detect the same signal from significantly different angles in multi-platform case [22]. In single platform localization this is not a problem since the sensors are close to each other.

The localization method is very similar to the multi-platform case. In multi-platform case, one platform is chosen as the reference platform and TDOA values are calculated according to this platform. In single-platform case, this is not the case. There is no reference sensor. The TDOA between two sensors is measured at different platform positions and the measurement points are always changing. The RDOA values between sensors are as in Equation (4-26). It is important to note the differences between Equations (4-6) and (4-26).

$$\begin{aligned} \|\boldsymbol{p}-\boldsymbol{r}_{\mathbf{1},front}\| - \|\boldsymbol{p}-\boldsymbol{r}_{\mathbf{1},back}\| &= g_1 \\ &\vdots \\ \|\boldsymbol{p}-\boldsymbol{r}_{N,front}\| - \|\boldsymbol{p}-\boldsymbol{r}_{\mathbf{1},back}\| &= g_N \end{aligned} \tag{4-25}$$

All the equations in (4-6) are written according to the reference sensor position $\boldsymbol{r_1}$. This enabled to write the equations in a matrix form by defining the $\boldsymbol{x}$ vector as target coordinates and the distance between target and reference platform. The $\boldsymbol{x}$ vector is found with an LS estimator since there are more equations than the unknown number. On the other hand in Equation (4-26) there is not a single reference sensor. All TDOA values are calculated according to the sensor at the back. So it can be said that there are N different reference points which are the position of the sensors at the back of the platform at each measurement point. So the new $\boldsymbol{x}$ vector consists of target positions and the distance between target and all N reference points. In other words the size of $\boldsymbol{x}$ grows with measurement number and its size is always larger than the number of equations (N). This is why there is no

closed form solution for single-platform case. In single-platform localization method, MLE is used to find the target position.

4.5.1 Maximum Likelihood Estimator

Maximum Likelihood estimation in multi-platform and single-platform cases are very similar. MLE for multi-platform case is explained in Section 4.4.2. In this section MLE for single-platform will be analyzed but the details of the estimator will not be given one more time. Only the differences between multi-platform and single-platform cases will be specified.

In multi-platform case, the TDOAs are written according to a chosen reference sensor position $(\boldsymbol{r}_1)$. The Jacobian matrix used in estimator was calculated as in Equation (4-24).

In single platform case, the TDOAs are calculated between two sensors on the platform. Let name these sensors as "front" and "back" sensors and choose the one at the back as reference sensor. Then the Jacobian matrix will be calculated as follows:

$$\boldsymbol{J}(k) = \begin{bmatrix} \dfrac{\left(\hat{\boldsymbol{p}}_{ML}(k) - r_{1,front}\right)^T}{\left\|\hat{\boldsymbol{p}}_{ML}(k) - r_{1,front}\right\|} - \dfrac{\left(\hat{\boldsymbol{p}}_{ML}(k) - r_{1,back}\right)^T}{\left\|\hat{\boldsymbol{p}}_{ML}(k) - r_{1,back}\right\|} \\ \vdots \\ \dfrac{\left(\hat{\boldsymbol{p}}_{ML}(k) - r_{N,front}\right)^T}{\left\|\hat{\boldsymbol{p}}_{ML}(k) - r_{N,front}\right\|} - \dfrac{\left(\hat{\boldsymbol{p}}_{ML}(k) - r_{N,back}\right)^T}{\left\|\hat{\boldsymbol{p}}_{ML}(k) - r_{N,back}\right\|} \end{bmatrix} \tag{4-26}$$

In the same way, the error vector used in the ML estimator is modified for single-platform case as follows:

$$\boldsymbol{h}(\boldsymbol{p}) = \begin{bmatrix} \left\|\boldsymbol{p} - \boldsymbol{r}_{\boldsymbol{1,front}}\right\| - \left\|\boldsymbol{p} - \boldsymbol{r}_{\boldsymbol{1,back}}\right\| - \tilde{g}_1 \\ \vdots \\ \left\|\boldsymbol{p} - \boldsymbol{r}_{\boldsymbol{N,front}}\right\| - \left\|\boldsymbol{p} - \boldsymbol{r}_{\boldsymbol{N,back}}\right\| - \tilde{g}_N \end{bmatrix}_{Nx1} \tag{4-27}$$

In above equation $\tilde{g}_i$ for $i = 1, \dots, N$ represents the noisy RDOA values between two sensors on the platform. These RDOA values are much smaller than the ones in multi-platform case.

The other difference between multi-platform and single platform algorithms is in error covariance matrices. In multi-platform case, since the TDOA values are measured according to a reference sensor, the error covariance matrix is not diagonal as indicated in Equation (4-8). However for single-platform case since there is no common reference, covariance matrix can be considered as a diagonal matrix:

$$\mathbf{\Sigma} = \sigma_n^2 \begin{bmatrix} 1 & 0 & \dots & 0 \\ 0 & \ddots & \ddots & \vdots \\ \vdots & \ddots & \ddots & 0 \\ 0 & \dots & 0 & 1 \end{bmatrix} \tag{4-28}$$

where σ_n^2 is the RDOA noise variance.

MLE Algorithm:

1. Estimate the TDOA values between the reference platform and other platforms with a TDOA estimation algorithm.
2. Obtain the measurement covariance matrix $\mathbf{\Sigma}$ as defined in Equation (4-28).
3. Start with an initial estimate and calculate the error vector for this estimate which is defined in Equation (4-27).
4. Calculate the Jacobian matrix $\boldsymbol{J}(0)$ for the initial estimate as in Equation (4-26).
5. Perform GN search algorithm which updates position estimate by updating error vector and Jacobian matrix at each step as in Equation (4-23).
6. End the search algorithm when the defined update criterions are met. The final $\widehat{\boldsymbol{p}}_{ML}(k)$ value is the ML estimate of the target position.

In single platform case, an initial estimate can't be obtained with a closed form estimator as explained before. A position estimate found with another algorithm

or an initial value which is close enough to the actual target position to avoid divergence can be used as initial estimate.

4.6 Combined Method for Position Estimation

In Section 3.6, emitter localization method which uses both bearing and frequency measurements is presented. In simulations, it is shown that the combined method outperforms bearing only and DSF only methods. In this section, beside the bearing and frequency measurements, TDOA measurements are also used in the localization method. The derivation of combined method is very similar to the combined method presented in Section 3.6 which uses both bearing and frequency measurements. So the details will not be repeated in this section one more time. Jacobian matrix, error vector and covariance matrix which are used in single-platform ML estimator are defined in Equations (4-26), (4-27) and (4-28) respectively. To include the TDOA measurements in ML estimator, these terms are added to the pre-defined corresponding vector or matrix which are defined in Equations (3-40), (3-39) and (3-38) respectively and the combined versions are obtained. The combined covariance matrix of measurement noise vector is as in Equation (4-29). As in bearing-only case, there is no relation between TDOA measurements and the center frequency of the emitted signal. So a zeros column is added to the end of the Jacobian matrix of TDOA method while combining the Jacobian matrices.

$$\boldsymbol{K}_{comb} = diag\{\sigma_{\theta_1}^2, \sigma_{\theta_2}^2, \dots, \sigma_{\theta_N}^2, \sigma_{\phi_1}^2, \sigma_{\phi_2}^2, \dots, \sigma_{\phi_N}^2, \sigma_{f_1}^2, \sigma_{f_2}^2, \dots, \sigma_{f_N}^2, \sigma_{n_1}^2, \dots, \sigma_{n_N}^2\} \quad (4\text{-}29)$$

$$\boldsymbol{J}_{comb} = \begin{bmatrix} \boldsymbol{J}_{Bearing} \\ \boldsymbol{J}_{DSF} \\ \boldsymbol{J}_{TDOA} \end{bmatrix} \quad (4\text{-}30)$$

where $\boldsymbol{J}_{TDOA}$ is defined as follows

$$\boldsymbol{J}_{TDOA}=\begin{bmatrix} \frac{(\hat{\boldsymbol{p}}_{ML}(k)-r_{1,front})^T}{\|\hat{\boldsymbol{p}}_{ML}(k)-r_{1,front}\|}-\frac{(\hat{\boldsymbol{p}}_{ML}(k)-r_{1,back})^T}{\|\hat{\boldsymbol{p}}_{ML}(k)-r_{1,back}\|} & 0 \\ \vdots & \vdots \\ \frac{(\hat{\boldsymbol{p}}_{ML}(k)-r_{N,front})^T}{\|\hat{\boldsymbol{p}}_{ML}(k)-r_{N,front}\|}-\frac{(\hat{\boldsymbol{p}}_{ML}(k)-r_{N,back})^T}{\|\hat{\boldsymbol{p}}_{ML}(k)-r_{N,back}\|} & 0 \end{bmatrix} \quad (4\text{-}31)$$

MLE Algorithm:

1. Estimate the AOA, received frequency and TDOA values at each measurement point with a direction-finding, frequency estimation and TDOA estimation algorithm.
2. Obtain the measurement covariance matrix $\boldsymbol{K_{comb}}$ as defined in Equation (4-29).
3. Start with an estimate and calculate the combined error vector for this estimate.
4. Calculate the Jacobian matrix $\boldsymbol{J}_{comb}$ for the initial estimate as in Equation (4-30) .
5. Perform GN search algorithm which updates estimate by updating error vector and Jacobian matrix at each step as in Equation (3-41).
6. End the search algorithm when the defined update criterions are met. The final $\hat{\boldsymbol{x}}_i$ value is the ML estimate of the parameters.

4.7 Simulation Results

Simulations are made for both multi-platform and single platform emitter localization algorithms. In single platform simulations, the same path used in bearing-only and DSF method is used. For multi-platform case a different scenario is created.

For multi-platform localization, target is chosen at $(x_P, y_P, z_P) = (30,30,0)km$. The platforms are positioned at $(0,0,30)km$, $(0,20,30)km$, $(20,0,30)km$, $(20,20,30)km$ and $(0,10,15)km$. In other words, platforms are at the corners of a $20kmx20km$ square and an extra platform is used at $(0,10,15)km$ to avoid singularity. The platforms positions should be chosen well. Otherwise the $(\boldsymbol{A}^T\boldsymbol{A})$ matrix in Equation (4-19) will be singular and become non-invertible. The target-platform geometry is as shown below:

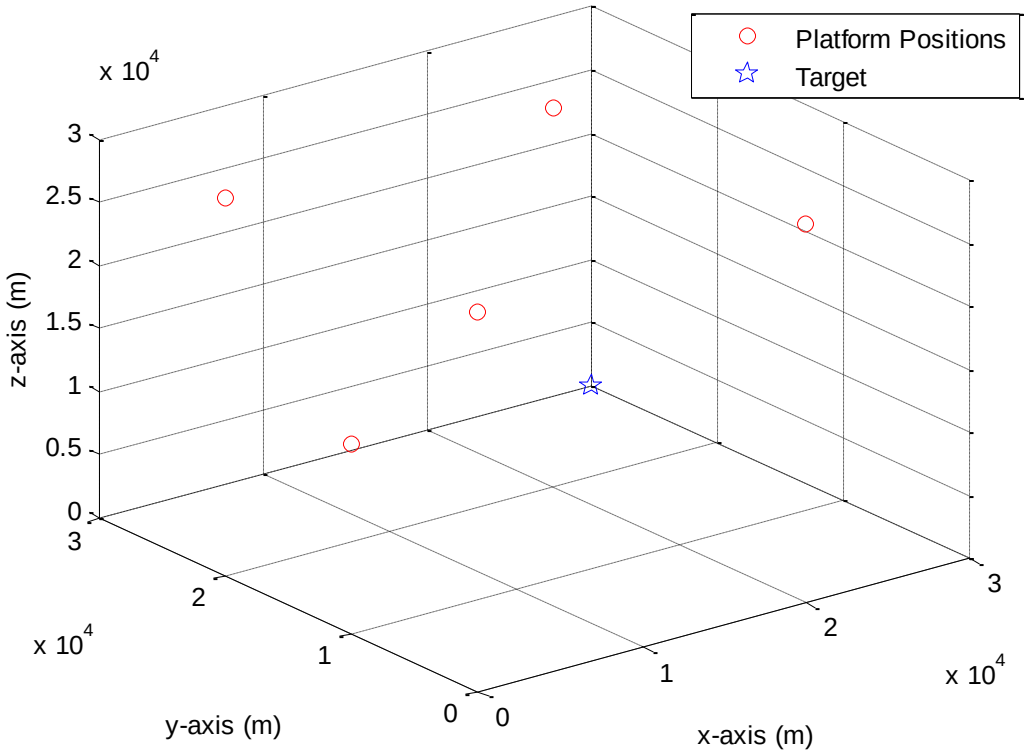

Figure 4-2 : Used target-platform geometry in multi-platform case

To see the effect of TDOA error on estimator accuracy, the standard deviation of the TDOA estimates is changed between 1e-12 sec and 1e-7 sec. For higher TDOA errors the ML estimator starts to diverge. TDOA standard deviation is changed

between these values. The performance comparison of LS estimator and ML estimator is seen in Figure 4-3. As seen from this figure, ML estimator attains the CRLB while LS performs poorly as σ_{TDOA} increases.

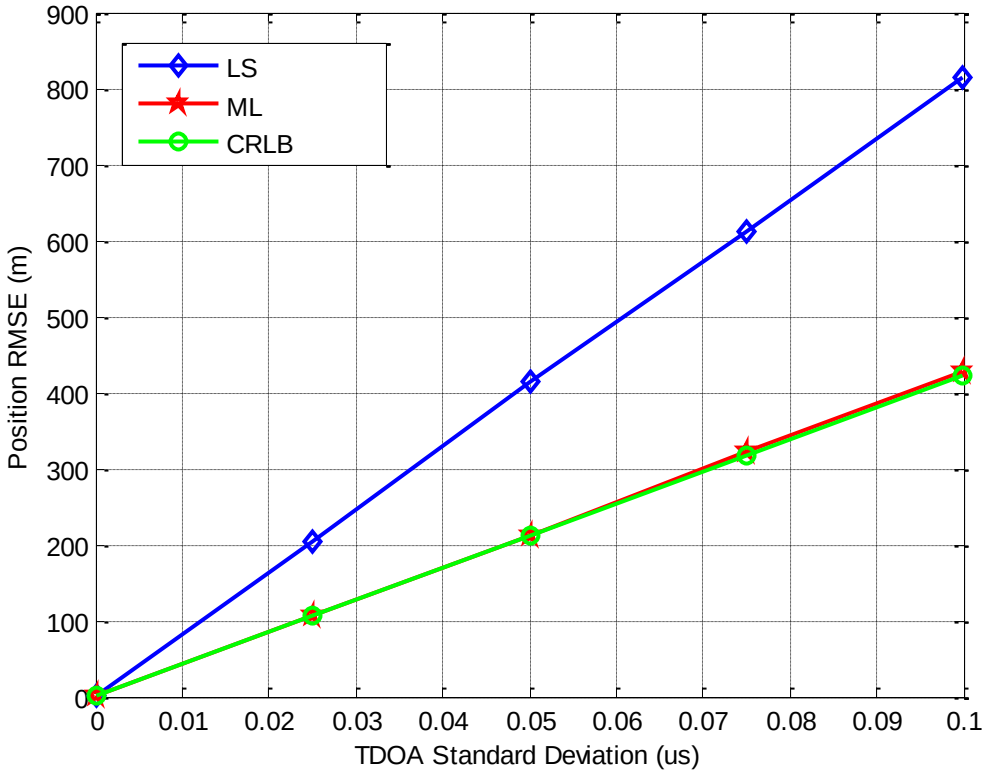

Figure 4-3 : RMS error for target position

Target-platform geometry is another factor that affects estimator accuracy. By using the CRLB matrix, error ellipsoid parameters can be calculated as explained in Section 2.5. Smaller ellipsoid means better estimator accuracy. For different targets, error ellipsoids are plotted around the actual target positions. Since error ellipsoids are hard to visualize, the projections of the ellipsoids are taken on x-y plane and the projected ellipses are plotted. As the hyperboloids defined by the TDOA values become orthogonal to each other, the estimator accuracy gets better. The target at

$(x_P, y_P) = (10,10)km$ is the case where the estimator performs best. As hyperboloids get parallel, noise or small measurement errors can cause considerable errors in estimating the target position. This is called Geometric Dilution of Precision (GDOP). The farther away from the sensor baselines, the worse GDOP gets [1].

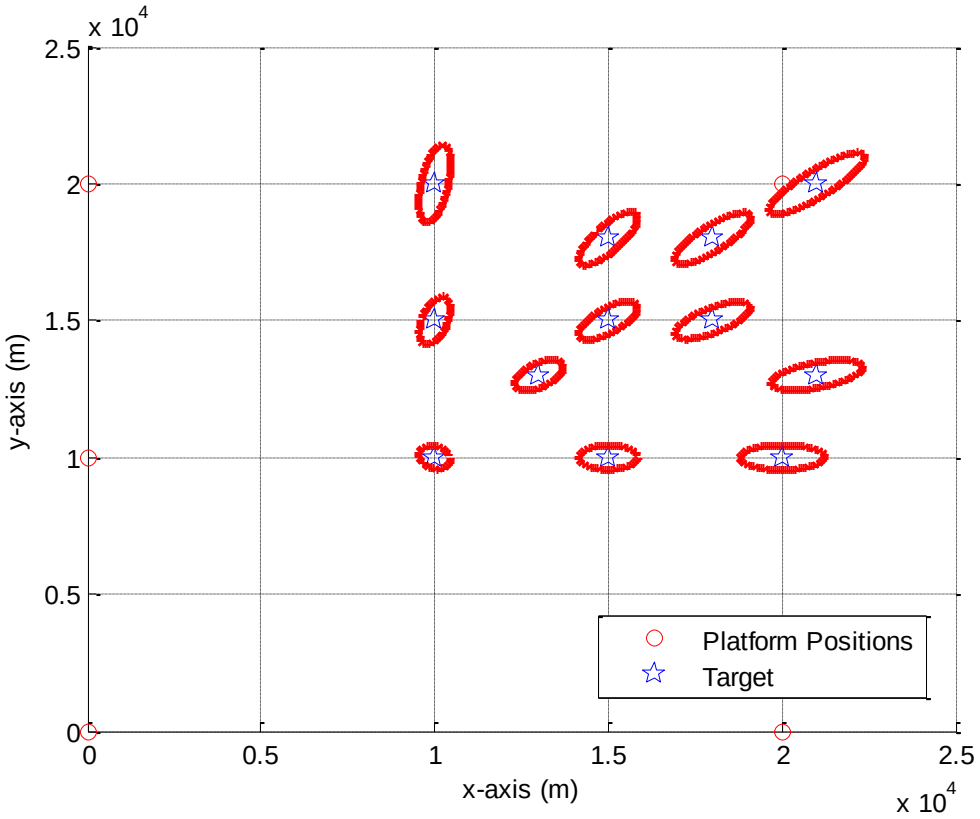

Figure 4-4 : Error ellipses for different target positions

For single platform TDOA localization simulations, the same scenario used in bearing-only and DSF localization algorithms is used. The target is at $(x_P, y_P, z_P) = (4000,3000,0)$. The platform is traveling with a constant speed $V = 100m/s$ and collects TDOA measurements at every 10 seconds. Platform starts its path at $(x_1, y_1, z_1) = (0,0,2000)$ with a velocity vector in the direction of $\theta = 90$ and

$\phi = 0$. After collecting 4 measurements, velocity vector changes in the direction of $\theta = 45$ and $\phi = -5$. 4 measurements are taken along this path and the velocity vector changes to the direction $\theta = 310$ and $\phi = 0$ and collects 4 more measurements. At each measurement point the TDOA is measured between sensors on the same platform. The distance between sensors is chosen as $d = 10m$ unless otherwise stated. The general scenario is as follows:

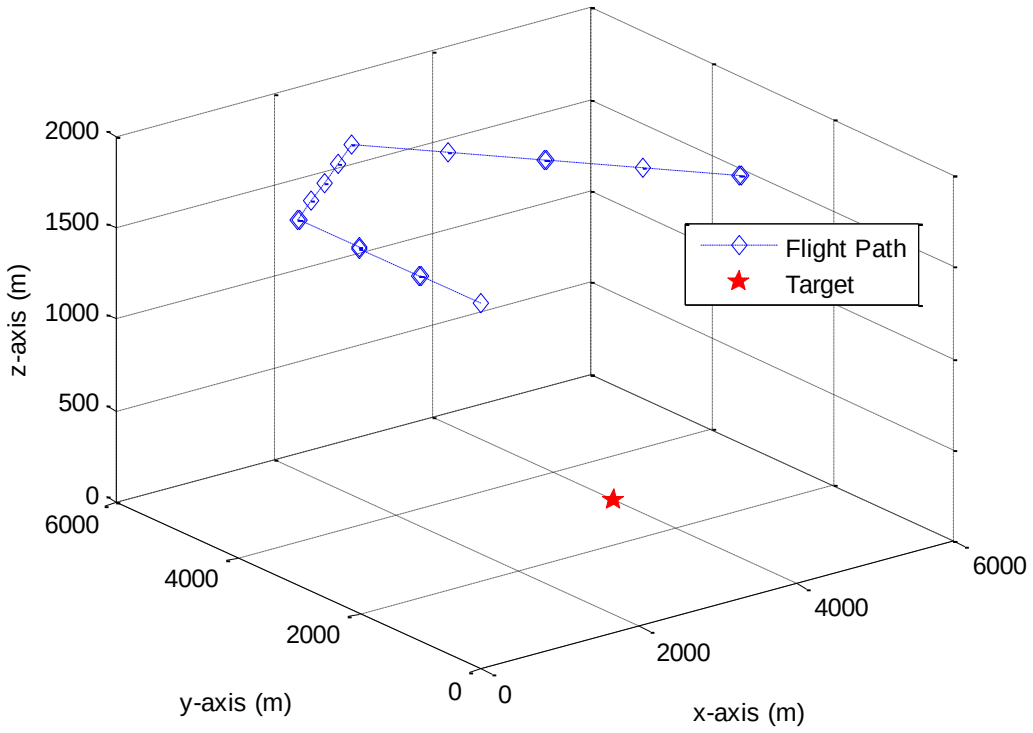

Figure 4-5 : Scenario used in the single-platform simulations

To see the effect of TDOA measurement error on localization accuracy, standard deviation of the TDOA measurement error is changed between 1nsec and 5nsec. For higher TDOA error, ML estimator starts to diverge and estimation cannot be found. Initial target position which is used in ML estimator is obtained by adding random error on actual target position. The distance between sensors is chosen as

$d = 10m$. As expected as TDOA error increases, the accuracy of the estimator decreases and ML estimator starts to diverge from CRLB.

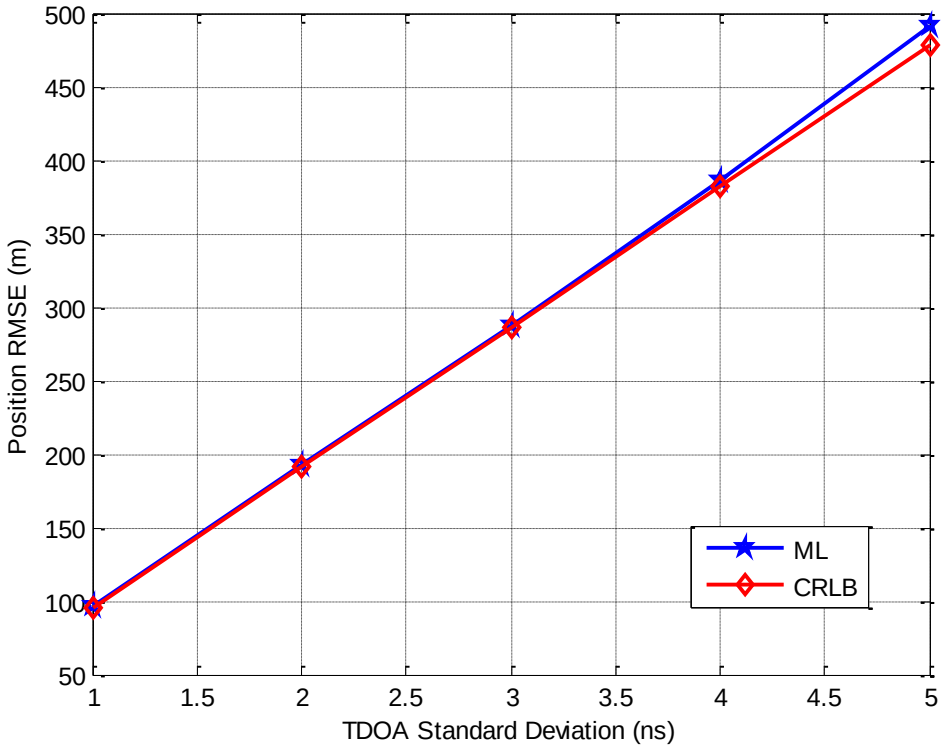

Figure 4-6: RMS error for target position when d=10m

To see the effect of the distance between sensors, TDOA error is kept constant at 1ns and distance between sensors is changed between 10m and 50m.

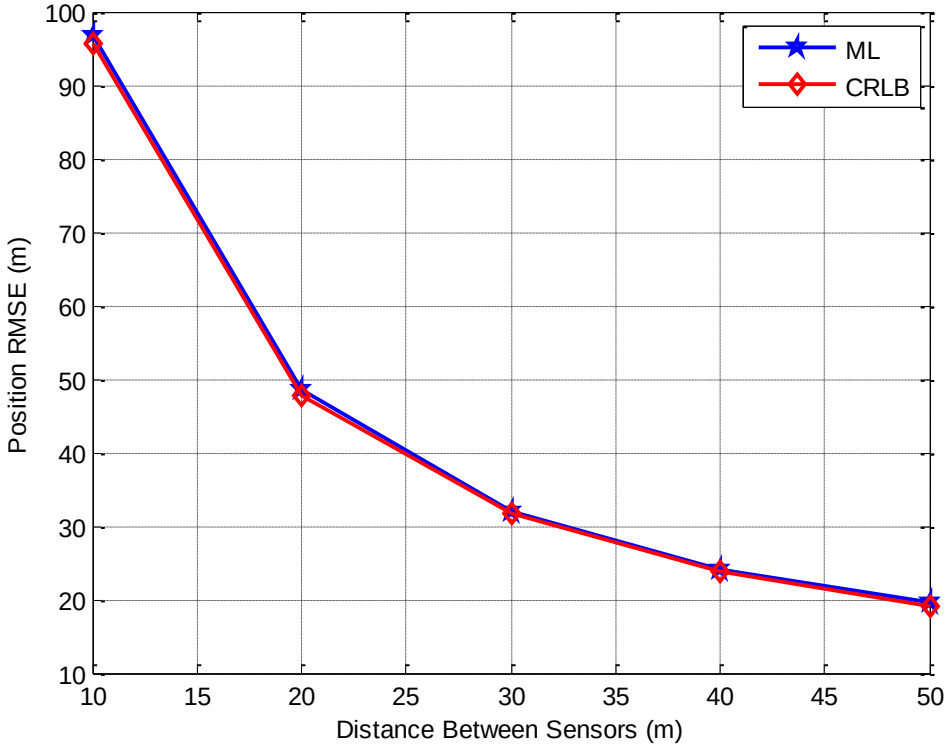

Figure 4-7 : RMS error for target position when $\sigma_{TDOA} = 1n\,\mathrm{sec}$

It is observed from Figure 4-7 that, as the distance between sensors is increased, the estimator performance gets better. For larger distances between sensors, larger TDOA values occur and the effect of the noise gets smaller.

Performance comparison of DSF method, bearing method (BM), TDOA method and the combined method (CM) which uses all parameters is done by using the projections of the error ellipsoids on x-y plane. The ellipses are as shown in Figure 4-8. Azimuth and elevation angles' standard deviations are chosen as 3 degrees, frequency standard deviation is 70 Hz and TDOA standard deviation is 1nsec. The emitted signal frequency is 10GHz and the distance between sensors on the platform which are used in TDOA method are chosen as 10m. The probabilities of the ellipses are 0.95.

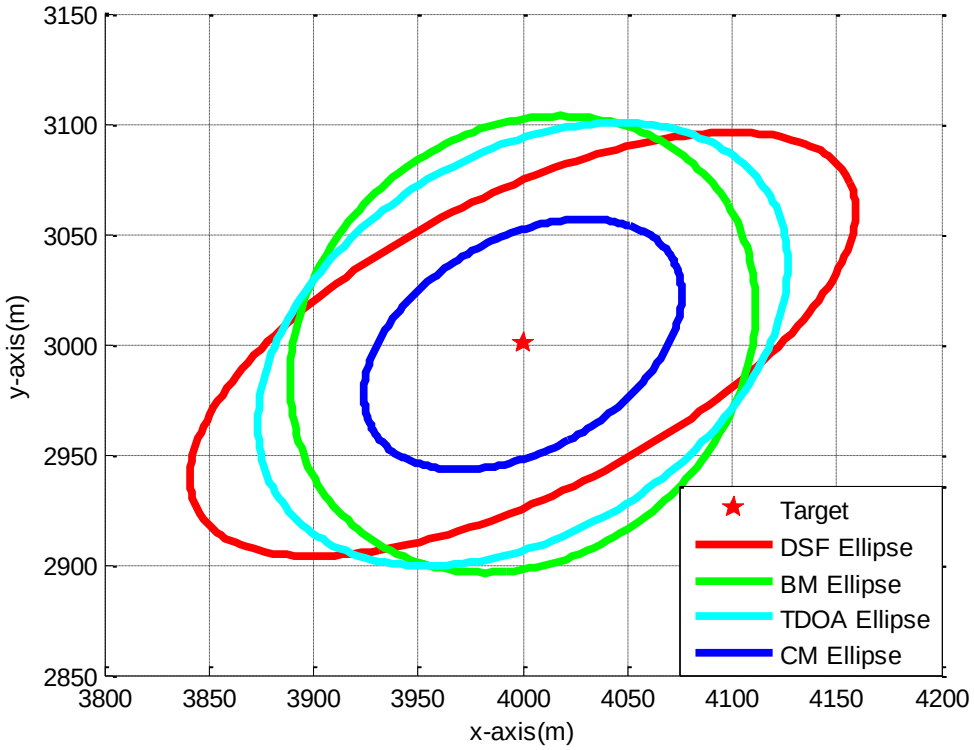

Figure 4-8 : Comparison of error ellipses for different methods

As seen from the figure, the ellipse for the combined method is smallest which means the estimates are confined in a smaller area. This means that the performance of the combined method is better than all the other methods as expected. In Figure 4-9, the estimates obtained with the algorithms are seen. Since error ellipsoids are hard to visualize, the algorithms are implemented with the knowledge that the target is on $z = 0$ plane and the slice of the error ellipsoids are plotted.

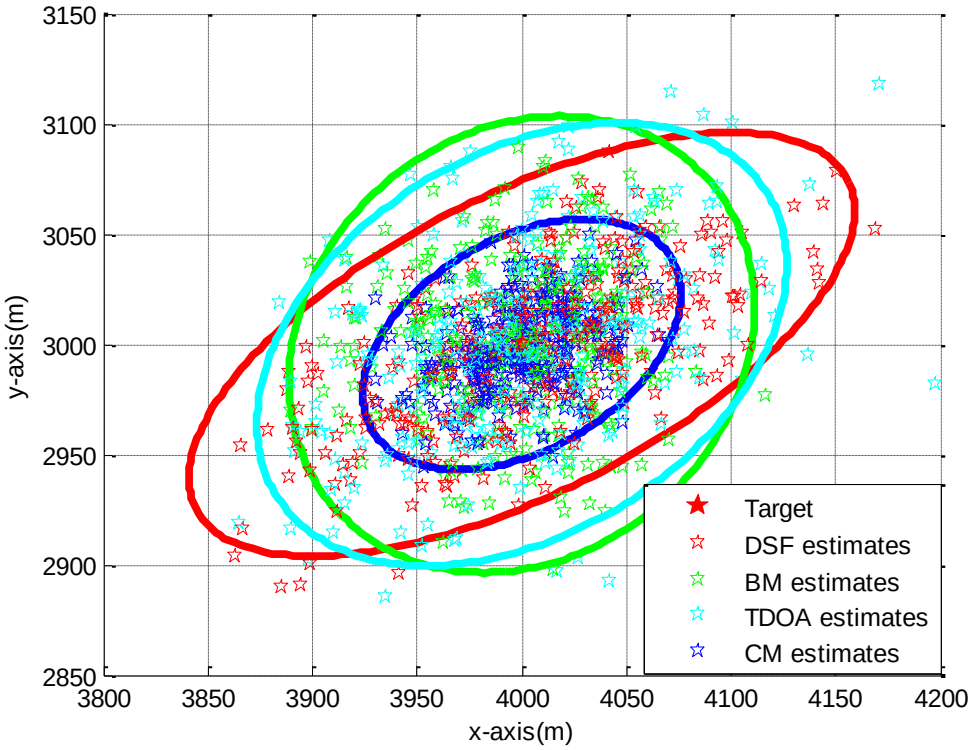

Figure 4-9 : The estimates obtained with different algorithms

In this thesis two hybrid algorithms are implemented. First bearing and frequency measurements are combined to find a target position. Then by adding TDOA values another hybrid algorithm is implemented. To see the effect of TDOA measurements to estimator accuracy, error ellipses for two hybrid algorithms are plotted in Figure 4-11.

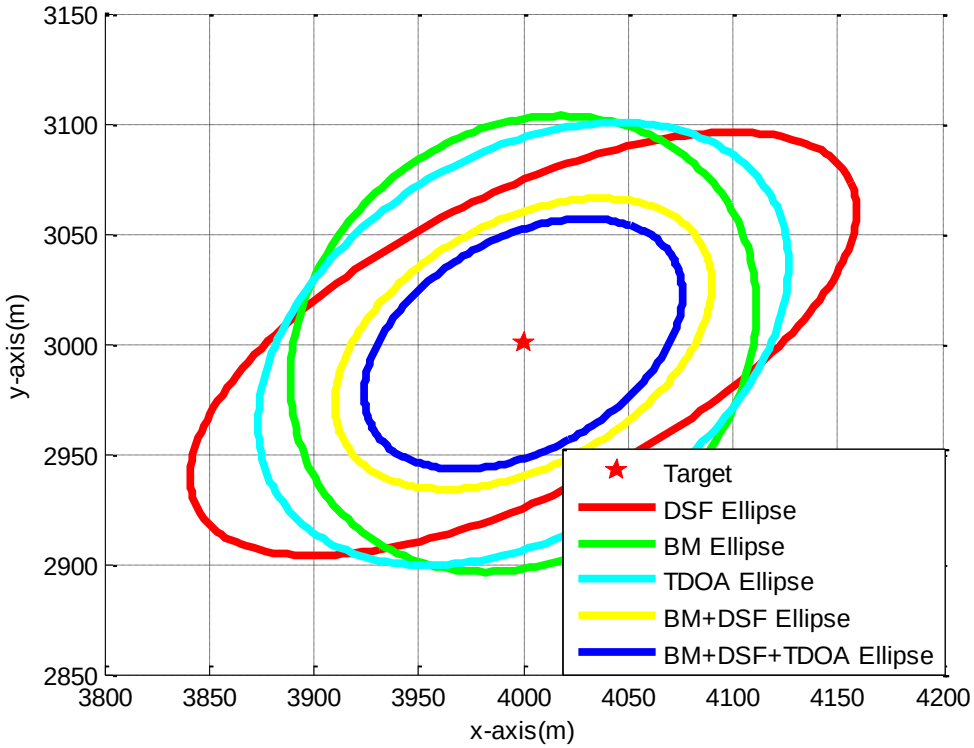

Figure 4-10 : Comparison of error ellipses for hybrid algorithms

As seen in Figure 4-10 the error ellipse (yellow) for the hybrid algorithm which uses bearing and frequency measurements is larger than the ellipse (blue) of hybrid algorithm which uses TDOA measurement in addition to bearing and frequency measurements. The improvement in estimator accuracy is observed by using error ellipses. An important point in Figure 4-10 is that the error ellipse alignments for BM and TDOA methods are similar. Since in single-platform TDOA localization method, the sensors where TDOA value is calculated are very close to each other. So the hyperbolas created in these sensors pairs are similar with DF lines.

In simulations, first the case where standard deviations of azimuth and elevation angles are fixed to 3 degrees and TDOA error is fixed to 1nsec is examined. The

standard deviation of the frequency measurements are changed between 10Hz and 90Hz. The results are as in Figure 4-11.

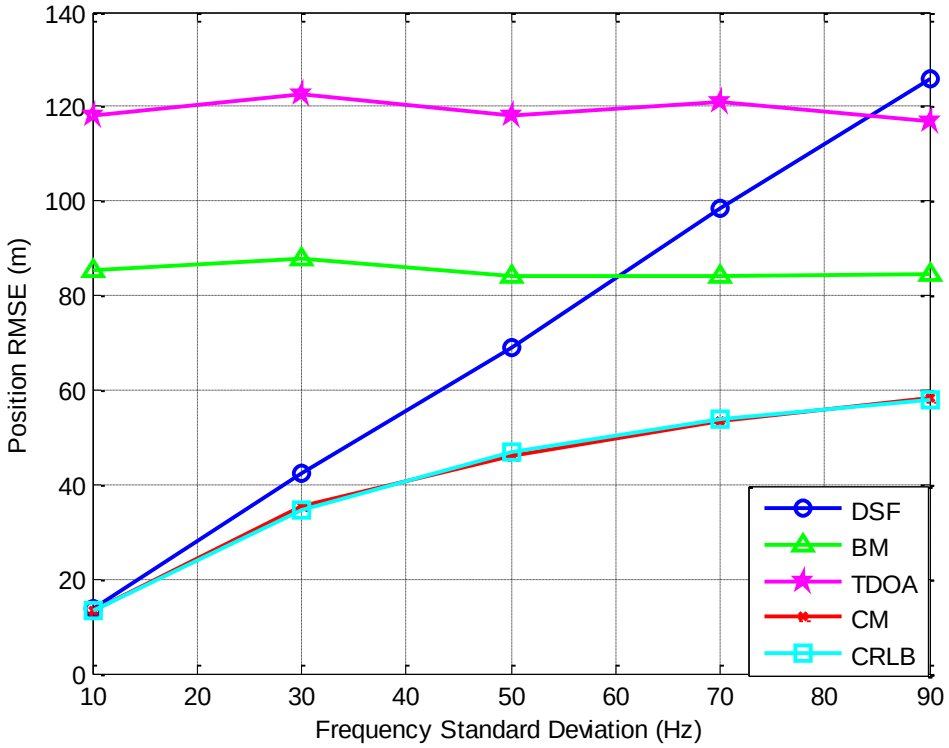

Figure 4-11 : Performance comparison of algorithms for different frequency standard deviations

To see the algorithm performances for different angle measurement standard deviations, bearing standard deviations are changed between 1° and 5°. Frequency standard deviation is fixed to 50Hz and TDOA standard deviation is fixed to 1 nsec.

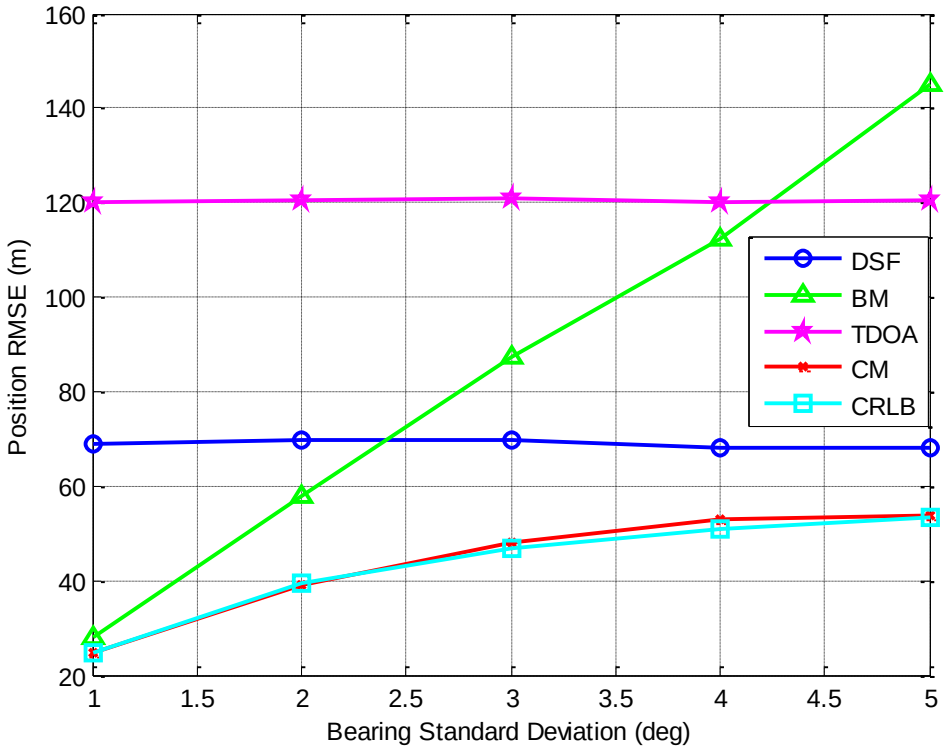

Figure 4-12 : Performance comparison of algorithms for different bearing standard deviations

To see the algorithm performances for different TDOA measurement standard deviations, TDOA standard deviations are changed between 0.5 and 1.5 nsec. Frequency standard deviation is fixed to 100Hz and bearing standard deviation is fixed to 5°.

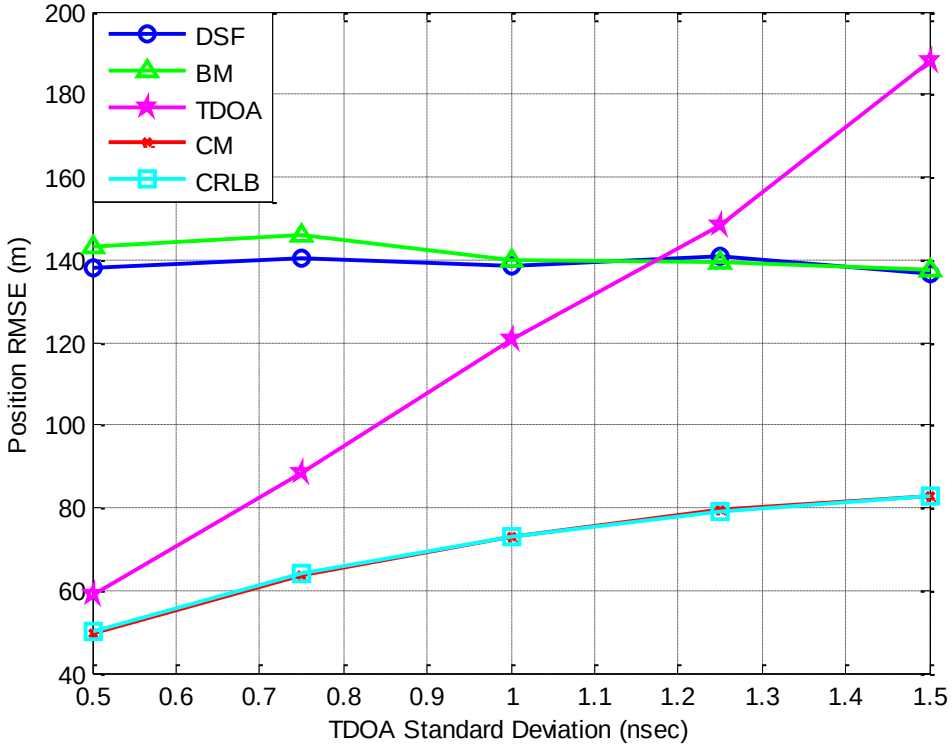

Figure 4-13 : Performance comparison of algorithms for different TDOA standard deviations

In all plots above it is observed that the combined ML method meets CRLB.

CHAPTER 5

CONCLUSIONS

In this thesis, different localization algorithms in 3D are considered. In the scenarios the target is stationary and the locator system is moving on its trajectory. The algorithms are examined mainly in three parts.

In the first group, bearing-only localization algorithms are analyzed. First the closed form estimators are presented which are OVE, PLE and WIVE. In WIVE algorithm, the estimate obtained with PLE is used. Then ML estimator is presented which uses the estimate obtained with WIVE as initial estimate and finds the solution in an iterative way. GN search algorithm is used in ML estimator. Position accuracies are calculated for different azimuth and elevation standard deviations for all these methods and it is observed that ML estimator has the best performance among all other methods. On the other hand, performance of WIVE algorithm is close to MLE and its computational complexity is relatively low. In these bearing-only localization methods, position is estimated after all measurements are collected. A recursive emitter localization method is presented which uses EKF. In this method, an initial position estimate is found with a few measurements and it is updated as a new measurement arrives without the need of storing old measurements. This method is useful when memory is an important criterion in the system.

In second group, Doppler-shift-based algorithms are considered. Due to the relative motion between platform and target there is a Doppler shift in frequency. By using the LS and ML algorithms, the position of the target and the emitted frequency are estimated. After implementing both bearing-only and DSF methods, these two

algorithms are combined in the ML estimator. It is observed that both position and frequency estimation is better in the combined method.

Finally TDOA based localization methods are considered. First multi-platform case is analyzed where the platforms are positioned at different locations. In TDOA based localization method, one platform is chosen as reference and TDOA values are measured according to this platform. By using this single reference platform, TDOA equations can be expressed in a matrix equation where the distance to the reference platform is modeled as an unknown variable. This property enables a closed form estimate (LS). By using this closed form estimate as an initial estimate, ML estimate of the TDOA method is obtained. Position accuracies are calculated for different TDOA standard values and it is observed that ML estimator performance is better than the LS as expected. For single-platform case, it is assumed that there are two sensors on the platform and the TDOA between these two sensors is measured. Platform is moving along its trajectory and measures the TDOA values between these two sensors at different positions. In this method, the reference sensor is the one at the back but at each measurement point the reference sensor is at a different position. So when TDOA equations are written in matrix form, the distance of the platform to the reference sensor is always changing and all these distance are added to the vector as an unknown. Number of unknowns is always greater than the number of equations. So closed form estimate is not available for a single-platform TDOA. It is assumed that an initial estimate of the target is known and ML estimate is obtained. Performance of the algorithm is analyzed for different TDOA values and sensor distances and observed that algorithm performance gets better as the distance between sensors on the platform gets longer. It is shown that in single-platform TDOA method, since TDOA values are much smaller than multi-platform TDOA method, it is more sensitive to noise.

After analyzing all algorithms, all methods are combined in the ML framework. The performance of the combined method is compared with all methods individually and it is shown that combined method is better as expected.

In simulations, to gain an idea about the performance of the algorithms, the error ellipsoid concept is examined. The ellipsoid parameters are obtained from CRLB matrix which represents the minimum achievable error for unbiased estimators. The error ellipsoids are plotted around the true target positions. It is explained that a smaller ellipsoid corresponds to a better estimator performance. For all algorithms, error ellipsoids are obtained using the CRLB matrices and error ellipsoid parameters are obtained. ML estimator performances are compared with the related CRLB values and shown that ML estimators meet CRLB. Since error ellipsoids are hard to visualize, the projection and slice of the ellipsoid are taken on x-y plane. Error ellipsoid around true target positions are plotted for different target positions and the effect of target-platform geometry on algorithm performance is shown.

As a future work, simulations can be done with real trajectory and measurement data. In this thesis, Cartesian coordinates are used. It is assumed that platform is on smooth x-y plane. The geometry of Earth and terrain data is not taken into account. By using digital terrain elevation data (DTED) and an earth model, algorithms can be analyzed in a more practical scenario.

REFERENCES

[1]. Poisel, R.A., "Electronic Warfare Target Location Methods", Boston, Artech House, 2005.

[2].Poisel, R.A., "Introduction to Communication Electronic Warfare Systems", Artech House, Norwood MA, 2002.

[3].Stansfield, R.G., "Statistical Theory of DF Fixing", Journal of IEEE 14, Part IIIA, 15, 1947, pp.762-770

[4].Gavish, M., Weiss, A.J., "Performance Analysis if Bearing-Only Target Location Algorithms", IEEE Transactions on Aerospace and Electronic Systems, Vol. 28, No.3, 1992, pp. 817-828.

[5].Nardone, S.C., Lindgren A.G., Gong, K.F., "Fundamental Properties and Performance of Conventional Bearings-Only Target Motion Analysis", IEEE Transactions on Automatic Control, Vol. AC-29, No. 9, September 1984.

[6].Foy, W.H "Position-Location Solutions by Taylor-Series Estimation", IEEE Transaction on Aerospace and Electronic Systems, Vol. AES-12, No. 2, March 1976, pp. 187-194.

[7].Torrieri, D.J "Statistical Theory of Passive Location Systems", IEEE Transactions on Aerospace and Electronic Systems, Vol.20, No.2, 1984, pp.183-197.

[8].Doğançay, K., Hmam, H., "Optimal Angular Sensor Separation for AOA Localization", ELSEVIER Signal Processing 88 (2008) pp.1248-1260.

[9].Chan Y.T. and Towers, J.J, "Passive Localization From Doppler-Shifted Frequency Measurements", IEEE Transactions on Signal Processing, Vol.40, No.10, October 1992.

[10]. Lee, B.H., Chan, Y.T., Chan, F., Du, H., Dilkes, F.A., "Doppler Frequency Geolocation of Uncooperative Radars", IEEE, 2007.

[11]. Becker, K., "An Efficient Method of Passive Emitter Location", IEEE Transactions on Aerospace and Electronic Systems, Vol.28, No.4 October 1992.

[12]. Becker, K., "Passive Localization of Frequency-Agile Radars from Angle and Frequency Measurements", IEEE Transactions on Aerospace and Electronic Systems, Vol. 35, No. 4, October 1999, pp. 1129-1144.

[13]. Fowler, M.L., "Analysis of Single-Platform Passive Emitter Location with Terrain Data", IEEE Transaction on Aerospace and Electronic Systems, Vol.37, No.2, April 2001.

[14]. Chan,Y.T. and Ho, K.C. "A Simple and Efficient Estimator for Hyperbolic Location", IEEE Transactions on Signal Processing, Vol. 42,No.8, August 1994, pp.1905-1915.

[15]. Bakhoum, E.G.,"Closed-Form Solution of Hyperbolic Geolocation Equations", IEEE Transactions on Aerospace and Electronic Systems Vol.42, No.4, October 2006.

[16]. Mellen G.M., "Closed-Form Solution for Determining Emitter Location Using Time Difference of Arrival Measurements", IEEE Transactions on Aerospace and Electronic Systems, Vol. 39, No.3, July 2003, pp.1056-1058

[17]. Drake, S., Doğançay, K. "Geolocation by Time Difference of Arrival Using Hyperbolic Asymptotes", IEEE International Conference on Acoustics, Speech and Signal Processing, Vol.2, 2004, pp.ii-361-4

[18]. Doğançay, K., Gray, D. A., "Closed-Form Estimators for Multi-Pulse TDOA Localization", Proceedings of the Eighth International Symposium on Signal Processing and Its Applications, Sydney, Australia, August 2005, Vol.2, pp.543-546.

[19]. Yang, B.,"Different Sensor Placement Strategies for TDOA Based Localization", ICASSP 2007.

[20]. Hmam, H., "Scan-Based Emitter Passive Localization", IEEE Transactions on Aerospace and Electronic Systems, Vol.43 No.1, January 2007.

[21]. Doğançay, K. "A Closed-Form Pseudolinear Estimator for Geolocation of Scanning Emitters", IEEE International Conference on Acoustics, Speech and Signal Processing, 2010.

[22]. Hmam, H., Doğançay, K., "Passive Localization of Scanning Emitters", IEEE Transactions on Aerospace and Electronic Systems, Vol. 46, No. 2, April 2010.

[23]. Doğançay, K., "UAV Path Planning for Passive Emitter Localization", IEEE Transactions on Aerospace and Electronic Systems, Vol. 48, No. 2, April 2012.

[24]. Doğançay, K., Ibal G., "Instrumental Variable Estimator for 3D Bearings-Only Emitter Localization", ISSNIP, 2005.

[25]. Dersan, A."Passive Radar Localization by TDOA Measurements" M.Sc. Thesis, Middle East Technical University, September 2001.

[26]. Mahafza, B.R., "Radar Systems Analysis and Design Using MATLAB", Chapman&Hall/CRC, 2000.

[27]. Batuman, E., "Comparison and Evaluation of Three Dimensional Passive Source Localization Techniques", M.Sc. Thesis, Middle East Technical University, June 2010.

[28]. Yıldırım, B., "A Comparative Evaluation of Conventional and Particle Filter Based Radar Target Tracking", M.Sc. Thesis, Middle East Technical University, November 2007.

[29]. Bar-Shalom, Y., Li, X. R., and Kirubarajan, T., "Estimation with Applications to Tracking and Navigation", John Wiley & Sons, NY, 2001.

[30]. University of Binghamton EE521- Lecture Notes of Mark Fowler.

[31]. Ribeiro, M.I., "Gaussian Probability Density Functions: Properties and Error Characterization", 2004.

[32]. Gai, J., Chan, F., Chan, Y.T., "Frequency Estimation of Uncooperative Coherent Pulse Radars", MILCOM, 2007.

[33]. Hoyer, E.A., Stork, R.F., "The zoom FFT using complex modulation", IEEE Proc. ICASSP,1977:78-81

[34]. Aboutanios, E., Mulgrew, B., "Iterative frequency estimation by interpolation on Fourier coefficients",IEEE Trans. Signal Process., 53(4),pp.1237-1241,2005

[35]. Doğançay, K. , "Emitter Localization using Clustering-Based Bearing Association", IEEE Transactions on Aerospace and Electronic Systems, Vol. 41, No.2, April 2005.

[36]. Çamlıca, S., "Recursive Passive Localization Methods Using Time Difference of Arrival", M.Sc. Thesis, Middle East Technical University, September 2009.

[37]. Torrieri, D.J. , "Arrival Time Estimation by Adaptive Thresholding", IEEE Trans. Aerosp. Electron. Syst. Vol. AES-10, no.2, pp. 178-184, March 1974.

[38]. Azaria, M. and Herts, D. "Time Delay Estimation by Generalized Cross Correlation", IEEE Transactions on Acoustics, Speech and Signal Processing, vol. ASSP-32, pp.280-285, Apr. 1984.

[39]. Quazi, A.H., "An Overview on the Time Delay Estimate in Active and Passive Systems for Target Localization", IEEE Transactions on Acoustics, Speech and Signal Processing, Vol. ASSP-29, No.3, June 1981.

[40]. Lee, K.E., Ahn D.M., Lee, Y., Cho, S., and Chun, J., "A Total Least Squares Algorithm For The Source Location Estimation Using Geo Satellites", MILCOM 2000. 21st Century Military Communications

Conference Proceedings, Los Angeles, California, USA, Vol. 1, October 2000, pp.271-275.